UAB
Universitat Autònoma de Barcelona

Cellular High-Density Lipoprotein-mediated Cholesterol Trafficking: Pathophysiological Mechanisms and Therapeutic Strategies in Cardiovascular and Alzheimer's Disease

Carla Borràs Querol

Cellular High-Density Lipoprotein-mediated Cholesterol Trafficking: Pathophysiological Mechanisms and Therapeutic Strategies in Cardiovascular and Alzheimer's Disease

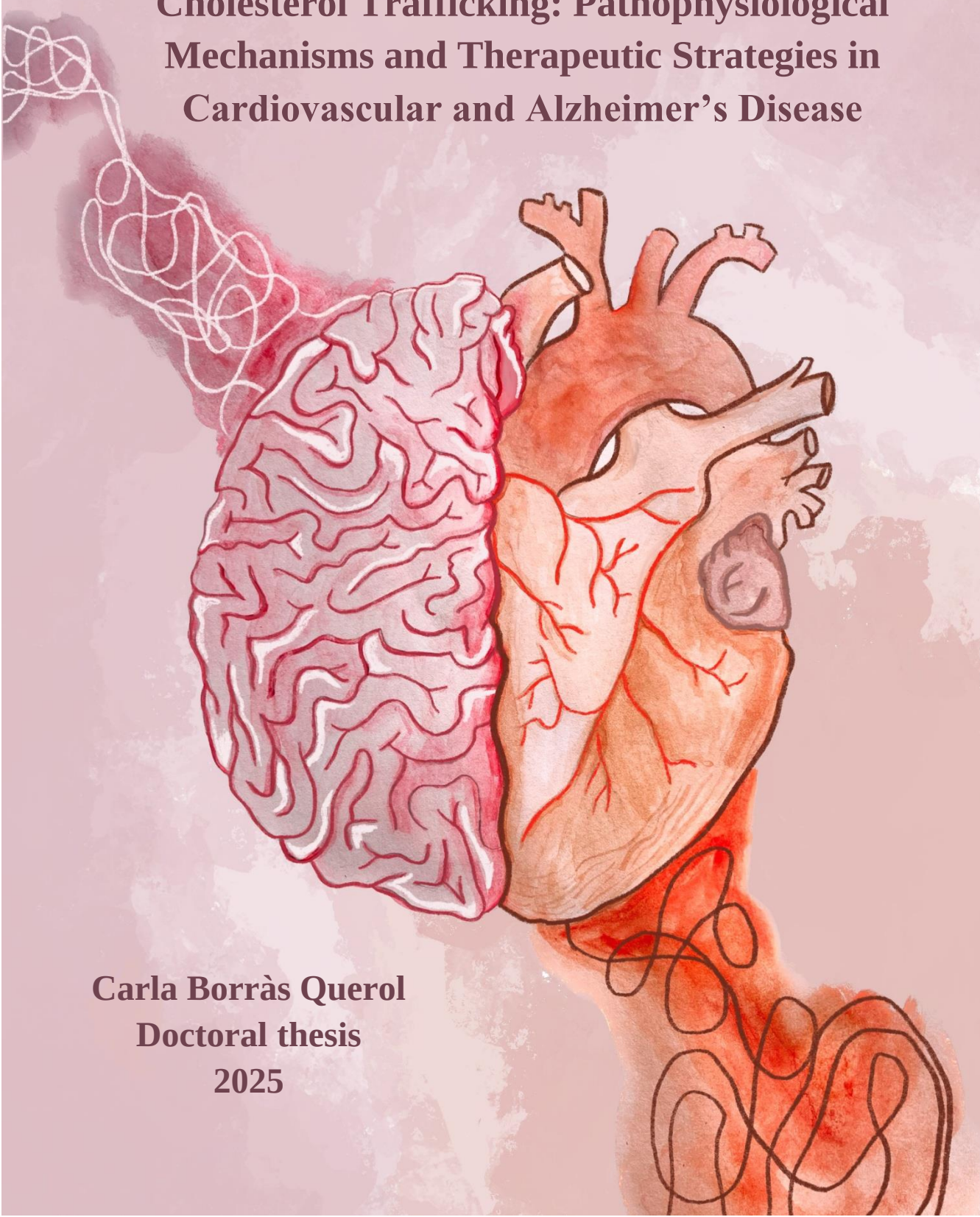

Carla Borràs Querol

Doctoral thesis

2025

DOCTORAL THESIS

Cellular High-Density Lipoprotein-mediated Cholesterol Trafficking: Pathophysiological Mechanisms and Therapeutic Strategies in Cardiovascular and Alzheimer's Disease

Carla Borràs Querol

2025

This thesis was researched and written in the **Pathophysiology of Lipid-Related Diseases group** at the Institut de Recerca Sant Pau

Cellular High-Density Lipoprotein-mediated Cholesterol Trafficking: Pathophysiological Mechanisms and Therapeutic Strategies in Cardiovascular and Alzheimer's Disease

Carla Borràs Querol

Doctoral Program in Biochemistry, Molecular Biology and Biomedicine

Department of Biochemistry and Molecular Biology

Universitat Autònoma de Barcelona

Dr. Joan Carles Escolà Gil

Director

Dr. Mireia Tondo Colomer

Director

Dr. Francisco Blanco Vaca

Director and tutor

TABLE OF CONTENTS

INDEX OF FIGURES

INDEX OF TABLES

ABBREVIATIONS

ABC: ATP-binding cassette

ACAT: acyl-cholesterol acyl transferase

AD: Alzheimer’s disease

ANOVA: analysis of variance

APO: apolipoprotein

APOBEC-1: APOB mRNA editing enzyme

APP: amyloid precursor protein

Aβ: amyloid beta

BBB: blood bran barrier

BSA: bovine serum albumin

cDNA: complementary DNA

CETP: cholesteryl ester transfer protein

CNS: central nervous system

cpm: counts per minute

CSF: cerebrospinal fluid

CVD: cardiovascular disease

DHPE: 1,2-Dihexadecanoyl-sn-Glycero-3-Phosphoethanolamine

DMEM: Dulbecco's Modified Eagle's Medium

DMPC: 1,2-dimyristoyl-sn-glycero-3-phosphocoline

EC: endothelial cell

FBS: fetal bovine serum

FDG: fluorodeoxyglucose

FH: familial hypercholesterolemia

HDL: high-density lipoprotein

HMGCR: 3-hydroxy-3-methylglutaryl coenzyme A reductase

IDL: intermediate-density lipoprotein

LCAT: lecithin cholesterol acyltransferase

LDL: low-density lipoprotein

LDLR: LDL receptor

LDLRAP1: LDLR adaptor protein 1

LPDF: lipoprotein-depleted fraction

LPL: lipoprotein lipase

LRP1: LDLR-related protein 1

LXR: liver X receptor

MBD: methyl-β-cyclodextrin

MRI: magnetic resonance imaging

NPC1L1: Niemann–Pick-C1-like-1

PBS: phosphate-buffered saline

PCSK9: proprotein convertase subtilisin/kexin type 9

PET: positive emission tomography

PLTP: phospholipid transfer protein

PSEN: presenilin

p-Tau: phosphorylated Tau

RA: retinoic acid

RCT: reverse cholesterol transport

rHDL: reconstituted HDL

SD: standard deviation

SR-B1: scavenger receptor B1

SREBP2: sterol regulatory element-binding protein 2

TAGLN: transgrelin

TBST: tris-buffered saline with 0.05% Tween-20

t-Tau: total Tau

VLDL: very low-density lipoprotein

VLDLR: VLDL receptor

VSMC: vascular smooth muscle cell

ABSTRACT

Cholesterol transport is a fundamental process in maintaining cellular homeostasis. Its disruption has been linked to cardiovascular disease (CVD) and Alzheimer's disease (AD). This thesis comprises three complementary studies investigating the regulation of cholesterol trafficking in the contexts of atherosclerosis and neurodegeneration. Although the studies share methodologies to assess cholesterol efflux and reverse cholesterol transport (RCT), each work applies these approaches to disease-specific cellular and animal models, addressing distinct mechanistic pathways.

The first study examines the impact of proprotein convertase subtilisin/kexin type 9 (PCSK9) inhibition on cholesterol metabolism in familial hypercholesterolemia (FH). Using paired samples from FH patients before and after treatment with the PCSK9 inhibitor evolocumab, we demonstrate cholesterol efflux from macrophages was not affected following PCSK9 inhibition. However, it promotes a redistribution of macrophage-derived cholesterol by decreasing low-density lipoprotein (LDL)-associated cholesterol and increasing high-density lipoprotein (HDL)-bound cholesterol in plasma. Similar redistribution was observed in PCSK9 antibody-treated FH mice (heterozygous LDL receptor-deficient mice expressing human APOB100), resulting in enhanced macrophage-to-feces RCT due to accelerated hepatic clearance of LDL particles. These findings support a role for PCSK9 inhibition in positively modulating

macrophage-specific RCT, which represents an additional atheroprotective effect beyond LDL-lowering in FH.

The second study investigates cholesterol metabolism in vascular smooth muscle cells (VSMCs), which are key contributors to foam cell formation and atherogenesis. Upon cholesterol loading, VSMCs undergo a phenotypic switch that reduces their cholesterol efflux capacity, and diminishes *in vivo* RCT. Activation of liver X receptors (LXRs) restores cholesterol efflux from lipid-laden VSMCs and enhances RCT. Additionally, inhibition of acyl-CoA:cholesterol acyltransferase (ACAT) improves efflux capacity by preventing cholesterol esterification and increasing free cholesterol availability. Notably, LXR activation combined with ACAT inhibition exerts a synergistic effect that maximizes cholesterol removal from VSMCs. These results demonstrate that cholesterol loading impairs VSMC-mediated RCT, a hallmark of the foam cell-like phenotype, which can be pharmacologically restored by LXR activation and ACAT inhibition either individually or in combination.

The third study focuses on cerebrospinal fluid (CSF)-mediated cholesterol transport in AD. CSF HDL-like particles, primarily composed of APOE, facilitate the delivery of astrocyte-derived cholesterol to neurons. This process is critical for membrane remodeling and myelination. Using CSF samples from AD patients and control subjects, we show that cholesterol efflux from astrocytes to CSF HDL-like particles remains unaltered in AD. However, CSF HDL-like particles from AD patients display a markedly reduced ability to deliver cholesterol to neurons. This deficit is not influenced by the presence of hallmark AD biomarkers Aβ or tau proteins. Instead, we demonstrate that APOE isoforms play a critical role:

reconstituted HDL particles containing APOE4 show significantly reduced neuronal cholesterol uptake compared to those with APOE3. These findings highlight an isoform-dependent mechanism by which APOE4 contributes to impaired cholesterol delivery to neurons in AD.

Together, these studies deepen our understanding of cholesterol transport mechanisms in CVD and AD. They also underscore the importance of molecular regulators, such as PCSK9, LXR and ACAT, and APOE isoforms, in modulating cholesterol dynamics and disease pathology

RESUM

El transport del colesterol és essencial per al manteniment de la homeòstasi cel·lular. La seva alteració s'associa amb la malaltia cardiovascular (CVD) i la malaltia d'Alzheimer (AD). Aquesta tesi comprèn tres estudis complementaris que investiguen la regulació del transport de colesterol en l'arteriosclerosi i la neurodegeneració. Tot i que els tres estudis comparteixen metodologies per avaluar l'eflux de colesterol i el transport revers de colesterol (RCT), cadascun les aplica en models cel·lulars i animals específics per abordar diferents qüestions mecanístiques.

El primer estudi va examinar l'impacte de la inhibició de la proproteïna convertasa subtilisina/kexina tipus 9 (PCSK9) en el metabolisme del colesterol en el context de la hipercolesterolèmia familiar (FH). Utilitzant mostres aparellades de pacients amb FH abans i després del tractament amb evolocumab, es va observar que la inhibició de PCSK9 no afecta l'eflux de colesterol dels macròfags. No obstant, indueix una redistribució del colesterol derivat dels macròfags, disminuint el colesterol associat a lipoproteïnes de baixa densitat (LDL) i augmentant en lipoproteïnes d'alta densitat (HDL). En un model murí humanitzat de FH (ratolins heterozigots deficients del receptor LDL que expressen APOB100 humana) tractat amb anticossos contra PCSK9, es va observar un efecte similar que va donar lloc a un augment del RCT dels macròfags a causa d'un aclariment hepàtic accelerat de les LDL. Aquests resultats recolzen un efecte positiu de la inhibició de PCSK9 sobre el RCT dels macròfags, com a acció

ateroprotectora addicional que transcendeix la seva capacitat de reduir el colesterol LDL en la FH.

El segon estudi va investigar el metabolisme del colesterol en les cèl·lules musculars llises vasculars (VSMCs), ja que es consideren una de les principals fonts de cèl·lules escumoses que promouen l'arteriosclerosi. Es va observar que, després de la càrrega de colesterol, les VSMCs experimenten un canvi fenotípic que disminueix la seva capacitat d'eflux de colesterol i redueix el RCT. L'activació dels receptors X hepàtics (LXRs) va restaurar la capacitat d'eflux de les VSMCs carregades de colesterol i va augmentar el RCT. Així mateix, la inhibició de l'enzim acil-CoA:colesterol aciltransferasa (ACAT) també va millorar aquesta capacitat, ja que prevé l'esterificació del colesterol i, per tant, incrementa la disponibilitat de colesterol lliure. La combinació de l'activació de LXRs i la inhibició d'ACAT va tenir un efecte sinèrgic que va maximitzar l'eliminació de colesterol de les VSMCs. Aquests resultats indiquen que la càrrega de colesterol indueix un fenotip de cèl·lula escumosa en VSMCs caracteritzat per un RCT defectuós, que pot ser restaurat mitjançant estratègies farmacològiques específiques.

El tercer estudi es va centrar en el transport de colesterol mediat pel líquid cefaloraquidi (CSF) en la AD. Les lipoproteïnes del CSF, similars a HDL i formades principalment per APOE, faciliten el transport de colesterol des d'astròcits a neurones. Es van utilitzar mostres de CSF de pacients amb AD i controls per estudiar l'eflux de colesterol des d'astròcits, que va ser similar en ambdós grups. No obstant, les lipoproteïnes del CSF de pacients amb AD van mostrar una capacitat reduïda per transportar colesterol a les neurones. Aquest defecte no es va veure influenciat per Aβ o tau. En canvi,

es va demostrar que les isoformes d'APOE juguen un paper clau: partícules reconstituïdes d'HDL que contenien APOE4 van mostrar una capacitat significativament menor d'entregar colesterol a les neurones en comparació amb les que contenien APOE3. Això destaca un mecanisme dependent d'isoforma mitjançant el qual l'APOE4 contribueix al transport alterat de colesterol en la AD.

En conjunt, aquests estudis aprofundeixen en la comprensió dels mecanismes de transport de colesterol en la CVD i la AD, i subratllen la importància de reguladors moleculars com PCSK9, LXRs, ACAT i les isoformes d'APOE en la dinàmica del colesterol i la progressió d'aquestes malalties.

RESUMEN

El transporte de colesterol es esencial para el mantenimiento de la homeostasis celular. Su alteración se relaciona con la enfermedad cardiovascular (CVD) y la enfermedad de Alzheimer (AD). Esta tesis comprende tres estudios complementarios que investigan la regulación del transporte de colesterol en la arteriosclerosis y la neurodegeneración. Aunque los tres estudios comparten metodologías para evaluar el eflujo de colesterol y el transporte reverso de colesterol (RCT), cada uno las aplica en modelos celulares y animales específicos para abordar diferentes cuestiones mecanísticas.

El primer estudio examinó el impacto de la inhibición de la proproteína convertasa subtilisina/kexina tipo 9 (PCSK9) sobre el metabolismo del colesterol en la hipercolesterolemia familiar (FH). Utilizando muestras pareadas de pacientes con FH antes y después del tratamiento con evolocumab, se demostró que la inhibición de PCSK9 no afecta el eflujo de colesterol desde macrófagos. Sin embargo, induce una redistribución del colesterol derivado de macrófagos, disminuyendo el colesterol asociado a lipoproteínas de baja densidad (LDL) y aumentándolo en lipoproteínas de alta densidad (HDL). En un modelo murino humanizado de FH (ratones heterocigotos deficientes del receptor LDL que expresan APOB100 humana) tratado con anticuerpos contra PCSK9, se observó un efecto similar que resultó en un incremento del RCT desde macrófagos debido a un aclaramiento hepático acelerado de las LDL. Estos resultados respaldan un efecto positivo de la inhibición de PCSK9 sobre el RCT desde macrófagos, como acción ateroprotectora adicional que trasciende su capacidad de reducir el colesterol LDL en la FH.

El segundo estudio investigó el metabolismo del colesterol en las células musculares lisas vasculares (VSMCs), ya que se consideran una de las principales fuentes de células espumosas que promueven la arteriosclerosis. Se observó que, tras la carga de colesterol, las VSMCs experimentan un cambio fenotípico que disminuye su capacidad de eflujo de colesterol y reduce el RCT. La activación de los receptores X hepáticos (LXRs) restauró la capacidad de eflujo de las VSMCs cargadas de colesterol y aumentó el RCT. Asimismo, la inhibición de la enzima acil-CoA:colesterol aciltransferasa (ACAT) también mejoró dicha capacidad, ya que previene la esterificación del colesterol y, por consiguiente, aumenta la disponibilidad de colesterol libre. La combinación de la activación de LXRs y la inhibición de ACAT tuvo un efecto sinérgico que maximizó la eliminación de colesterol de las VSMCs. Estos hallazgos indican que la carga de colesterol induce un fenotipo de célula espumosa en VSMCs caracterizado por un RCT defectuoso, que puede ser restaurado mediante estrategias farmacológicas específicas.

El tercer estudio se centró en el transporte de colesterol mediado por el líquido cefalorraquídeo (CSF) en la AD. Las lipoproteínas del CSF, similares a HDL y formadas principalmente por APOE, facilitan el transporte de colesterol desde astrocitos a neuronas. Se emplearon muestras de CSF de pacientes con AD y controles para el estudio del eflujo de colesterol desde astrocitos, el cual fue similar en ambos grupos. Sin embargo, las lipoproteínas del CSF de pacientes con AD mostraron una capacidad reducida para transportar colesterol a neuronas. Este defecto no se vio influenciado por Aβ o tau. En cambio, se demostró que las isoformas de APOE desempeñan un papel clave: partículas reconstituidas de HDL que contenían APOE4 mostraron una capacidad significativamente menor de entregar colesterol a las neuronas en comparación con aquellas con APOE3. Esto destaca un mecanismo dependiente de isoforma mediante el cual APOE4 contribuye a un transporte alterado de colesterol en AD.

En conjunto, estos estudios profundizan en la comprensión de los mecanismos de transporte de colesterol en la CVD y la AD, y subrayan la importancia de reguladores moleculares como PCSK9, LXRs, ACAT y las isoformas de APOE en la dinámica del colesterol y la progresión de estas enfermedades.

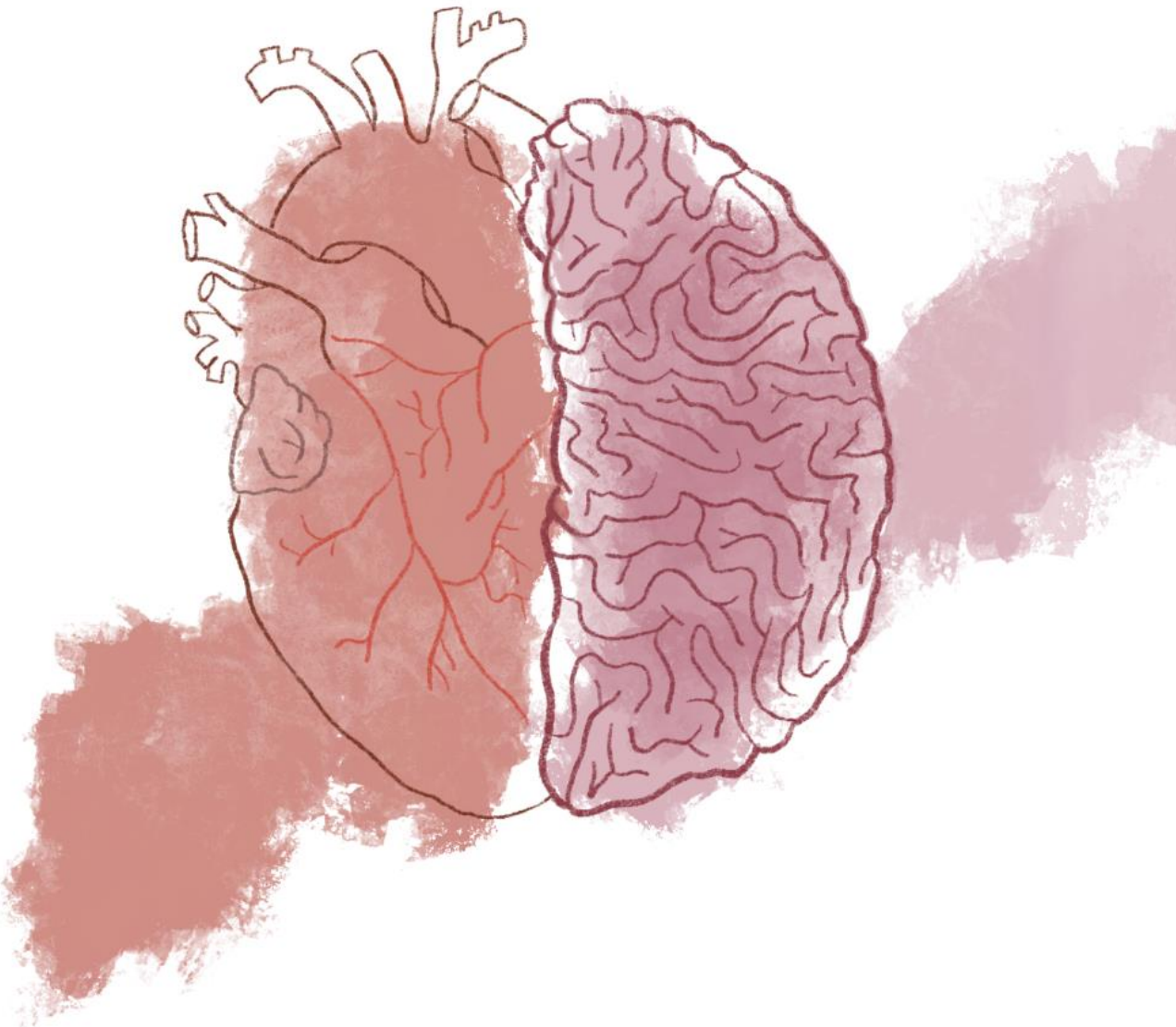

CHAPTER I

INTRODUCTION

1. CHOLESTEROL IN THE BODY

Cholesterol is a lipid molecule belonging to the sterol family. Its name is derived from the Greek words "chole", meaning bile, and "stereos", meaning solid, combined with the suffix "ol", for alcohols. Cholesterol was first identified as a component of gallstones over two centuries ago, but its complete molecular structure was not elucidated until 1932.[1] Cholesterol plays a crucial role in human pathophysiology and has been extensively studied for its involvement in different diseases. It is a major constituent of cell membranes, a precursor for hormone and metabolite synthesis, and a key molecule for cell signaling, transport and nerve conduction.[1]

In mammals, cholesterol can be obtained from two main sources: **dietary intake**, also known as exogenous cholesterol or dietary cholesterol, and ***de novo* biosynthesis**, known as endogenous cholesterol. It is considered that nearly 70% of total cholesterol originates from *de novo* biosynthesis, while the remaining 30% is derived from food intake.[1]

1.1.Cholesterol functions

Cholesterol has a unique composition that makes it an ideal component for forming cell membranes as part of lipid bilayers. It plays a crucial role in maintaining membrane fluidity due to its conformation and interactions with surrounding lipids. Cholesterol is also essential for the formation of membrane rafts, which are critical for immune signaling, cytoskeleton maintenance and membrane trafficking. Furthermore, it ensures the proper functioning of membrane receptors, ion channels and transporters.[1]

Cholesterol acts as a precursor for the synthesis of bile acids, steroid hormones, and vitamin D, representing a fundamental molecule in numerous metabolic processes. Notably, it plays a vital role during embryonic and fetal development, contributing to implantation, placental homeostasis, and organogenesis.[1]

The central nervous system (CNS) accounts for more than 20% of the whole body's cholesterol, thus it is considered the most cholesterol-rich organ. The majority of brain cholesterol is present in myelin sheaths, which are essential for synaptic function. A smaller portion resides in plasma membranes of glial cells and neurons.[2]

1.2. Cholesterol *de novo* biosynthesis

In mammals, all nucleated cells can synthesize cholesterol; however, hepatocytes produce the largest amount, indicating the liver as the primary organ responsible for cholesterol production.[3]

Brain cholesterol metabolism is isolated from the rest of the body due to the presence of the blood bran barrier (BBB). During embryogenesis and childhood, neurons and glial cells synthetize large amounts of cholesterol to support myelinogenesis. As the brain matures into adulthood, neurons lose their ability to synthesize cholesterol and become reliant on cholesterol produced by glial cells.[4]

Cholesterol biosynthesis consists of a highly complex enzymatic pathway, involving the conversion of the precursor acetyl-CoA through the mevalonate pathway.[3] As a complex process, it is tightly controlled by three key regulators that are sensitive to cholesterol levels: one transcriptional regulator, sterol regulatory element-binding protein 2 (SREBP2), and two rate-limiting enzymes, 3-hydroxy-3-methylglutaryl coenzyme A reductase (HMGCR) and squalene monooxygenase. In cholesterol-depleted conditions, SREBP2 upregulates the transcription of HMGCR and squalene monooxygenase. Furthermore, these enzymes are modulated by post-transcriptional mechanisms, including ubiquitination and phosphorylation.[3]

2. CHOLESTEROL TRANSPORT AND LIPOPROTEIN METABOLISM

Cholesteryl esters and triglycerides are not soluble in blood and cerebrospinal fluid (CSF) due to their hydrophobic nature. Consequently, these molecules are enclosed within a hydrophilic monolayer composed of unesterified cholesterol, phospholipids and apolipoproteins (APOs), forming **lipoproteins** (**Figure 1**).[1]

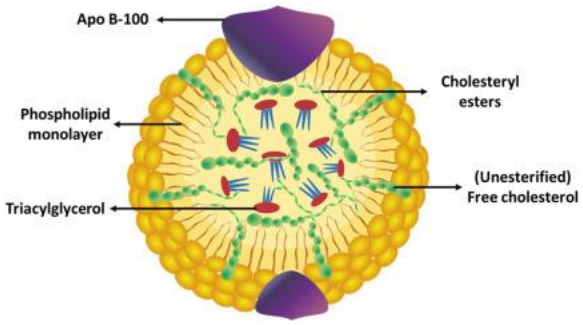

Figure 1. Lipoprotein structure. Lipoproteins consist of a hydrophilic monolayer, composed of unesterified cholesterol, phospholipids and apolipoproteins. In their nuclear core, lipoproteins contain triacylglycerides and cholesteryl esters in different proportions. Adapted from (Sonal Sekhar et al., 2020).[1]

2.1. APOs

APOs are essential for lipoprotein formation and metabolism, functioning as cofactors for enzymes and ligands for membrane receptors that enable lipid trafficking. The liver and intestine are primarily responsible for APO synthesis and degradation, although other tissues, such as the heart, have a residual turnover rate.[1] In the CNS, APOs are predominantly produced by astrocytes and microglia; however, neurons have been reported to produce them under stressful conditions, such as brain injury.[4] In the present thesis, we will focus on the most relevant APOs for plasma and CNS lipoproteins including APOA1, APOB, APOE and APOJ.

APOA1 is mainly produced in the liver and intestine. Structurally, it is formed of amphipathic α-helices that enable lipid binding, thus it is rapidly degraded when

not bound to lipids. As the major component of high-density lipoproteins (HDL), APOA1 plays a crucial role in cholesterol transport, while also exhibiting anti-inflammatory and antioxidant properties.[5] Although predominantly found in the bloodstream, small amounts of APOA1 are detected in the brain, where it associates to CNS lipoproteins. Studies suggest that APOA1 enters the brain through the BBB via scavenger receptor B1 (SR-B1), or other yet unidentified pathways.[6]

APOB exists in two primary isoforms, APOB48 and APOB100, which are encoded by the same gene but generated through RNA editing. APOB48 is a truncated form of the full-length APOB protein, APOB100. In humans, APOB48 is synthetized by enterocytes as a result of the abundant expression of APOB mRNA editing enzyme (APOBEC-1), and serves as component of chylomicrons. APOBEC-1 is absent in the human livers and, thus, only APOB100 is produced by hepatocytes and is present in very low-density lipoproteins (VLDL), intermediate density lipoproteins (IDL), low-density lipoproteins (LDL) and lipoprotein (a).[5] However, in mice, a significant fraction of the hepatic APOB transcripts are edited, producing both APOB48- and APOB100-containg lipoproteins.[7] APOB is pivotal for lipid transport to peripheral tissues. APOB100, in particular and when increased, is strongly associated with atherogenesis and cardiovascular complications.[5] In the CNS, APOB concentration is much more limited. Recent studies reported trace amounts of APOB in the brain, highlighting its possible link to neurodegenerative disorders.[8]

APOE production in the bloodstream is mainly attributed to the liver and macrophages, and is present in a wide range of lipoproteins, including chylomicrons, VLDL, IDL, and HDL.[5] In the brain, APOE is synthetized by astrocytes and is the primary protein component of CNS lipoproteins.[4] Structurally, APOE consists of three domains: the N-terminal domain, which enables receptor binding; the C-terminal domain, which contains the lipid-binding region; and the hinge region, which provides protein mobility. APOE exists in

three isoforms, APOE2, APOE3 and APOE4, determined by polymorphic alleles (ε2, ε3 and ε4), which encode changes in one or two amino acids in the N-terminal domain.[9] Globally, the APOE3 isoform is the most prevalent (80%), followed by APOE4 (14%), and APOE2 (6%).[10]

APOJ, also known as clusterin, is expressed in numerous tissues, including testis, ovaries, kidneys, and liver, and can be found in small amounts in HDL. In the brain, APOJ is synthesized by astrocytes, microglia, and injured neurons, and is a component of CNS lipoproteins. Moreover, APOJ contributes to different metabolic processes such as inflammation and apoptosis.[4]

2.2. Lipoproteins in the bloodstream

Lipoproteins mediate the transport of exogenous cholesterol from the small intestine to the liver, and endogenous cholesterol between the liver and peripheral tissues through the bloodstream. They are classified based on their density, which depends on their lipid content and APO composition. The main types of lipoproteins, arranged in ascending order of density are shown in **Figure 2**.

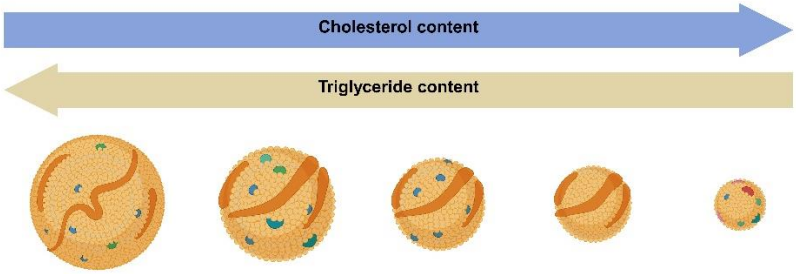

	Chylomicron	VLDL	IDL	LDL	HDL
Diameter (nm)	> 75	30 - 90	25 - 35	18 - 25	5 - 12
Density (g/mL)	< 0.95	0.95 - 1.006	1.006 - 1.019	1.019 - 1.063	1.063 - 1.210
Associated APOs	APOBB48, APOE	APOA4, APOB100, APOC1, C2, C3 APOE	APOB100, APOE	APOB100	APOA1, A2, A4, APOC1, C2, C3 APOE APOJ

Figure 2. Schematic diagram of main peripheral lipoproteins and their properties. Lipoproteins arranged in ascending order of cholesterol content and descending order of triglyceride content. Diameter (nm), density (g/mL) and associated APOs are indicated. Created with *Biorender.com*.

Their distinct densities have enabled their isolation by density gradient ultracentrifugation, a technique that has greatly facilitated their extensive study and characterization.[11]

Chylomicrons, VLDL and IDL are triglyceride-rich lipoproteins. Chylomicrons are synthesized in enterocytes and contain APOB48 as their main structural protein. They are responsible for transporting dietary triglycerides and cholesterol from the intestine to the liver. In contrast, VLDL and IDL are produced in the liver and their core protein is an APOB100 molecule. VLDLs act as carriers of endogenously synthesized lipids and are progressively hydrolyzed by lipoprotein lipase (LPL), resulting in the formation of IDLs. These, in turn, are further metabolized into LDL particles.[11]

LDL particles represent the primary cholesterol carrier in the bloodstream, delivering hepatic cholesterol and triglycerides to peripheral tissues, including muscle, adipose tissue, the gonads and the adrenal gland. Originating from the progressive metabolism of VLDL, each LDL particle contains a single APOB100 molecule, which is essential for receptor recognition and cellular uptake.[12]

HDL plays a pivotal role in transporting cholesterol from peripheral tissues to the liver for its elimination. HDL is attributed with multiple protective properties including anti-atherogenic, anti-inflammatory, anti-thrombotic, and anti-apoptotic effects.[13] APOA1 represents the most abundant protein within HDL, mainly with multiple molecules present in each particle. Additionally, HDL contains minor APOs, enzymes and proteins involved in complement activation, and inhibition of proteases and acute-phase reactions.[13]

HDL is considered a heterogeneous class of lipoproteins, with different subtypes identified depending on the isolation method used. Based on ultracentrifugation, they can be divided into HDL2, with a larger volume and richer in lipids, and HDL3, smaller in size and with a higher protein content. Based on two-dimensional agarose gel electrophoresis, HDL can be separated into preβ-

migrating particles, which have a very low lipid content and a nascent discoidal shape, and α-migrating particles, which represent mature spherical HDL particles with a higher lipid load.[14]

2.3.Lipoprotein receptors and cholesterol transporters

Different receptors and transporters are involved in lipoprotein and cholesterol metabolism. Here, the most relevant will be briefly described.

2.3.1. LDL receptor family

The LDL receptor (LDLR) family comprises a group of membrane receptors involved in the internalization of extracellular ligands such as lipoproteins, exotoxins and lipid-carrier complexes. Members of the LDLR family share structural segments including an extracellular ligand-binding domain, an epidermal growth factor domain, a transmembrane anchor domain, and a cytosolic domain (**Figure 3**).[15]

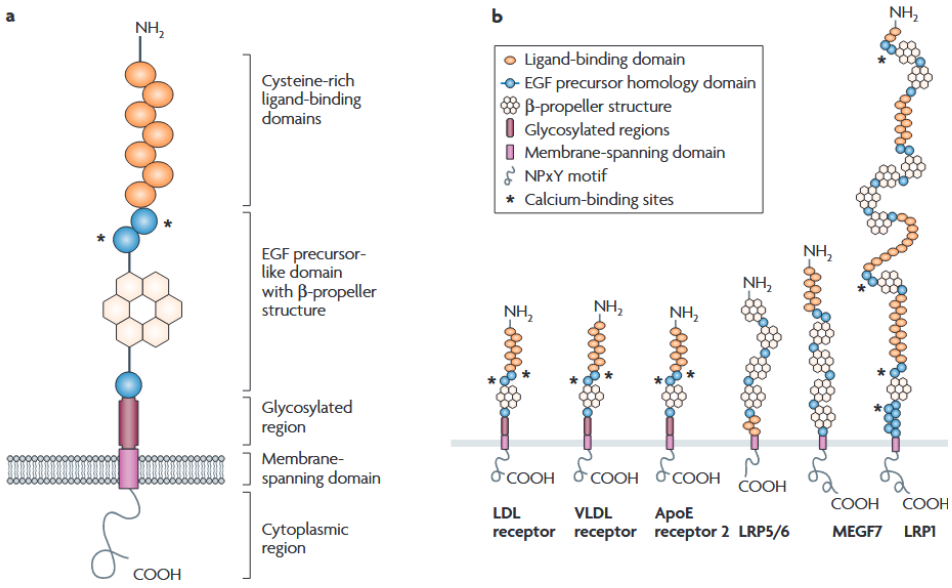

Figure 3. Structure of LDLR family members. (a) Schematic representation of shared structural motifs among LDL receptor family members. **(b)** Structural domains of selected receptors. Adapted from (Wassan et al., 2008).[15]

Notably, the intracellular domain facilitates receptor clustering, leading to the formation of invaginations necessary for receptor-ligand endocytosis into early endosomes. A critical component of this process is LDLR adaptor protein 1 (LDLRAP1), which stabilizes the association between the receptor and its ligand, and ensures efficient internalization.[16] Following endocytosis, the receptor-ligand complex is trafficked to endosomes, where the acid environment promotes dissociation. The receptor is then recycled back to the membrane to sustain its activity (**Figure 4A**).[17,18]

LDLR is ubiquitously expressed and is crucial for cholesterol homeostasis in most tissues, and, particularly in the liver. Being APOB100 and APOE its main ligands, LDLR participates in cellular uptake of remnant chylomicrons, VLDL and, mainly, LDL.[18]

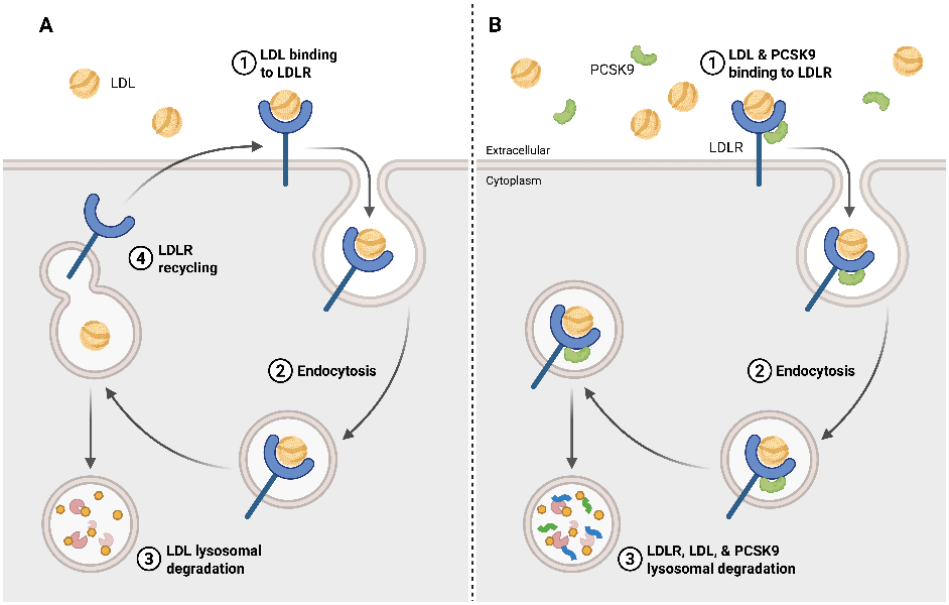

Figure 4. LDLR recycling and PCSK9-mediated regulation. **(A)** LDLR binds to LDL particles and the complex is is endocytosed. LDL particles are degrades, while LDLR is recycled back to the membrane. **(B)** In the presence of PCSK9, it binds to the LDL-LDLR complex and, following endocytosis, the whole complex is degraded. Created with *Biorender.com*

LDLR is tightly regulated at transcriptional and post-transcriptional levels. Upon decreased cellular cholesterol content, LDLR expression is enhanced through the SREBP2 transcription factor activation. Otherwise, when cholesterol levels increase, SREBP2 is inactive, thus maintaining LDLR transcription at low levels.[19] Post-transcriptionally, the presence of LDLR on the hepatocyte membrane is compromised by proprotein convertase subtilisin/kexin type 9 (PCSK9). PCSK9 is synthetized in the liver and binds to membrane-bound LDLR, inducing its endocytosis and subsequent lysosomal degradation, thereby inhibiting LDLR recycling back to the membrane (**Figure 4B)**.[20]

VLDL receptor (VLDLR) is expressed in adipose tissue, muscle, heart and endothelial cells (ECs). APOE is its major ligand, thus VLDLR supports the extrahepatic metabolism of triglyceride-rich lipoproteins, including VLDL and chylomicrons.[18]

LDLR-related protein 1 (LRP1) is widely expressed across tissues, with particularly high levels in the liver and brain. Its large extracellular domain enables the recognition of more than 40 ligands and is involved in a variety of metabolic processes, including the clearance of APOE-containing lipoproteins, inflammatory signaling, protease regulation, and vascular integrity.[18]

2.3.2. SR-B1

SR-B1 is a transmembrane protein that consists of a large extracellular domain, two transmembrane domains, and various short cytosolic domains. It is highly expressed in liver, adrenal gland, intestine, ovaries, testes, macrophages, and ECs, among others. SR-B1 plays a crucial role in the selective uptake of cholesteryl esters from HDL particles by the liver and steroidogenic tissues. Furthermore, it supports cellular cholesterol efflux to HDL, a key step in the anti-atherogenic RCT pathway.[21]

2.3.3. ATP-binding cassette transporters

ATP-binding cassette (ABC) transporters constitute a widespread superfamily of integral membrane proteins that mediate the translocation of substrates across cellular membranes in an ATP-dependent manner. Their structure typically comprises two highly conserved nucleotide-binding segments (also known as ABC domains) and two transmembrane domains. The ABC domains bind and hydrolyze two ATP molecules, inducing conformational changes necessary for substrate efflux. The transmembrane domains are more variable between family members and confer different ligand specificities (**Figure 5**).[22]

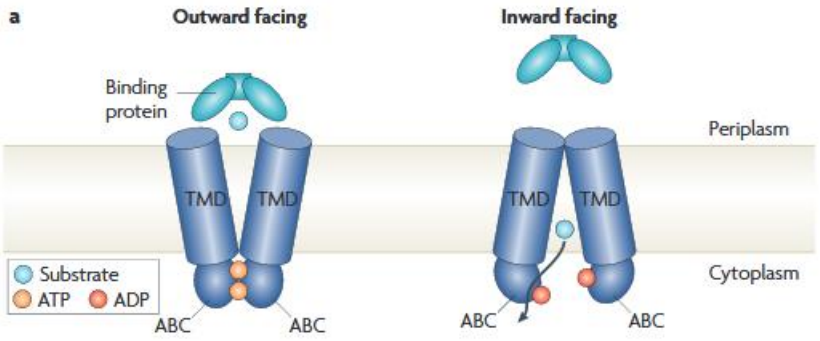

Figure 5. Molecular conformation of ABC transporters. ABC transporters alternate between two conformational states. Upon ligand binding, two ATP molecules are hydrolyzed, triggering a conformational change that facilitates substrate efflux. TMD: transmembrane domain. Extracted from (Rees *et al.*, 2009).[22]

ABCA1 and ABCG1 are ubiquitously expressed, but differ in structure and function. ABCA1 contains two extracellular domains that enable APOA1 binding, making it crucial in mediating the efflux of cholesterol and phosphatidylcholine to lipid-free APOA1. Differently, ABCG1 is a half-size ABC transporter, thus containing one domain of each type and requiring homodimerization for functionality. ABCG1 interacts with mature HDL particles to support further lipidation by cholesterol, phosphatidylcholine and sphingomyelin efflux.[23]

ABCG5 and ABCG8 are exclusively expressed in hepatocytes, enterocytes, epithelium and gallbladder, those receptor function as heterodimers and are responsible for sterol excretion.[24]

Importantly, the expression of ABC transporters is regulated by the nuclear transcription factor **liver X receptor (LXR)**. Under conditions of excess cholesterol, oxysterols are produced, and they serve as endogenous ligands for LXR. Upon LXR activation, it heterodimerizes with retinoid X receptor, enabling binding to the promoter regions and enhancing their expression.[25]

2.3.4. Niemann–Pick-C1-like-1 protein

Niemann–Pick-C1-like-1 (NPC1L1) protein is a transmembrane receptor primarily expressed in the small intestine, with lower levels also found in the liver. It plays a key role in the intestinal absorption of phytosterols and cholesterol. The expression of NPC1L1 is regulated by SREBP2 and LXR, both of which are responsive to intracellular cholesterol levels.[26]

2.4.Cholesterol intake and absorption

Exogenous cholesterol is solubilized by bile acids, forming micelles in the intestinal lumen. The absorption of these micelles in the small intestine is mediated by NPC1L1 protein. Within enterocytes, cholesterol is esterified with a fatty acid by acyl-cholesterol acyl transferase (ACAT) 2, and subsequently incorporated into chylomicrons, which are secreted into the lymphatic system to enter the circulation. Unesterified cholesterol is returned to the lumen via ABCG5/G8 transporters.[27]

2.5.Cholesterol transport in the bloodstream

Cholesterol transport comprises several receptors, transporters, enzymes and proteins. A scheme of the global cholesterol transport, involving peripheral lipoprotein metabolism is depicted in **Figure 6.**

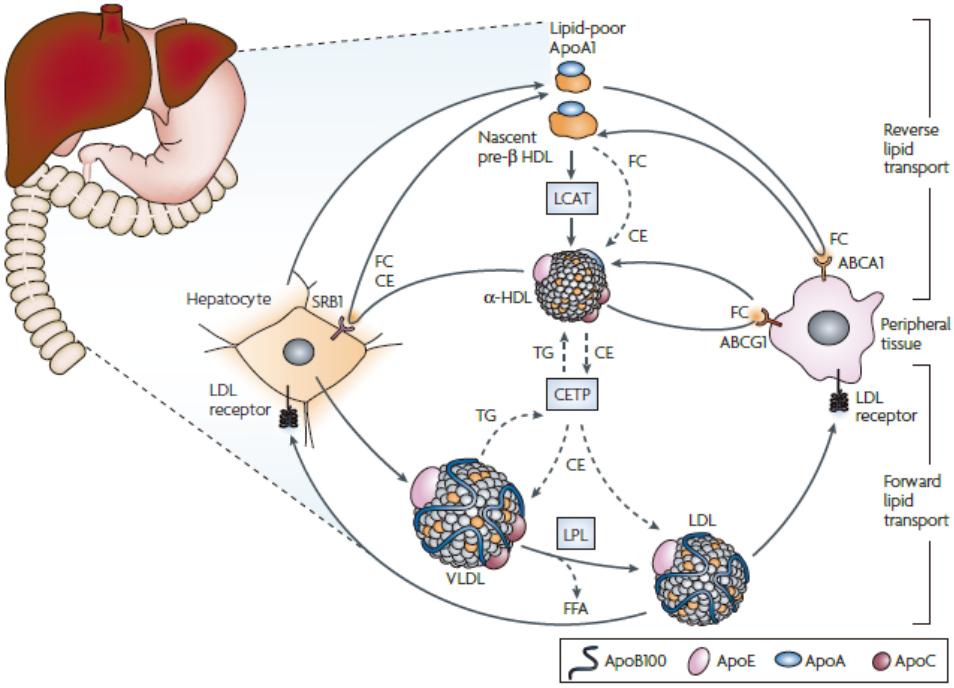

Figure 6. Peripheral cholesterol transport. Cholesterol transport categorized into two main pathways: forward cholesterol transport, which refers to the transport of cholesterol from hepatocytes to the peripheral tissues; and reverse cholesterol transport which encompasses the mechanisms by which cholesterol is returned from peripheral tissues to the liver. EC: ester cholesterol, FC: free cholesterol, FFA: free fatty acid, TG: triglyceride. Extracted from (Wasan *et al.*, 2008).[15]

2.5.1. Forward cholesterol transport

Cholesteryl esters in the liver, either from dietary or endogenous cholesterol, along with triglycerides, are transferred to newly synthetized VLDL particles that are secreted from hepatocytes (**Figure 6**). After the cleavage of triglycerides by LPL, VLDL particles transition into LDL particles, containing a relative higher proportion of cholesterol, and thus reducing their density (**Figure 2 and 6**).[28]

Upon reaching peripheral tissues, APOB100 interacts with cell membrane LDLR, triggering clathrin-mediated endocytosis of the LDL particle. Within the cell, LDL is released, cholesterol is used or esterified by ACAT1, and LDLR is recycled back to the membrane. However, LDLR expression is tightly regulated

according to intracellular cholesterol levels. Thus, excess LDL particles return to the liver via hepatic LDLR for cholesterol excretion to the bile (**Figure 6**).[28]

Besides LDLR, some cells, such as macrophages, express non-regulated membrane scavenger receptors, allowing them to internalize cholesterol regardless of their intracellular levels. Consequently, these cells accumulate cholesterol uncontrollably, resulting in the formation of foam cells, which are a determining factor in the development of atherosclerosis.[28]

2.5.2. Reverse cholesterol transport

Reverse cholesterol transport (RCT) is essential for cholesterol removal from peripheral cells. Throughout this process, HDL particles originate and undergo maturation to ultimately deliver cholesterol to the liver for its excretion. The first step of RCT is cholesterol efflux, which involves the externalization of cholesterol from cells. This process occurs through passive diffusion, in part mediated by SR-B1, or via active transport, facilitated by ABCA1 and ABCG1 transporters (**Figure 6**).[29]

Lipidation of free APOA1 molecules transforms them into pre-β HDL particles. Both APOA1 and pre-β HDL interact with ABCA1, promoting the efflux of cholesterol and phospholipids from cells. These nascent HDL particles are subsequently remodeled by lecithin cholesterol acyltransferase (LCAT). LCAT catalyzes the conversion of free cholesterol into cholesteryl esters, which are sequestered within the lipoprotein core. Alongside LCAT-mediated remodeling, further lipidation of HDL via ABCG1- and SR-B1-mediated cholesterol efflux results in the formation of mature HDL particles (**Figure 6**).[29]

Cholesteryl esters within HDL are selectively uptaken by SR-B1 at the hepatocyte membrane.[28] In humans, cholesteryl ester transfer protein (CETP) facilitates the exchange of cholesteryl esters from HDL to LDL particles, enabling their subsequent uptake by hepatic LDLR (**Figure 6**). Once in the liver, cholesterol is eliminated through the bile, either in its unesterified form or after its conversion

into bile acids. The ABCG5/G8 heterodimer mediates cholesterol excretion into the bile duct, allowing its transport to the intestinal lumen for eventual elimination.[29]

RCT is particularly important in macrophages and vascular smooth muscle cells (VSMC) that accumulate cholesterol in the arterial wall.

2.6. CNS lipoproteins

Lipoproteins in the CNS facilitate the transport of cholesterol throughout the brain and the CSF. CNS lipoprotein concentrations are approximately 1 to 10% respect to those in plasma. The size and density of brain lipoproteins are similar to peripheral HDL particles; therefore, they are also referred to as **HDL-like particles**. Despite their similarities, CNS lipoproteins exhibit a broader size range (8-22 nm) than plasma HDL and a distinct APO composition.[30]

Unlike peripheral HDL, APOE is the main component in CNS lipoproteins, with APOJ present in their nascent discoidal forms,[31] and APOA1 in the more mature forms, although not being synthetized in the brain.[32,33]

2.7. Cholesterol transport in the CNS

A schematic representation of cholesterol transport in the CNS is shown in **Figure 7**. Cholesterol, APOE and APOJ are primarily synthetized by astrocytes and glial cells. Cholesterol efflux from astrocytes is mediated by ABCA1 and ABCG1 transporters. Initially, lipid-free or poorly lipidated APOE and APOJ interact with ABCA1, forming nascent discoidal particles. APOA1 from the bloodstream may also contributes to the formation of these particles.[32,34,35] Then, these nascent lipoproteins acquire additional lipids through ABCG1,[36] and undergo enzymatic remodeling by LCAT, ultimately maturing into spherical HDL-like particles.[31]

Once they reach the neuron membrane, these lipoproteins interact with different receptors including LRP1 and LDLR, leading to cholesterol uptake by neurons.[37]

Of note, oxysterols can flux across the BBB. Neurons convert excess cholesterol into 24-hydroxycholesterol to be transferred to the bloodstream and ultimately reach the liver. Conversely, 27-hydroxycholesterol represents the most abundant cholesterol metabolite in circulation and can diffuse into the brain, where it promotes various functions.[38]

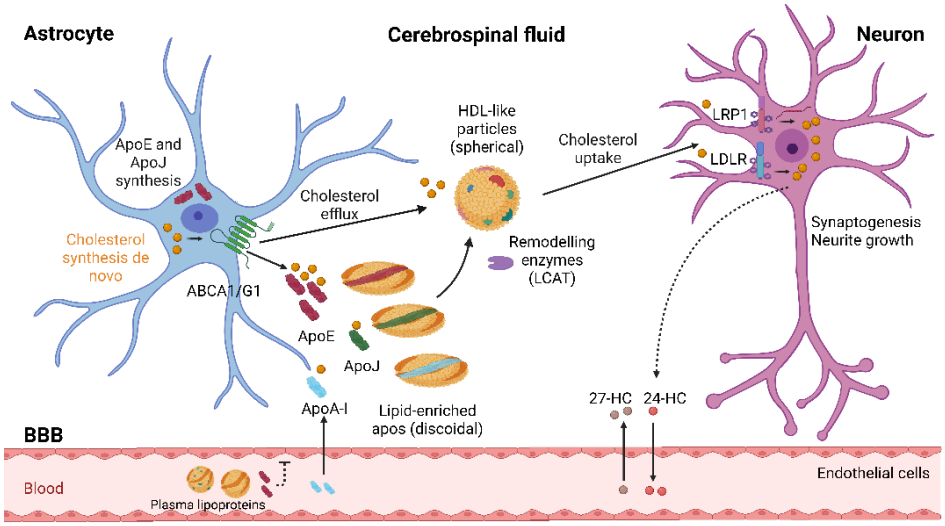

Figure 7. Cholesterol trafficking in the brain. Astrocyte-derived cholesterol is effluxed via ABCA1 and ABCG1 transporters, leading to the synthesis of lipoproteins containing APOE, APOJ and APOA1. These CNS lipoproteins, also known as HDL-like particles, interact with LDLR and LRP1 at the neuronal membrane to facilitate cholesterol uptake. Created with *Biorender.com*.

For a comprehensive review of cholesterol transport mechanisms in the CNS, see *Publication 1, ANNEX.*

3. CARDIOVASCULAR DISEASE

3.1. Etiology and risk factors

Cardiovascular diseases (CVDs) represent the leading cause of death worldwide. According to the World Health Organization, they account for approximately 17.9 million deaths annually, with one-third occurring prematurely before the age of 70. CVDs comprehend a wide range of disorders affecting the heart and blood vessels. In addition to their life-threatening nature, these conditions can reduce quality of life and lead to long-term disability.[39]

Cardiovascular pathologies can be classified depending on the affected region of the body. Coronary artery disease, cerebrovascular disease, and peripheral artery disease, involve reduction or obstruction of blood flow to the heart, the brain, and extremities, respectively. Other conditions are categorized regarding their underlying cause, including cardiomyopathies, rheumatic heart disease or pulmonary embolism.[40]

Nowadays, the major cardiovascular risk factors include hypertension, hyperlipidemia, smoking, alcohol consumption, unhealthy dietary habits sedentary lifestyle, obesity and diabetes.[41,42] Furthermore, genetic predisposition significantly influences CVD prevalence, and contributes to certain risk factors such as hyperlipidemia or diabetes.[43]

3.2. Atherosclerosis

Atherosclerosis is the main cause of reduced blood flow in large arteries, which can eventually lead to complete obstruction. It is considered a slow-progression disease since the formation of atherosclerotic plaques is initiated many years before clinical symptoms arise.[44]

Atherosclerosis is characterized by lipid accumulation and inflammation within the arterial wall. It involves the interplay of various metabolic processes, including lipid modification, activation of inflammatory responses, fibrosis, calcification,

and cellular dysfunction, among others. Consequently, the atherosclerotic process can be divided into different stages, classifying plaques as initial, growing, or advanced (**Figure 8**).[45]

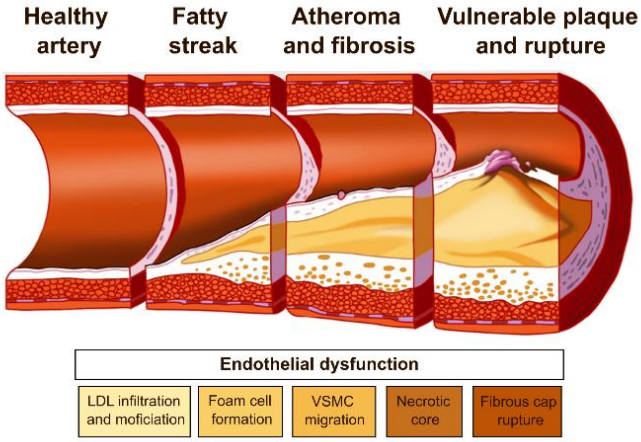

Figure 8. Progression of atherosclerosis. Schematic representation of arterial wall changes throughout the progression of atherosclerotic lesions, highlighting key pathological hallmarks Adapted from: https://www.lipidtools.com/atherosclerosis-and-cardiovascular-risk/.

3.2.1. Arterial wall composition

Arteries are composed of three distinct layers: the tunica intima, the tunica media and the tunica adventitia (**Figure 9**).[46]

The **tunica intima** is the innermost layer, directly facing the lumen of blood vessels. It consists of a monolayer of ECs, which serve as the first line of defense by acting as a selectively permeable barrier. This layer is also supported by collagen and elastin fibers.

The **tunica media** is primarily composed of VSMCs, and along with collagen, elastin, and proteoglycans, they form concentric layers known as lamellar units. In larger arteries, microvessels, named vasa vasorum, perfuse the media to provide necessary nutrients to the cells.

The **tunica adventitia** is the outermost layer of the artery, consisting mainly of fibroblasts and collagen, providing structural support and anchorage to surrounding tissues.

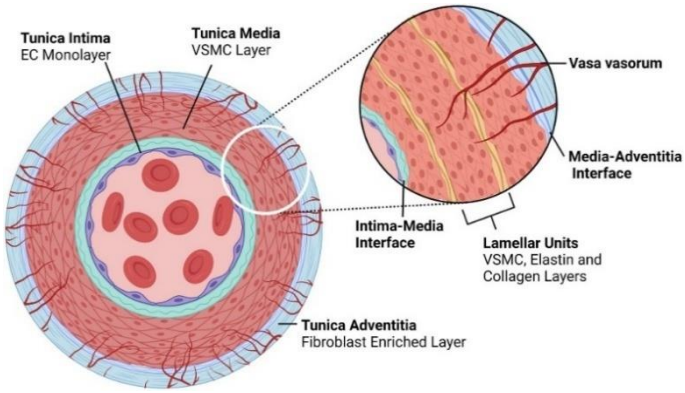

Figure 9. Schematic diagram of the artery structure. Arteries are composed of three layers: the tunica intima, the tunica media and the tunica adventitia. Extracted from (Bax *et al.*, 2022).[46]

3.2.2. Pathophysiology of atherosclerosis

Formation and progression of the atherosclerotic lesion

Atherosclerotic lesion formation begins with endothelial dysfunction, triggered by pathological processes such as oxidative stress, disturbed shear stress and lipid accumulation from excess circulating LDL particles. Under these conditions, ECs lose their protective functions, becoming more permeable and enabling LDL infiltration and retention within the arterial wall.[45]

Once inside the intima, LDL particles undergo oxidative and enzymatic modifications, triggering adhesion and recruitment of leukocytes, particularly monocytes. Upon infiltration, monocytes mature into macrophages which, through the uncontrolled uptake of modified LDL particles, transition into foam cells. (**Figure 10**).[47]

In parallel, VSMC from the media migrate into the intima and also internalize modified LDL particles. This process induces a phenotypic switching by the loss of the common VSMC markers, such as α-smooth muscle actin, myosin heavy chain and transgrelin (TAGLN), alongside the gain of macrophage-like traits, including the expression of CD68 and Mac-2. As a result, VSMC acquire a macrophage-like cell phenotype, contributing to foam cell formation (**Figure 10**).[48] Hence, the role of VSMCs in atherosclerotic lesions has been extensively underestimated, despite their contribution to at least half of foam cell population in human coronary artery atheromas and more than one-third in murine models.[49,50]

The accumulation of foam cells within the arterial wall, along with the pro-inflammatory environment, result in the formation of fatty streaks, the earliest visible feature of atherosclerosis, and progressing to atheroma formation.

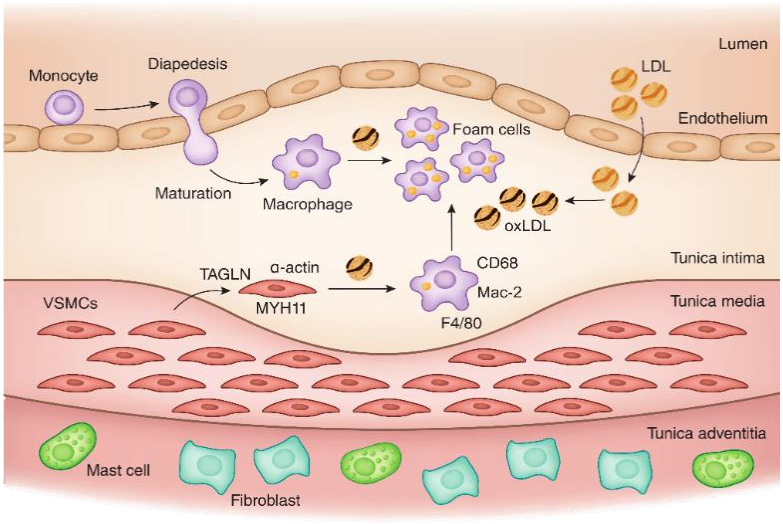

Figure 10. Sources of foam cells in atherosclerotic lesions. Foam cells originate from the uncontrolled uptake of modified LDL by macrophages and VSMC that have undergone a phenotypic switch of cell markers. oxLDL: oxidized LDL. Adapted from (Rosenfeld, 2015).[47]

Advanced lesion and rupture

Advancing to the fibrous plaque stage, foam cell death leads to the formation of a necrotic core composed of cell debris and cholesterol. This process is accompanied by the migration of VSMCs to the lesion and the secretion of large amounts of extracellular matrix, forming the fibrous cap. Acting as a protective barrier, the fibrous cap stabilizes the plaque and prevents the necrotic core from rupture. Following fibrosis, atherosclerotic plaques undergo calcification, characterized by the deposition of calcium phosphate crystals as pericytes and VSMCs differentiate into bone-like cells (**Figure 11A**).[51,52]

When the atherosclerotic plaque ruptures, it is exposed to circulating blood, triggering platelet activation. Concurrently, coagulating pathways are stimulated, resulting in thrombin production and the subsequent conversion of fibrin. Altogether, these events culminate in the formation of a thrombus within the vessel lumen, obstructing blood flow and potentially causing severe clinical complications (**Figure 11B**).[51,52]

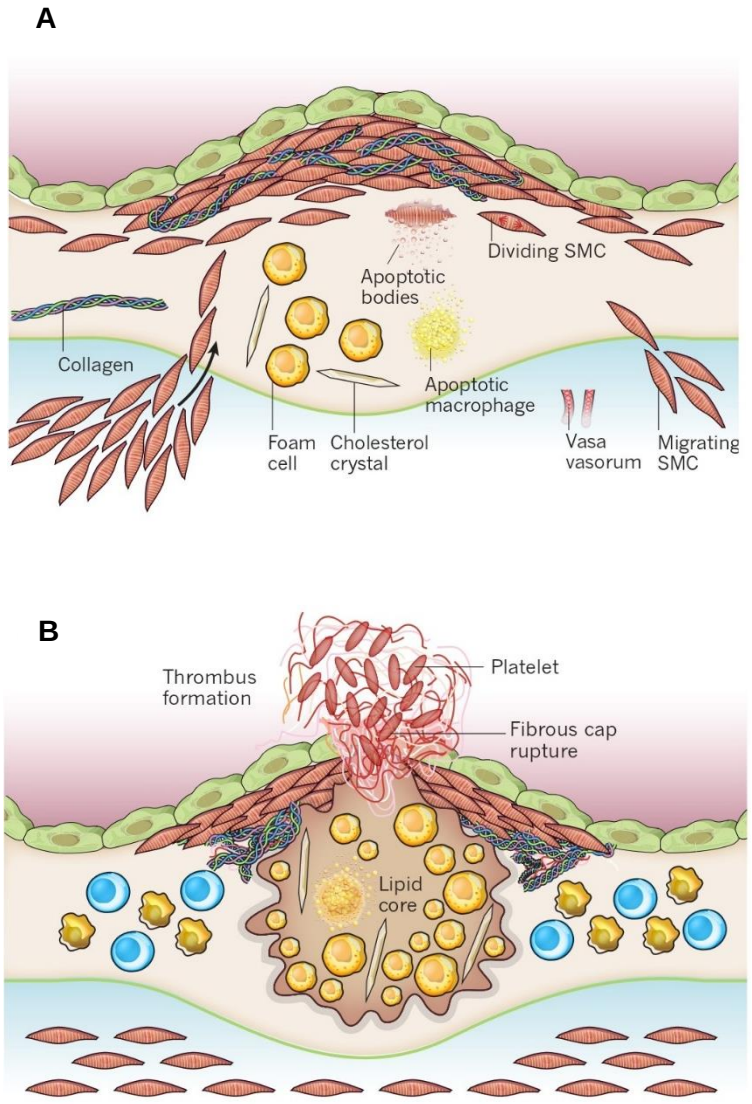

Figure 11. Advanced lesion and rupture. (A) Lesion progression involves migration and proliferation of VSMCs into the intima, forming a fibrous cap around the lipid or necrotic core, derived from dead cells**. (B)** Thrombus formation leads to rupture of the fibrous cap and subsequent coagulation, compromising blood flow. Adapted from (Libby *et al.*, 2011).[51]

3.3.Familial hypercholesterolemia

Familial hypercholesterolemia (FH) is the most common genetic form of hyperlipidemia, affecting approximately 1 in 300 individuals in the general population.[53] FH is characterized by significantly elevated plasma LDL cholesterol levels, resulting in an inherently high risk of premature coronary heart disease. Importantly, FH can present in either homozygous or heterozygous form, with the homozygous variant being significantly more severe but far less prevalent (1 to 300,000).[54]

3.3.1. Pathophysiology

FH is a monogenic disease with mostly autosomal dominant inheritance caused by mutations in the ***LDLR, APOB*** **or** ***PCSK9*** genes.

The majority of FH cases (approximately 85%) are attributed to ***LDLR*** mutations, with over 1,600 different variants identified in this gene. They can be classified based on the specific function affected, including synthesis, transport from the endoplasmic reticulum to the Golgi, binding to LDL particles, internalization by hepatocytes, and membrane recycling.[55]

Mutations in the ***APOB*** gene account for about 10% of FH cases, with the Arg3500Gln mutation being the most prevalent. This mutation leads to the production of a defective APOB100 protein at the binding site, impairing its interaction with LDLR.[55]

In contrast, ***PCSK9*** mutations are considered rare, representing less than 5% of FH cases. Notably, only severe functional deficits result in pathological mutations, which are characterized by a gain of function. Increased PCSK9 activity induces LDLR degradation, ultimately rising plasma LDL levels.[55]

Importantly, mutations in the ***LDLRAP1*** gene cause an autosomal recessive form of the disease, a rare condition affecting less than 1 in a population of one million. This form presents with a clinical severity similar to homozygous FH.[56]

3.3.2. Diagnosis

The diagnostic criteria for FH rely in four key parameters: lipid levels, family history, physical examination, and genetic analysis. Various clinical guidelines based on a scoring system that incorporates these parameters are available.[57–59]

Lipid levels, particularly LDL cholesterol levels, are essential for diagnosis. According to the European Atherosclerosis Society consensus, different scores are assigned based on LDL cholesterol concentrations, which are categorized into four groups ranging from 155 to over 325 mg/dL.

Family history is also highly relevant, especially if a family member has suffered from premature coronary heart disease. Additionally, a first-degree relative with elevated LDL cholesterol and/or tendon xanthomas increases the risk of FH diagnosis.

Physical examination is important as well, with the presence of tendon xanthomas and/or corneal arcus further increasing the risk of FH.

Finally, **genetic analysis** is a key tool for confirming FH diagnosis. The identification of a causative genetic mutation is definitive for diagnosing FH. However, the absence of a detectable mutation does not exclude its diagnosis as there seem to be polygenic forms of FH and, other forms of as yet unknown origin.

3.3.3. Treatment

Upon an FH diagnosis, both pharmacological therapy and lifestyle modifications are essential for effective disease management. Different pharmacological approaches are depicted in **Figure 12**.[60]

Since their discovery, **statins** have been the most widely used therapy for FH. Their main mechanism of action involves the inhibition of HMGCR, thereby lowering cholesterol synthesis and reducing its plasma levels. Furthermore, by reducing mevalonate production, statins exert multiple pleiotropic effects such as decreased LDL oxidation, improved endothelial function, inhibition of cholesterol

esterification, and reduced platelet aggregation.[61] Nevertheless, statins could induce in some patients different side effects, such as muscle pain and damage, elevated plasma glucose levels, and liver toxicity.[61]

Ezetimibe reduces cholesterol absorption by inhibiting the NPC1L1 protein in the intestine, which leads to reduced dietary cholesterol uptake and, consequently, lower plasma cholesterol levels. Ezetimibe is commonly used as a second-line therapy alongside statins to potentiate their cholesterol lowering effects.[62]

PCSK9 inhibitors are usually monoclonal antibodies that selectively bind circulating PCSK9, preventing its interaction with LDLR and subsequent degradation. As a result, LDLR levels at the hepatocyte membrane increase, enhancing cholesterol clearance from the blood.[63] Evolocumab and alirocumab are two monoclonal antibodies that efficiently reduce LDL cholesterol levels when used on a background of statin therapy.[64,65]

Inclisiran is a small interfering RNA that targets PCSK9 mRNA for its degradation, thereby reducing the translation of PCSK9 protein and boosting the number of LDLR at the hepatocyte membrane. Remarkably, only two doses per year are required due to its long-term effect. It is currently prescribed in combination with statins for patients who do not reach lipid targets with statins.[62]

Bempedoic acid functions as an inhibitor of ATP-citrate lyase, a key enzyme in the cholesterol biosynthesis pathway. It is administered as a prodrug and becomes selectively activated in hepatocytes, thus minimizing the risk of myotoxicity. Currently, bempedoic acid is usually prescribed in combination with other lipid-lowering therapies.[66]

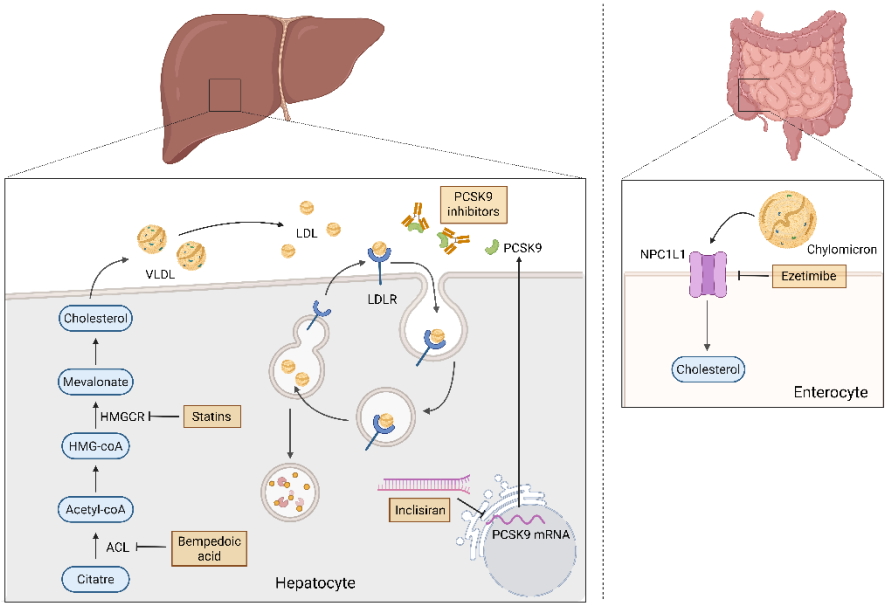

Figure 12. Therapeutic strategies for FH. Overview of various therapeutic agents used in FH, depicting their mechanism of action in the liver and intestine. Created with *Biorender.com*.

3.3.4. Genetically engineered mouse models

The development of genetically modified mice has been instrumental in advancing the study of FH. Particularly, **LDLR-deficient mice** have served as a valuable model for investigating the pathophysiology of the disease and for identifying potential therapeutic targets.

Homozygous LDLR-knockout (LDLR-/-) mice exhibit markedly elevated plasma cholesterol levels due to the impaired clearance of circulating LDL, with cholesterol concentrations reaching extremely high levels when animals are fed a high-fat diet. Moreover, this hypercholesterolemic state is accompanied by the formation of massive atherosclerotic lesions, especially in the aortic root and aortic valves, establishing these mice as a robust model for atherosclerosis research.[67]

Heterozygous LDLR-deficient (LDLR+/-) mice display a moderate increase in plasma cholesterol levels, as the remaining LDLR expression retains partial functionality and enables residual LDL clearance.

LDLR−/−APOBEC1−/− mice lack both the LDLR and the APOBEC1 enzyme. This causes very high levels of mouse APOB100 and LDL-cholesterol in their blood, leading to severe atherosclerosis.

Human APOB100 transgenic mice represent a knock-in model carrying the human *APOB100* gene, serving as a pivotal model for the comprehensive study of LDL metabolism. These mice exhibit elevated levels of LDL despite normal expression of LDLR, highlighting the role of APOB100 in lipoprotein homeostasis. Moreover, when crossed with LDLR-deficient mouse, they produce a more humanized and severe model of homozygous FH by combining defective LDL clearance with human-like lipoprotein profiles.[68,69]

4. ALZHEIMER'S DISEASE

Alzheimer's disease (AD) is the most common form of dementia, accounting for 60 to 80% of all cases. Currently, over 55 million people worldwide suffer from dementia, and this number is projected to triple by 2050.[70] AD is a neurodegenerative disorder characterized by progressive mental and cognitive decline, leading to difficulties in communication and reasoning, memory loss, and, ultimately, complete dependence.[71]

Ageing is the strongest non-modifiable risk factor for AD, with a prevalence of 3% between ages 65 and 75, increasing to 17% between 75 and 84, and peaking at 32% in those over 85. Other non-modifiable risk factors include sex, race and genetics.[72] Regarding modifiable risk factors, unhealthy lifestyle factors, head injuries, and metabolic and vascular diseases, including HF, atherosclerosis, hypertension, obesity, smoking and diabetes, have been linked to an increased risk of AD onset.[71,73]

4.1.Pathophysiology

Histologically, AD is defined by the abnormal accumulation of extracellular amyloid beta (Aβ) forming **amyloid plaques**, and intracellular hyperphosphorylated Tau filaments forming **neurofibrillary tangles** in neurons.

4.1.1. Aβ pathology

Aβ is a peptide produced by the cleavage of the amyloid precursor protein (APP), a transmembrane protein processed by three different proteases: α-, β- and γ-secretases. Depending on the secretase involved and the number of cleavages, APP undergoes either the non-amyloidogenic or the amyloidogenic pathway **(Figure 13).** In the **non-amyloidogenic pathway**, APP is first cleaved by α-secretase, generating a soluble APPα fragment, and then by γ-secretase, producing short, non-plaque forming derivatives. Conversely, the **amyloidogenic pathway**, is initiated by β-secretase cleavage, releasing a soluble APPβ fragment, followed

by γ-secretase cleavage, which produces $A\beta_{38-42}$ monomers. Among these, $A\beta_{42}$ is particularly insoluble and prone to forming toxic oligomers, which eventually aggregate into amyloid plaques that are deposited in the brain.[74,75]

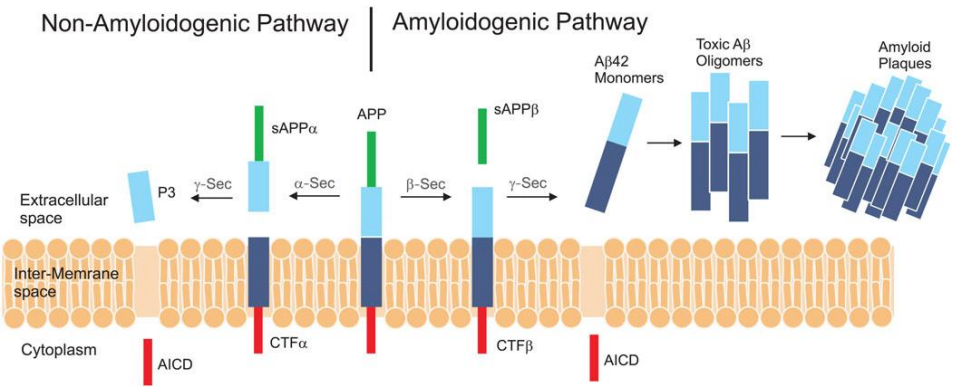

Figure 13. Schematic representation of APP processing pathways. APP can be processed via the non-amyloidogenic or the amyloidogenic pathway. The amyloidogenic pathway leads to the production of Aβ oligomers, which aggregate and form amyloid plaques. Extracted from (Bachurin *et al.*, 2017).[75]

Various factors regulate secretase activity. Noteworthy, γ-secretase is regulated by presenilin 1 (PSEN1) and 2 (PSEN2), and their disruption results in γ-secretase dysfunction, increasing Aβ oligomers production.[76]

In AD excessive accumulation of insoluble Aβ monomers, and their product, amyloid plaques, accumulate extracellularly, and are believed to negatively impact neuronal function. Therefore, various hypotheses support the idea that Aβ overproduction and aggregation play a central role in the initiation and progression of the disease.[76] Certainly, familial forms of AD, which represent approximately 1% of cases, are caused by mutations in the *APP*, *PSEN1*, and *PSEN2* genes.[77,78]

4.1.2. Tau pathology

Tau is a microtubule-associated protein primarily located in neuronal axons. It plays a crucial role in microtubule stabilization as well as in axonal transport,

synaptic plasticity, and cell signaling. Tau undergoes different post-transcriptional modifications such as phosphorylation, acetylation, and methylation. Notably, phosphorylation is essential for its normal function; however, excessive and uncontrolled phosphorylation leads to the formation of hyperphosphorylated Tau, which aggregates and precipitates into **neurofibrillary tangles**.[79]

Elevated Tau levels, alongside with neurofibrillary tangles, are a hallmark of AD and have been shown to compromise microtubule assembly, axonal transport, and synaptic function. Nonetheless, Tau pathology in AD patients is usually accompanied by the presence of Aβ plaques, thus indicating that Tau may not be the main trigger of the disease.[80]

Altogether, Aβ and Tau pathologies disrupt brain homeostasis by contributing to neuronal loss, microglia activation, neuroinflammation, mitochondrial dysfunction, and impaired calcium metabolism.[80] These pathological processes begin years before the clinical onset of AD, providing a critical window for early diagnosis and therapeutic intervention.

4.1.3. APOE and genetic risk factors

Sporadic or late-onset AD is the most common form of the disease, prompting genome-wide association studies to identify genetic risk factors.

Several AD-associated genes involved in neural-immune system, synaptic activity, endocytosis, and lipid metabolism pathways have been identified. Importantly, cholesterol metabolism-related AD-risk genes include *APOE, APOJ, ABCA7, ABCG1* and *SREBP2*.[81–83] Among these, APOE is the only gene with a significant association with Aβ or Tau pathologies.[84]

In this regard, the link between **APOE-ε4 allele** and AD prevalence was established over three decades ago, making it the most robust and reproducible genetic risk factor for late-onset AD.[85,86] Recently, APOE-ε4 homozygosity has been recognized as a distinct genetic form of AD.[87] The APOE4 isoform has been

associated to impaired Aβ clearance while promoting Aβ production, aggregation and deposition. Furthermore, APOE4 has been reported to enhance Tau phosphorylation. Regarding lipid metabolism, different studies have shown that APOE4 is associated with reduced lipid binding, alongside increased cholesterol synthesis and accumulation, oxidative stress and lipid peroxidation.[38] Nonetheless, APOE4 has not been thoroughly investigated in the context of cholesterol transport mediated by CNS lipoproteins.

4.2.Diagnosis

In the recent years, the diagnostic paradigm for AD has undergone a fundamental shift from a clinical, symptom-based to a biologically defined diagnosis This evolution reflects growing evidence that AD pathology begins many years before the appearance of cognitive symptoms. Hence, current diagnostic criteria emphasize the identification of underlying biological changes using validated biomarkers, which enable earlier detection and the potential of preclinical intervention.[88]

Historically, imaging techniques such as magnetic resonance imaging (MRI) and Fluorodeoxyglucose-positive emission tomography (FDG-PET) were primary to identifying brain atrophy and reduced brain metabolism, markers of neurodegeneration. Additionally, CSF collection via lumbar puncture and analysis was pivotal in confirming AD pathology through the detection of amyloid and Tau alterations.[89,90]

More recently, advances in the understanding of AD pathophysiology and the emergence of blood-based biomarkers have transformed the diagnostic landscape. The current biomarker system is divided into two classes:

Core 1 biomarkers, which include, amongst others, **amyloid PET, CSF $A\beta_{42}/A\beta_{40}$ ratio,** and **plasma phosphorylated Tau (p-Tau) 217**. Abnormalities in any of these are sufficient to establish a biological diagnosis of AD.

Core 2 biomarkers, which include, amongst others, **Tau PET,** and **other CSF p-Tau and total-Tau (t-Tau) forms.** These biomarkers primarily inform about disease staging.[88]

It is important to note that, biomarker testing in cognitively normal individuals is currently limited to research settings. Nonetheless, the incorporation of biomarker-based criteria into clinical practice underscores a broader movement toward precision medicine in neurodegenerative diseases, which may allow testing on asymptomatic individuals in the near future.[88]

4.3.Treatment

The therapeutic landscape of AD has evolved significantly thanks to the approval of monoclonal antibodies that target Aβ peptides. These anti-amyloid immunotherapies aim to slow disease progression by promoting the clearance of toxic Aβ species from the brain. Aducanumab and lecanemab represent the first disease-modifying therapies approved for the treatment of early-stage AD.[91]

Aducanumab is a human IgG1 monoclonal antibody that targets Aβ aggregates, including both oligomers and fibrils. It received approval by FDA in June 2021, based on its demonstrated ability to reduce amyloid plaque burden. However, due to controversial clinical efficacy, its clinical use is restricted.[91]

Lecanemab is also a human IgG1 monoclonal antibody that preferentially binds to soluble Aβ protofibrils, which are especially neurotoxic. Lecanemab was approved in January 2023, and it showed more robust clinical results and a more favorable safety profile, making it the most promising therapy to date.[91]

Despite these advances, symptomatic management remains an essential component of AD care. Pharmacological treatment of cognitive and symptoms mainly target neurotransmitter disturbances through monotherapy or combination therapy using **cholinesterase inhibitors** (donepezil, rivastigmine, galantamine), or **glutaminergic regulation** via the NMDA receptor antagonist memantine.[92]

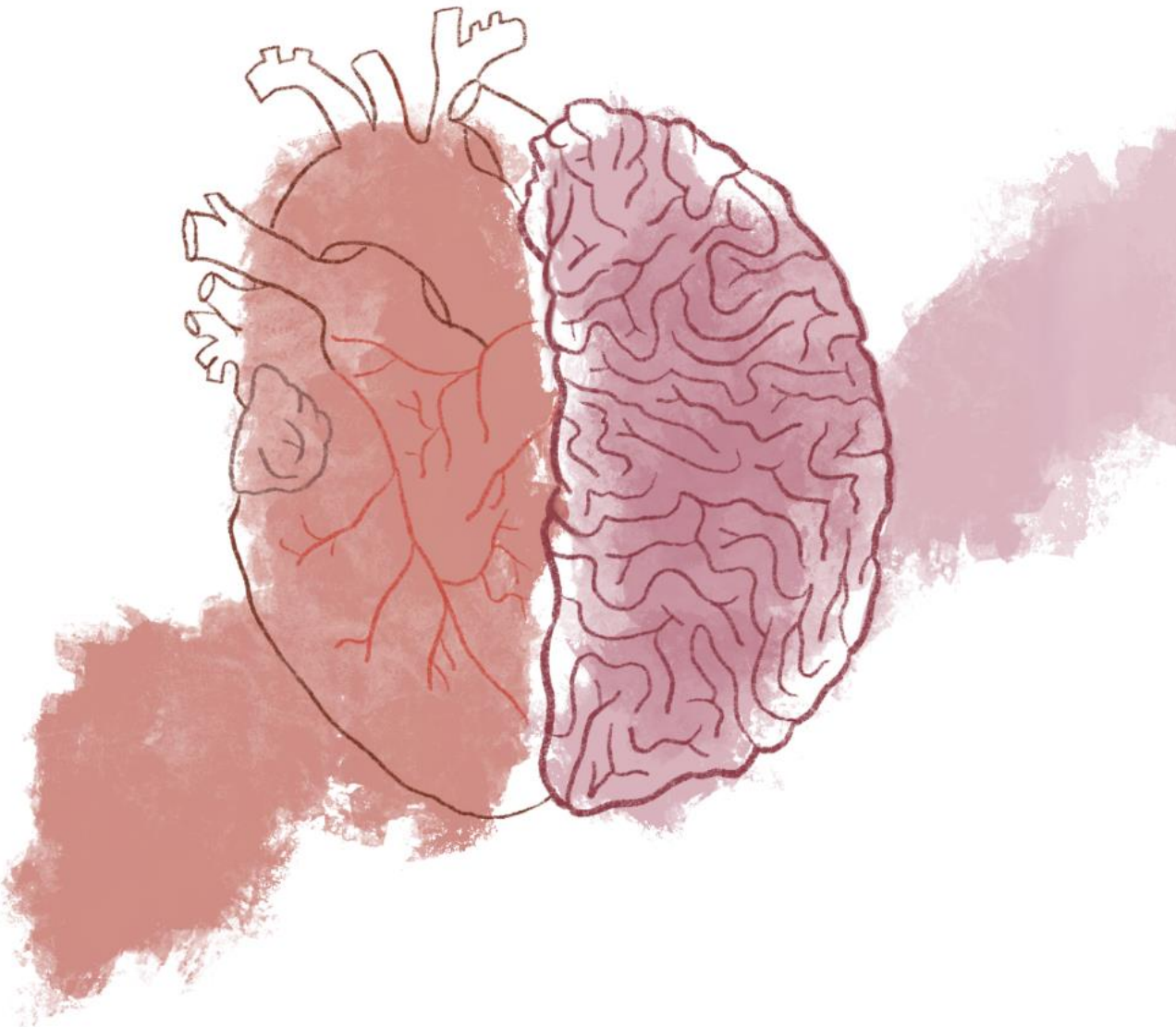

CHAPTER II

HYPOTHESES AND OBJECTIVES

This thesis aimed to investigate key mechanisms of cholesterol transport in the contexts of CVD and AD, structured into three interconnected works.

Work 1: PCSK9 Inhibition and Cholesterol Efflux in FH

Heterozygous FH subjects show reduced cholesterol efflux from macrophages to plasma compared to normolipidemic individuals. We hypothesize that PCSK9 inhibition therapy can restore the cholesterol efflux capacity of macrophages exposed to heterozygous FH plasma and normalize the overall macrophage-specific RCT capacity in an FH mouse model.

Objectives:

- To quantify macrophage cholesterol efflux to plasma obtained from FH patients before and after PCSK9 inhibitor treatment.
- To analyze the redistribution of macrophage-derived cholesterol among lipoprotein subclasses following PCSK9 inhibition.
- To assess the impact of PCSK9 antibody treatment on macrophage-specific RCT in a mouse model of FH.

Work 2: Cholesterol Efflux from VSMCs in Atherogenesis

Macrophages have traditionally been considered the primary contributors to foam cell formation, however, growing evidence suggests that VSMCs play a significant role in plaque development. We hypothesize that cholesterol efflux is impaired in VSMCs undergoing foam cell transformation, and that this impairment can be reversed by activating LXR or inhibiting ACAT, thereby restoring their RCT capacity.

Objectives:

- To evaluate the ability of various cholesterol acceptors to promote cholesterol efflux from VSMCs before and after foam cell induction via methyl-β-cyclodextrin (MBD)-cholesterol loading.
- To investigate the effect of LXR activation on the overall RCT rate from VSMCs to feces in vivo.
- To determine whether ACAT inhibition restores cholesterol efflux capacity and the overall RCT rate in VSMC-derived foam cells.
- To assess whether the combination of LXR activation and ACAT inhibition produces a synergistic effect on cholesterol efflux and the overall RCT rate in VSMC-derived foam cells.

Work 3: CSF-Mediated Cholesterol Transport in AD

We hypothesize that CSF from AD patients exhibits impaired cholesterol transport between astrocytes and neurons, potentially due to altered function of APOE4-containing HDL-like particles.

Objectives:

- To compare CSF-mediated cholesterol efflux from astrocytes using CSF samples from control subjects and AD patients under baseline conditions and following ABCA1 and ABCG1 activation.
- To determine CSF-mediated cholesterol uptake by neurons using CSF samples from control subjects and AD patients and whether it is influenced by Aβ peptide or tau protein.
- To synthesize reconstituted HDL (rHDL) nanoparticles containing either APOE3 or APOE4, and assess the impact of APOE isoforms on cholesterol transport between astrocytes and neurons.

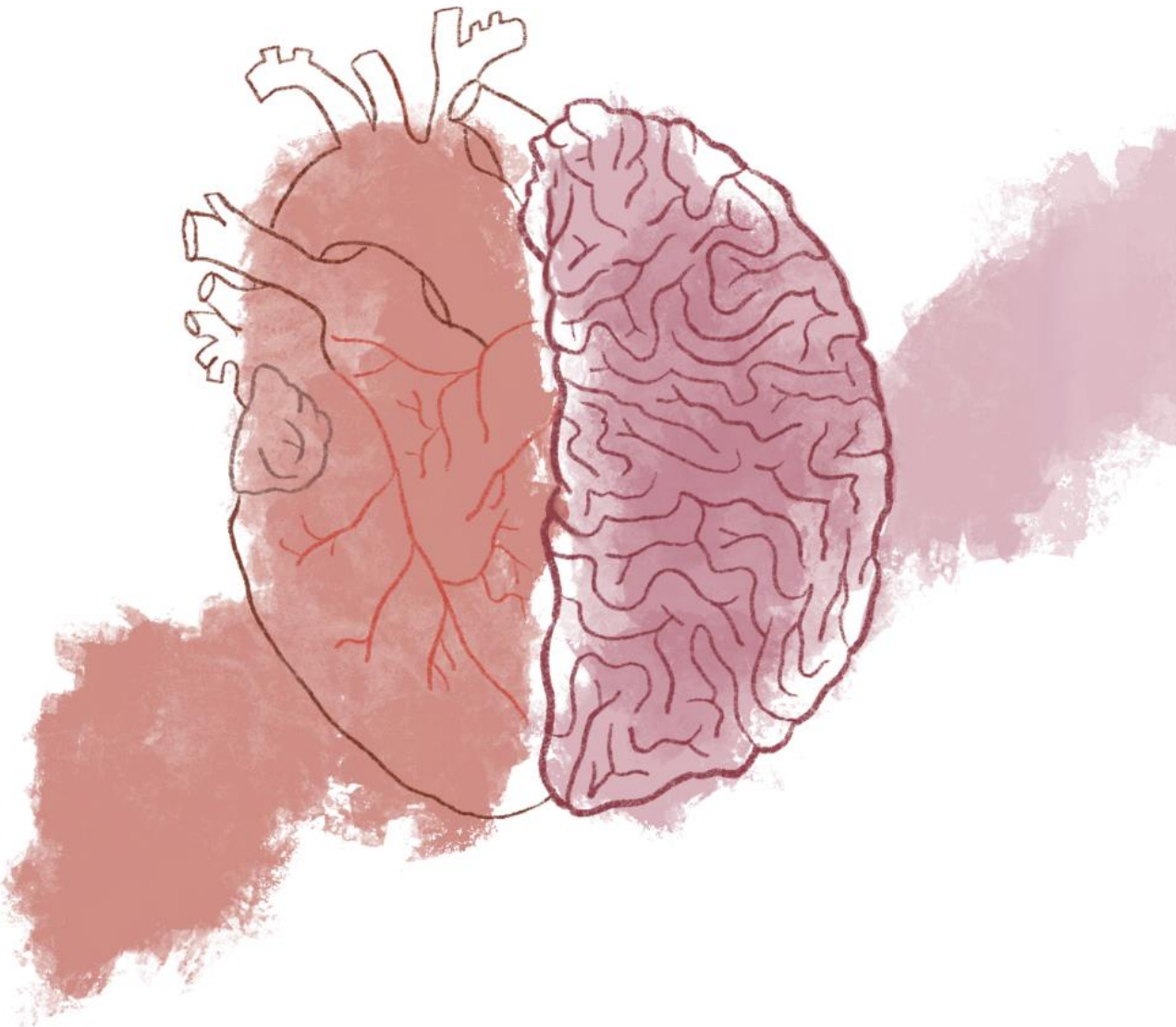

CHAPTER III

MATERIALS AND METHODS

This section is divided into three parts, each describing the specific methods used in the corresponding work. Importantly, while each work required specific approaches, common methodologies were employed to address the different research objectives. In particular, all three works share core techniques for investigating cholesterol transport both *in vitro* and *in vivo*, applied to different cellular and mouse models relevant to CVD and AD, respectively.

METHODOLOGY FOR WORK 1

1. Human samples and analysis

1.1. Plasma samples

The study included plasma samples from 14 adult patients with FH collected before and after treatment with a PCSK9 inhibitor at Hospital Universitario Ramón y Cajal (Madrid, Spain). All subjects initiated PCSK9 inhibition therapy due to LDL-cholesterol levels remaining above recommended targets despite receiving high-intensity statin therapy combined with ezetimibe.[57] The patients were treated with 140 mg of evolocumab (Amgen, Thousand Oaks, CA) administered every 14 days, with an average interval of 49 days between baseline and post-treatment sample collection. Additionally, pooled plasma samples from normolipidemic donors were obtained at Hospital de la Santa Creu i Sant Pau.

The study was conducted in accordance with the ethical principles outlined in the Declaration of Helsinki and was approved by the Ethical and Clinical Investigation Committee of Hospital Universitario Ramón y Cajal and of Hospital de la Santa Creu i Sant Pau (protocol codes C-GEN-007 and IIBS-APO-2013-105).

1.2. Lipid-related parameters analysis

Plasma total cholesterol, HDL-cholesterol, triglycerides, APOA1 and APOB were measured using the COBAS 6000/501c autoanalyzer (Roche Diagnostics, Basel, Switzerland). Cholesterol (3039773190) and triglycerides (20767107322) were determined by enzymatic assays, whereas APOA1 (3032566122) and APOB (3032574122) concentrations were quantified using immunoturbidimetric assays (all reagents from Roche Diagnostics). Since all samples had triglyceride levels below 4.5 mmol/L, LDL-cholesterol was calculated using the Friedewald equation:[93]

$$LDL\ cholesterol = Total\ cholesterol - HDL\ cholesterol - \frac{Triglycerides}{5}$$

PLTP activity was measured using a commercial assay kit that detects the transfer of a fluorescent substrate from a donor particle in the presence of plasma samples (Merck, Darmstadt, Germany). CETP activity was assessed with a CETP assay kit (Merck), which measures the CETP-mediated transfer of a neutral fluorescent lipid from a substrate to a physiological acceptor, independently of endogenous plasma lipoprotein concentrations. LCAT activity was determined using a fluorometric method that evaluates phospholipase activities (Merck).

1.3. Lipoprotein isolation by ultracentrifugation

Plasma lipoproteins were isolated by sequential ultracentrifugation based on their different density ranges: VLDL (≤ 1.006 g/mL), LDL (1.019-1.063 g/mL) and HDL (1.063-1.210 g/mL). Fresh samples were subjected to stepwise density adjustments using potassium bromide (KBr), followed by ultracentrifugation in a fixed-angle rotor (50.3, Beckman Coulter, Fullerton, CA) at 100,000 x g for 24 hours at 4ºC.

Plasma was initially adjusted to a density of 1.006 g/mL using a density buffer composed of 0.05 g/L chloramphenicol, 8.75 g/L sodium chloride, 0.37 g/L EDTA (all from Merck), and 0.08 g/L gentamicin (Laboratorios Normon, Madrid, Spain). Subsequent density adjustments were made using KBr solutions prepared from the 1.006 g/mL stock, according to Radding and Steinberg's equation:[94]

$$grams\ of\ KBr = \frac{Volume\ x\ (final\ density - initial\ density)}{1 - (0.312\ x\ final\ density)}$$

Isolation steps were performed as follows:

- **VLDL:** The plasma sample was adjusted to a 1.006 g/mL, and centrifuged. The upper layer (≤ 1.006 g/mL), containing the VLDL fraction, was carefully collected.

- **LDL:** The infranatant from the previous step was adjusted to a density of 1.063 g/mL and centrifuged. The resulting upper layer (1.006–1.063 g/mL), corresponding to the LDL fraction, was collected.
- **HDL**: The remaining infranatant was then adjusted to 1.210 g/mL and centrifuged. The upper layer (1.063–1.210 g/mL) was recovered as the HDL fraction.
- **Lipoprotein-depleted fraction** (**LPDF)**: The final infranatant (> 1.210 g/mL), representing the LPDF, was collected.

Alternatively, ultracentrifugation can be performed in two single steps to isolate a specific lipoprotein fraction. This is achieved by first discarding lipoproteins with lower densities and then adjusting the infranatant to the target density for the desired lipoprotein fraction.

Importantly, when isolated lipoproteins were used in experimental procedures, KBr was removed by desalting through PD-10 column (Merck) using phosphate-buffered saline (PBS) as the elution buffer.

1.4. APOB-depleted plasma

HDL and LPDF can be obtained more rapidly and with smaller sample volumes by removing all APOB-containing lipoproteins. For APOB-depleted plasma preparation, samples were mixed with 0.44 mmol/L phosphotungstic acid and 20 mmol/L magnesium chloride (both from Merck), then centrifuged at 10,500 x *g* for 2 minutes and the resulting supernatant contained HDL fraction and LPDF.

2. Cell culture model

J774A1.1 mouse macrophages (TIB67™, ATCC®, Manassas, VA) were cultured in Dulbecco's Modified Eagle's Medium (DMEM) high glucose with L-glutamine and with sodium pyruvate (Corning, Corning, NY) supplemented with 10% fetal bovine serum (FBS, Pan Biotech, Aidenbach, Germany) and 100 U/mL

penicillin/streptomycin (Dominique Dutscher, Brumath, France). The cells were maintained in 75 cm^2 cell culture flasks and incubated at 37ºC in a humidified atmosphere containing 5% CO_2. The culture medium was replaced every 48 hours, and cells were scrapped when they reached confluence.

3. *In vitro* cholesterol transport study

3.1. Macrophage-derived cholesterol efflux

In vitro and *ex vivo* cellular cholesterol efflux was evaluated using a radiochemical method (**Figure 14**).[95] Macrophages were seeded at a density of 2 x 10^5 cells/well in 6-well plates and allowed to grow for 72 hours in complete medium. Subsequently, the radiolabelling step was performed by incubating the cells with DMEM containing 1 µCi/well of [1α,2α(n)-^{3}H]cholesterol (Revvity, Waltham, MA) and 5% FBS for 48 h. After labelling, the macrophages were equilibrated overnight in DMEM supplemented with 0.2% free fatty acid bovine serum albumin (BSA, Merck). The following day, cholesterol efflux was initiated by incubating the cells for 4 hours with various cholesterol acceptors added to the medium.

For *in vitro* assays, cholesterol acceptors included pooled plasma samples from normolipidemic individuals (2.5%, v/v) and mature HDL isolated from the same pool (25 µg/mL of APOA1). LDL, also isolated from the same pool, was added at different concentrations ranging from 0 to 25 µg/mL of APOB. HDL and LDL were prepared by sequential ultracentrifugation as described in **section 1.3, Work 1**.

For *ex vivo* assays, cholesterol acceptors consisted of plasma from FH patients collected before and after treatment with evolocumab (see **section 1.1, Work 1**). Plasma or APOB-depleted plasma (see **section 1.4, Work 1**) was added at a concentration of 2.5% (v/v) of the original sample volume, corresponding to 25 µL for plasma and 75 µL for APOB-depleted plasma (equivalent to the lipoprotein-depleted fraction derived from 25 µL of plasma).

After the 4 hour-incubation, the medium was collected and centrifuged at 250 x *g* for 5 minutes to remove non-adherent cells. The adherent cell layer was lysed with 0.1 mol/L NaOH (Merck), followed by incubation with gentle agitation for 48 hours at 4ºC. Lysates were then collected and sonicated for at least 1 hour. Both medium and cell fractions were mixed with 4 mL of scintillation fluid (Ultima Gold™ F, Revvity) in 20 mL Super Polyethylene Vials (Revvity), and [^{3}H]cholesterol radioactivity was quantified in counts per minute (cpm) with an LS 6500 Multi-purpose Scintillation Counter (247971-G, Beckman Coulter, Brea, CA).

Cholesterol efflux (%) was calculated as follows:

$$\text{Cholesterol efflux (\%)} = \frac{[^3\text{H}]\text{cholesterol in the medium}}{\text{Total } [^3\text{H}]\text{cholesterol (medium + cells)}} x\ 100$$

To further assess cholesterol distribution, lipoprotein fractions (VLDL, LDL, HDL and LPDF) were isolated from the efflux medium by sequential ultracentrifugation (see **section 1.3, Work 1**), and the associated radioactivity was measured to determine the proportion of macrophage-derived cholesterol present in each fraction.

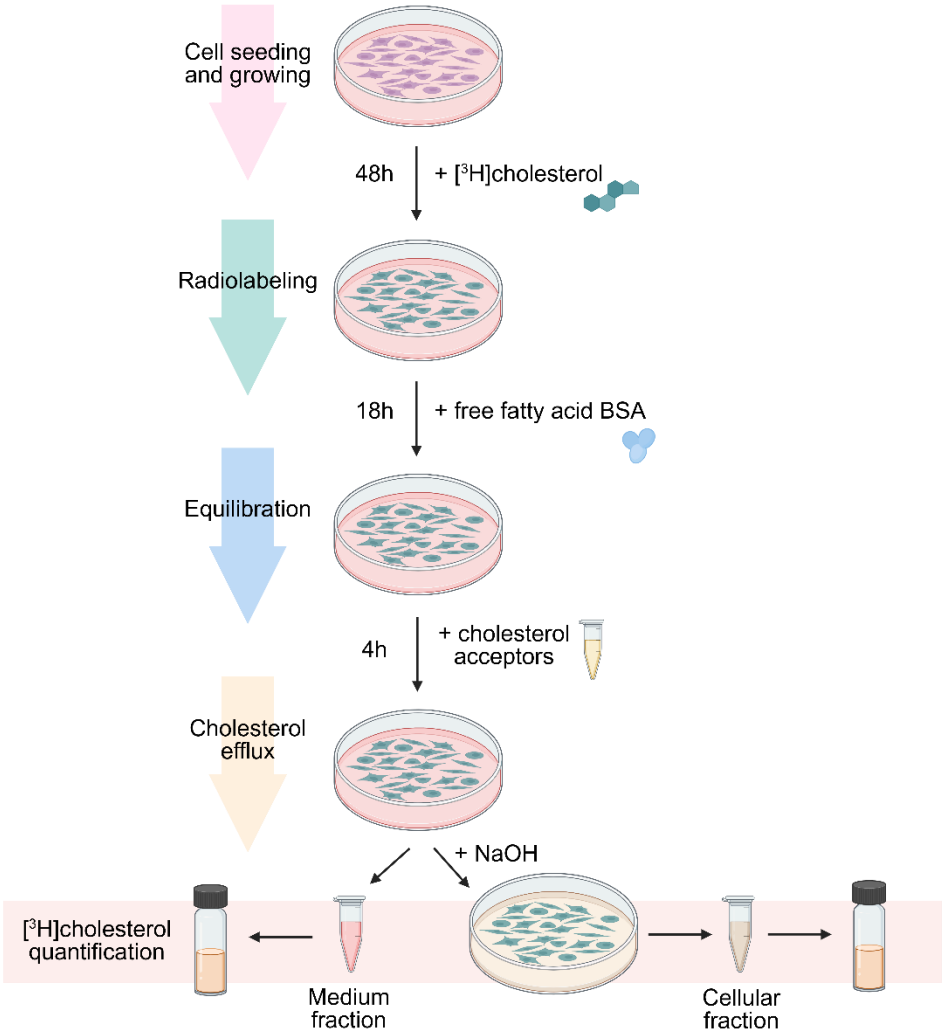

Figure 14. Schematic representation of the cholesterol efflux assay. Cells are first seeded and cultured under standard conditions. Radiolabeling is then performed by incubating the cells with [^{3}H]cholesterol for 48 hours. Following this, an equilibration step is conducted overnight using medium supplemented with fatty acid-free BSA. The next day, cholesterol acceptors are added for a 4 hour-incubation. Subsequently, the medium is collected, and NaOH is added to lyse the adherent cells. Finally, [^{3}H]cholesterol in both medium and cellular is quantified by liquid scintillation counting. Created with *Biorender.com*.

4. Mouse models, treatments and sample analysis

4.1. Mouse models

For the *in vivo* studies, wild-type (LDLR+/+) mice (#000664, Jackson Laboratories, Bar Harbor, ME), LDLR-deficient (LDLR−/−) mice (#002207, Jackson Laboratories) and human APOB100 transgenic (LDLR+/+ hAPOB100) mice (#1004-M, Taconic Biosciences, Rensselaer, NY), all on a C57BL/6 background, were obtained. To generate heterozygous LDLR-deficient mice expressing human APOB100 (LDLR+/− hAPOB100), LDLR−/− mice were crossed with hAPOB100 transgenics. Genotyping was performed via PCR on genomic DNA extracted from tail tips using *Ldlr*-specific primers (Jackson Laboratories) and the presence of the hAPOB100 transgene was confirmed by measuring serum human APOB levels.

Mice were housed under standard conditions (22 °C, 12-hour light/dark cycle) with *ad libitum* access to food and water. Both male and female mice aged 8–10 weeks were used in the experiments.

All procedures were reviewed and approved by the Institutional Animal Care and Use Committee of the Sant Pau Research Institute and authorized by the Animal Experimental Committee of the local government authority (Generalitat de Catalunya, authorization number 10626) in accordance with the Spanish Law (RD 53/2013) and European Directive 2010/63/EU. All procedures were conducted at the Animal Experimentation Service, certified under ISO 9001:2015 standards.

Throughout all experiments, mice of the same genotype and age were randomly assigned to groups to ensure equal sample sizes, and all animals were included in the analyses. Whenever feasible, experiments were conducted in a blinded fashion with respect to sample origin to minimize bias.

4.2. Diet and treatment

Mice were fed a Western-type diet (TD.88137, Harlan Teklad, Madison, WI), which contains 21% fat and 0.2% cholesterol, for a period of four weeks. Concurrently, mice received weekly intraperitoneal injections of either 10mg/kg of the PCSK9 recombinant antibody PL-45134 (clone mAb1) or a vehicle solution (PBS). The recombinant antibody PL-45134, provided by Amgen has been reported to act as an efficient antagonist of mouse PCSK9 function.[96]

4.3. Lipid-related parameters analysis

Serum total cholesterol, triglycerides, HDL-cholesterol, human APOB, and the activities of PLTP and LCAT were assessed as described in **section 1.2, Work 1.** HDL-cholesterol was specifically measured in APOB-depleted serum. To analyze cholesterol distribution across lipoprotein classes, VLDL, LDL, HDL, and LPDF fractions were isolated by sequential ultracentrifugation (see **section 1.4, Work 1**), and cholesterol concentrations within each fraction were subsequently quantified.

4.4. Western Blot analysis

Hepatic LDLR expression was assessed by Western Blotting. Liver tissues were lysed in RIPA buffer (50 mmol/L Tris-HCl, pH 7.5; 150 mmol/L NaCl; 1% NP40; 0.5% sodium deoxycholate; 0.1% SDS; 1 mmol/L EDTA) supplemented with protease inhibitor cocktail (Roche Diagnostics), phenylmethylsulfonyl fluoride (Merck) and sodium orthovanadate (Merck). Lysates were centrifuged at 12,000 x *g* for 15 minutes at 4ºC, and the supernatants were collected. Protein concentrations were determined using a BCA Protein Assay Kit (Thermo Fisher Scientific).

Protein extracts were mixed with a 4x Laemmli loading buffer (Thermo Fisher Scientific), heated at 95 ºC for 5 minutes, and 20 µg of protein per sample were resolved on 10% TGX Stain-Free precast gel (Bio-Rad) Following SDS-PAGE,

proteins were transferred onto 0.2 µm PVDF membranes (Bio-Rad), which were then blocked with 3% non-fat dried milk in Tris-buffered saline with 0.05% Tween-20 (TBST) for 15 minutes and incubated overnight at 4 °C with a Rabbit Anti-Mouse LDLR primary antibody (ab52818, Abcam, Cambridge, United Kingdom) at a 1:200 dilution. After three 10-minute washes with TBST, membranes were incubated for 1 hour with Anti-Rabbit IgG (H+L), HRP Conjugate, secondary antibody (W4011, Promega) at a 1:2000 dilution. Following three additional TBST washes, signal detection was performed using the Immun-Star™ Western Chemiluminescence Kit (Bio-Rad). TGX Stain-Free gels were activated post-electrophoresis for 1 minute. Images were acquired using the ChemiDoc XRS imaging system (Bio-Rad) and analyzed with Image Lab software (version 6.0.1, Bio-Rad). Band intensities were normalized to total protein using stain-free gel images as loading controls.[97,98]

5. *In vivo* cholesterol transport studies

5.1. Macrophage-specific RCT assay

A schematic representation of the RCT assay[95] is depicted in **Figure 15**.

J774A.1 macrophages were cultured in 75 cm^2 culture plates in complete medium for 72 hours. Cells were then labeled with 5 µCi/mL of [1α,2α(n)-^{3}H]cholesterol for 48 hours. After labeling, macrophages were washed and equilibrated overnight in medium containing 0.2% fatty acid–free BSA. Subsequently, cells were detached by scraping, resuspended in PBS, and pooled before intraperitoneal injection into mice (average of 1.7 x 10^6 macrophages containing 1.7 x 10^6 cpm per mouse; cell viability was 85%, assessed by trypan blue exclusion).

Following injection, mice were individually housed, and feces were collected over the next 48 hours. At the endpoint, mice were euthanized by cardiac puncture, and livers were harvested. Total serum [^{3}H]cholesterol radioactivity was quantified, and both APOB-depleted serum and the LDL fraction were isolated for [^{3}H]cholesterol measurement using liquid scintillation counting. Lipids were

extracted from liver and fecal samples by adding 10 mL of hexane-isopropanol (3:2, v/v, Merck) and incubating the mixture overnight. The following day, the extract was collected, and 3 mL of 0.5 mol/L sodium sulfate (Merck) were added. The mixture was gently mixed for 10 minutes and then centrifuged at 1,000 x *g* for 10 minutes, to separate the hexane and the isopropanol in two layers. The upper hexane layer containing lipids was collected, evaporated at room temperature and resuspended in 4 mL of scintillation liquid to quantify the [^{3}H]cholesterol content in the organic phase. The aqueous phase of fecal extracts was also evaporated, resuspended in 4 mL of scintillation liquid and used to determine [^{3}H]-labeled bile acid content. The [^{3}H]tracer detected in fecal bile acids was combined with the [^{3}H]cholesterol detected in feces to determine total fecal [^{3}H]tracer. Results were expressed as the percentage of the injected radioactive dose recovered in each compartment.

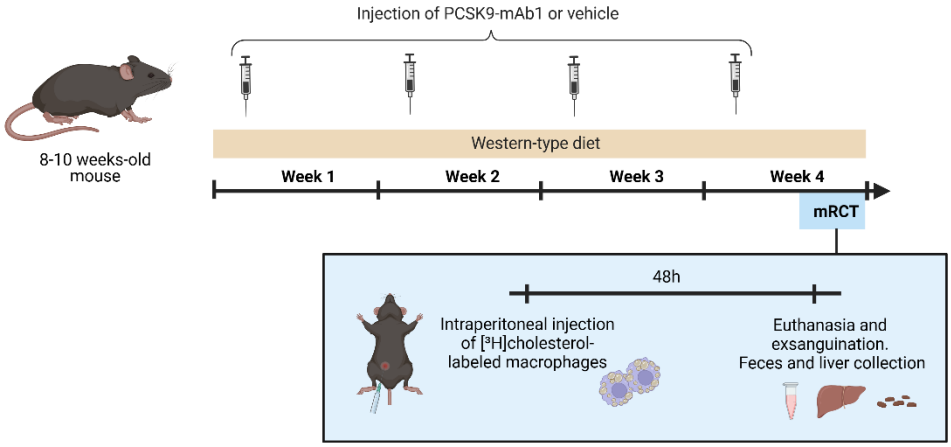

Figure 15. Schematic representation of macrophage-to-feces RCT assay. Eight-to-ten-week-old mice were injected with the PCSK9-mAb1 or the vehicle every 7 days and fed a Western-type diet for 4 weeks. Forty-eight hours before the end of the experiment, mice were intraperitoneally injected with J774A.1 macrophages loaded with [^{3}H]cholesterol and housed in individual cages. At the end of the experiment, mice were euthanized and exsanguinated via cardiac puncture, their livers were removed, and individual feces were collected. Created with *Biorender.com*.

5.2. HDL and LDL kinetics

A schematic representation of the kinetic assay[99] is shown in **Figure 16.**

For lipoprotein preparation, LDL and HDL fractions from pooled serum from LDLR+/− hAPOB100 mice were isolated by sequential ultracentrifugation as described in **section 1.3, Work 1**. Lipoprotein radiolabeling was performed by mixing 50 µL of 1µCi/µL cholesteryl-[1,2-^{3}H(N)] oleate solution (Revvity) and 1.8 mg of L-α-phosphatidylcholine from egg yolk (Merck), and the solvent was evaporated under a nitrogen stream. Two mL of 1.006 g/mL density buffer were added to the dried lipids, which were then resuspended by vortexing and sonicating for 10 minutes. The resulting [1,2-^{3}H(N)]cholesteryl oleate emulsion was mixed with 2 mL of isolated LDL or HDL, and 2 mL of non-inactivated human LPDF, serving as a source of CETP. The mixture was incubated for 18 hours at 37 ºC. Radiolabeled LDL and HDL were subsequently reisolated by ultracentrifugation and desalted as described in **section 1.3, Work 1**. Electrophoretic mobilities matched that of native lipoproteins, and more than 75% of the radioactivity was confirmed to be incorporated into LDL or HDL.

Each mouse received an intravenous injection of either radiolabeled LDL or HDL (400,000 cpm) in 0.1 mL of 0.9% NaCl via the retro-orbital venous plexus. Mice were then individually housed for fecal collection over the subsequent 48 h. Blood samples were collected at 2 minutes and 2, 6, 24 and 48 hours post-injection. At the endpoint, mice were euthanized by cardiac puncture, and livers were harvested. Radioactivity in serum, liver and feces was measured and expressed as previously described (**section 5.1, Work 1**). Serum decay curves were fitted on an exponential model, the fractional catabolic rate was calculated as the reciprocal area under the curve, and expressed as pools/hour.

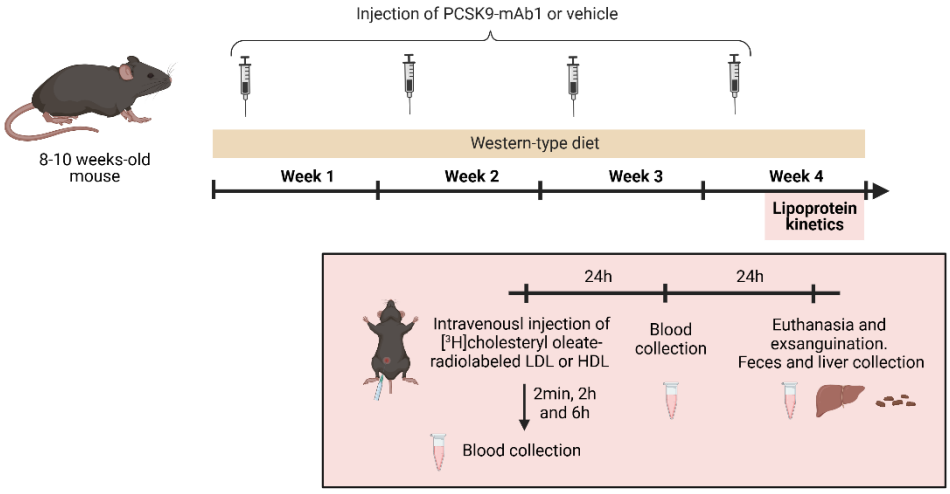

Figure 16. Schematic representation of lipoprotein cholesterol kinetics assays. LDL and HDL were isolated from a pooled serum of LDLR+/− hAPOB100 mice and incubated with [^{3}H]cholesteryl oleate preparation in the presence of CETP source (LPDF) to obtain radiolabeled LDL and HDL. Individually housed mice were treated with either PCSK9-mAb1 or the vehicle every 7 days and fed a Western-type diet for 4 weeks. Forty-eight hours before the end of the experiment, every mouse received an intravenous injection of radiolabeled autologous LDL or HDL. Blood was collected at the indicated times. At the end of the experiments, mice were euthanized, and their livers were removed, and individual stools were collected. Created with *Biorender.com*.

6. Statistical methods

Continuous data are presented as the mean ± standard deviation (SD). The Shapiro-Wilk normality test was conducted to assess the Gaussian distribution of data.

A paired t-test was conducted to compare plasma parameters of FH subjects before and after anti-PCSK9 treatment. Repeated measures two-way analysis of variance (ANOVA) followed by Šídák multiple comparison test was performed to compare macrophage cholesterol efflux to plasma and the amount of radiolabeled cholesterol in the different lipoprotein fractions before and after anti-PCSK9 treatment in *ex vivo* cholesterol efflux assays. A paired t-test was used to analyze the differences in the percentage of macrophage-derived cholesterol in LDL and HDL.

One-way ANOVA followed by a post-test for linear trend was used to compare the accumulation of radiolabeled cholesterol in LDL and HDL in *in vitro* assays, and two-way ANOVA followed by a Tukey's multiple comparisons test was employed to compare the different incubation times for each LDL concentration in cell-free studies.

The number of mice per group was estimated based on a significance level of 0.05, a statistical power of 80%, and an expected effect size of 6,500 cpm in the fecal excretion of macrophage-derived cholesterol. Unpaired t tests were used to compare the differences between mice groups receiving vehicle or PCSK9 antibody treatment.

GraphPad Prism version 8.0.2 for Windows (GraphPad Software, San Diego, CA) was used to perform all statistical analyses. A p-value ≤ 0.05 was considered statistically significant.

METHODOLOGY FOR WORK 2

1. Cell culture model, treatments and analysis

1.1. Cell culture model

Immortalized mouse aortic VSMCs (CRL-2797™, ATCC®) were cultured in DMEM supplemented with 10% FBS and 0.2 g/L G-418 (InvivoGen, San Diego, CA). The cells were maintained in 75 cm^2 cell culture flasks and incubated at 37ºC in a humidified atmosphere containing 5% CO_2. The culture medium was replaced every 48 hours, and cells were trypsinized when they reached confluence.

1.2. Cell treatments

For the experiments, VSMCs were seeded and cultured in complete medium for 24 to 72 hours. Subsequently, the cells were exposed to 20 µg/mL MBD-cholesterol (Merck) in 5% FBS-containing medium for 48 hours to induce a foam cell phenotype, representing the VSMC cholesterol-loading phase. Non-loading control cells were incubated with the same medium without MBD-cholesterol. Afterwards, the VSMCs underwent an LXR activation step, which involved treatment with an LXR agonist T0901317 (Cayman Chemicals, Ann Arbor, MI) at a concentration of 2 µmol/L, dissolved in dimethyl sulfoxide (Merck), for 18 hours. Untreated control cells were incubated with dimethyl sulfoxide alone as the vehicle (0.1% v/v). Non-loading and untreated control cells were considered the baseline conditions for the experiments (**Figure 17**).

For those experiments involving ACAT inhibition, the ACAT inhibitor Sandoz 58-035 (Santa Cruz Biotechnology, Dallas, USA) was added to the culture medium at a concentration of 10 µmol/L during all experimental steps.

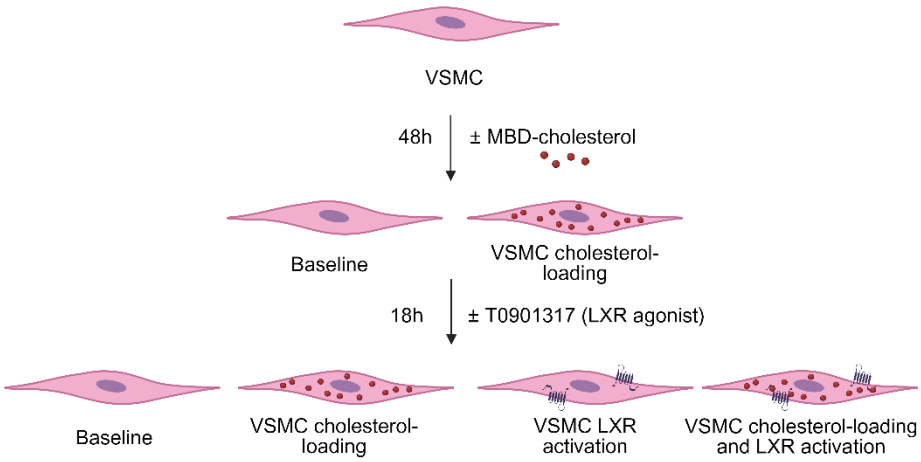

Figure 17. Depiction of VSMC cholesterol-loading and conditioning steps. VSMCs were cultured under baseline conditions or incubated with MBD-cholesterol, representing the cholesterol-loading phase, for 48 hours. Afterwards, VSMCs were treated with either the vehicle or the LXR agonist T0901317 for 18 hours, leading to four different experimental conditions. Created with *Biorender.com*.

1.3. Oil Red O and Bodipy-cholesterol staining

Oil Red O and Bodipy-cholesterol staining were performed to visualize the accumulation of neutral lipids within VSMCs. Cells were seeded into 6-well plates or individual plates of 3.5 cm^2 and treated according to the previously described experimental conditions (**section 1.2, Work 2**).

For Oil Red O staining, the cells were first washed twice with PBS before fixation with 4% paraformaldehyde (Thermo Fisher Scientific) for 10 minutes. Following fixation, the cells were washed twice with PBS and stained with an Oil Red O working solution, prepared by mixing 4 parts of distilled water with 6 parts of a 5 g/L Oil Red O solution (Merck) dissolved in isopropanol (Merck). The staining process was carried out for 1 hour. After staining, the cells were washed twice with distilled water, counterstained with a 1 g/L hematoxylin solution (Merck) for 1 minute, and rinsed again with distilled water. Images were acquired using an

inverted fluorescence phase-contrast microscope (Leica Microsystems, Wetzlar, Germany).

Bodipy-cholesterol (2.5 µmol/L, Merck) was added during the final 24 hours of the VSMC cholesterol-loading phase and to non-loading control VSMCs. Subsequently, the cells were washed with PBS and stained with a solution containing 0.5 µL of Hoechst and 1 µL of CellMask™ (Thermo Fisher Scientific) in 1 mL of PBS. Images were acquired using a Leica TCS SP5 X Tune confocal microscope (Leica Microsystems).

1.4. Thin-layer chromatography

Thin-layer chromatography analysis was performed to separate unesterified cholesterol from cholesteryl esters from VSMCs labeled or not with 1 µCi/well of [1α,2α(n)-^{3}H]cholesterol (Revvity) under the previously described experimental conditions (**section 1.2, Work 2**).

The cellular fraction was collected by adding 0.5 mL of 0.5 mol/L NaOH and incubating for 48 hours at 4ºC. Subsequently, lipids were extracted by adding 1 mL of hexane-isopropanol (3:2 v/v) and incubating the mixture for 1 hour. The following day, the extract was collected, and 300 µL of 0.5 mol/L sodium sulfate (Merck) were added. The mixture was gently mixed for 10 minutes and then centrifuged at 1,000 x *g* for 10 minutes, to separate the hexane and the isopropanol in two layers. The upper hexane layer containing lipids was collected and evaporated at room temperature. The dried lipid pellet was resuspended in 25 µL of chloroform (Merck) and applied onto a thin-layer chromatography plate (Merck). After, the plate was placed into a glass tank containing the mobile phase solution composed of hexane-diethyl ether-ethyl acetate (50:50:1.5, v:v:v, Merck) until the solvent front reached 5 cm from the top of the plate.

To quantify cellular lipids, plates were stained with a 5% phosphomolybdic acid ethanol solution (Merck) and compared to standards of free cholesterol (1.5 g/L) and esterified cholesterol (1 g/L). Images were acquired using a ChemiDoc XRS

Gel Documentation System (Bio-Rad) and data were quantified using Image Lab software (version 6.0.1, Bio-Rad). Cellular protein concentrations were determined using a BCA Protein Assay Kit (ThermoFisher Scientific).

To quantify the distribution of [^{3}H]cholesterol, plates were left overnight at room temperature and subsequently placed in a tank with iodine crystals (Merck) for 15 minutes to stain the lipids. The iodine-stained lipid bands were scraped from the plate and quantified by liquid scintillation counting.

1.5. Quantitative Real Time-PCR and flow cytometry analyses

For quantitative Real Time-PCR (qRT-PCR) analyses, total cellular RNA was extracted using the EZ-10 DNAaway RNA Miniprep kit (Bio Basic Inc., Markham, Ontario, Canada) and quantified by NanoDrop-2000 spectrophotometry (Thermo Fisher Scientific). Complementary DNA (cDNA) synthesis was performed using EasyScript®. First-Strand cDNA Synthesis SuperMix (Transgen Biotech, Beijing, China), and qRT-PCR amplification was conducted with GoTaq® Probe qPCR Master Mix (Promega, Madison, WI). TaqMan probes specific for *Abca1* (*Mm00442646_m1*), *Cd68* (*Mm03047343_m1*), *Tagln* (*Mm00441661_g1*) and *Actin* (*Mm00607939_s1*, used as an internal control) were obtained from Thermo Fisher Scientific (Waltham, MA). Reactions were carried out on a CFX96^{TM} Real-Time System (Bio-Rad, Hercules, CA) using the following thermal cycling conditions: 10 minutes at 95 °C, followed by 40 cycles of 95 °C for 15 seconds and 65 °C for 1 minute. Relative mRNA expression levels were calculated using the $2^{\Delta\Delta Ct}$ method.[100]

For flow cytometry, VSMCs were washed with PBS, trypsinized and resuspended in 100 µL of PBS containing 0.5% BSA at a concentration of 5 × 10^6 cells/mL. The cells were then fixed with 4% paraformaldehyde for 20 minutes and washed twice with PBS containing 0.5% BSA. After each wash, the cells were centrifuged at 250 x *g* for 5 minutes, and the supernatant was discarded. Permeabilization was performed by adding 0.1% Triton X-100 (Merck) for 10 minutes. Subsequently,

the cells were incubated with 5% Goat Serum (Thermo Fisher Scientific) to block non-specific binding. After blocking, CD68 staining was achieved by incubating the cells with 1:100 Rat anti-Mouse CD68 (FA-11 clone, Bio-Rad) for 30 minutes at 4ºC, followed by incubation with 1:4000 Goat anti-Rat IgG Alexa-488 (ab150157, Abcam) for 30 minutes. Finally, the cells were resuspended in 200 µL of PBS containing 0.5% BSA. After each step, the cells were washed twice. Controls were processed in parallel incubated without one of the antibodies.

Flow cytometry analysis was performed using a MACSQuant Analyzer (Miltenyi Biotec, Bergisch Gladbach, Germany). Data were acquired for 10,000 events within the gate representing viable single cells and analyzed using MACSQuant Software.

2. *In vitro* cholesterol transport study

2.1. VSMC-derived cholesterol efflux

Cellular cholesterol efflux was measured using a modified protocol of the previously described radiochemical method (**section 3.1, Work 1**) depicted in **Figure 18**. VSMCs were seeded at a density of 3 x 10^5 cells/well in 6-well plates and cultured in complete medium for 24 hours. Cells were then radiolabeled, either under baseline conditions or during the cholesterol-loading phase, for 48 hours. Following labeling, cells were equilibrated overnight. When indicated, LXR activation was performed during this step. The next day, cells were optionally pre-treated with the ABCA1 inhibitor probucol (Merck) at a concentration of 10 µmol/L for 2 hours.

Finally, fresh medium containing cholesterol acceptors was added to assess cholesterol efflux for 4 hours. Cholesterol acceptors were derived from pooled serum samples of wild-type C57BL/6J mice and included 25 µL of whole serum (2.5% v/v), 75 µL of APOB-depleted serum (equivalent to the lipoprotein-depleted fraction derived from 25 µL of plasma), or isolated HDL adjusted to a final concentration of 25 µg/mL of APOA1. At the end of the efflux assay,

radiolabeled cholesterol in the medium and in the cells was quantified by liquid scintillation counting, and cholesterol efflux was calculated as the percentage of total [^{3}H]cholesterol released from the cells.

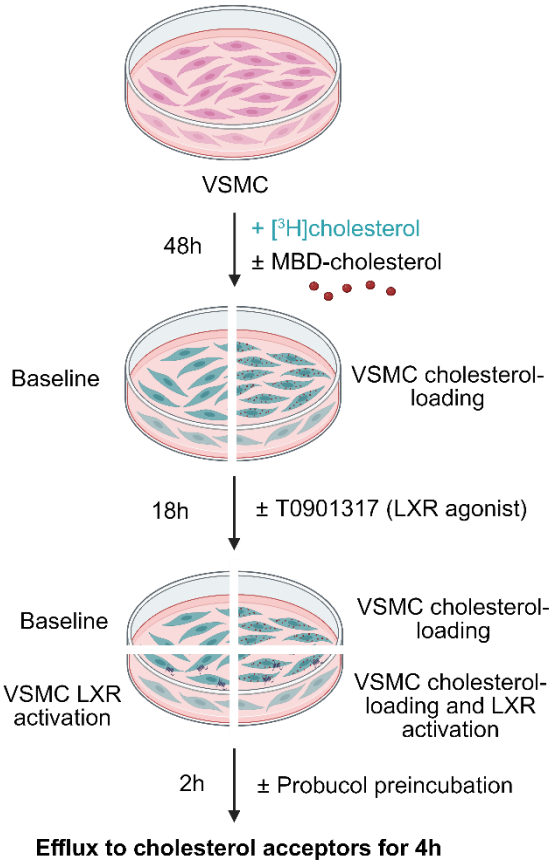

Figure 18. Schematic illustration of the VSMC cholesterol efflux assay. VSMCs were loaded with [^{3}H]cholesterol under baseline conditions or during exposure to MBD-cholesterol, representing the VSMC cholesterol-loading phase, for 48 hours. VSMCs were then treated with either the vehicle or the LXR agonist T0901317 for 18 hours. Subsequently, an optional preincubation with probucol, which was used to block ABCA1-mediated cholesterol efflux, was performed for 2 hours, followed by exposure to various cholesterol acceptors for 4 hours. Created with *Biorender.com*.

3. Mouse model and diet

Wild-type C57BL/6J (#000664, Jackson Laboratories) mice were obtained and housed under standard conditions with *ad libitum* access to food and water. Both male and female mice aged 8–10 weeks were used in the experiments. The experimental procedures were reviewed, approved and performed as aforementioned (**section 4.1, Work 1**).

Mice were fed a Western-type diet (TD.88137, Harlan Teklad), which contains 21% fat and 0.2% cholesterol, for a period of four weeks.

4. *In vivo* cholesterol transport study

4.1. VSMC-specific RCT assay

RCT method was adapted from the previously described in **section 5.1, Work 1**. VSMCs were cultured in 75 cm^2 cell culture flasks in complete medium for 72 hours. Subsequently, the cells were radiolabeled, either under baseline conditions or during the cholesterol-loading phase, for 48 hours. Following incubation, cells were washed and equilibrated overnight. Optionally, LXR activation was performed during this step. For experiments involving ACAT inhibition, the ACAT inhibitor was added during all experimental steps. The radiolabeled mouse VSMCs were then trypsinized, resuspended in PBS and pooled before intraperitoneal injection into mice (average of VSMCs and their associated cpm per mouse are described below; cell viability was higher than 90% in all conditions, assessed by trypan blue exclusion).

Following injection, mice were assigned to the different groups according to different cell treatment:

- Group 1: Mice injected with radiolabeled VSMCs under baseline conditions (2.1 x 10^6 VSMCs containing 1.4 x 10^6 cpm per mouse).
- Group 2: Mice injected with radiolabeled VSMCs under cholesterol-loading conditions (2.0 x 10^6 VSMCs containing 2.6 x 10^6 cpm per mouse).
- Group 3: Mice injected with radiolabeled VSMCs pre-treated with the LXR agonist (2.0 x 10^6 VSMCs containing 1.6 x 10^6 cpm per mouse).
- Group 4: Mice injected with radiolabeled VSMCs under cholesterol-loading conditions and pre-treated with the LXR agonist (3.2 x 10^6 VSMCs containing 2.8 x 10^6 cpm per mouse).
- Group 5: Mice injected with radiolabeled VSMCs under cholesterol-loading conditions and pre-treated with the ACAT inhibitor (1.8 x 10^6 VSMCs containing 1.8 x 10^6 cpm per mouse).
- Group 6: Mice injected with radiolabeled VSMCs under cholesterol-loading conditions and pre-treated with both the ACAT inhibitor and the LXR agonist (2.3 x 10^6 VSMCs containing 2.0 x 10^6 cpm per mouse).

Figure 19 depicts the cells injected in groups 1-4 and the following RCT protocol.

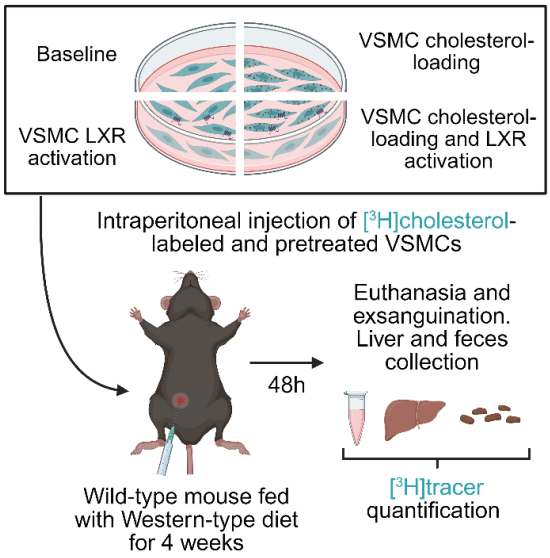

Figure 19. Schematic depiction of the VSMC-to-feces RCT assay. Mice were fed a Western-type diet for 4 weeks. VSMCs labelled with [^{3}H]cholesterol under baseline conditions or during exposure to MBD-cholesterol for 48 hours. Afterward, the cells were treated with either the vehicle or the LXR agonist T0901317 for 18 hours. The cells were then trypsinized, pooled and intraperitoneally injected into the mice 48 hours before the end of the experiment. At end point, mice were euthanized. Blood and liver were harvested, and feces over the last 48h were collected for [^{3}H]cholesterol measurement. Created with *Biorender.com*.

5. Statistical methods

Continuous data are presented as the mean ± SD. The Shapiro-Wilk normality test was performed to assess the Gaussian distribution.

In the *in vitro* results, unpaired t-tests were used to compare the differences between two groups. For *in vivo* assays, the number of mice per group was estimated based on a significance level of 0.05, a statistical power of 80%, and an expected effect size of 5,000 cpm in the fecal excretion of VSMC-derived cholesterol, and unpaired t-tests were used to compare the differences between two groups.

METHODOLOGY FOR WORK 3

1. Human samples and analysis

1.1. CSF samples

CSF samples were retrospectively selected from the SPIN cohort (Sant Pau Initiative on Neurodegeneration), a multimodal research cohort for the discovery and validation of biomarkers in neurodegenerative diseases. The cohort includes participants with various neurodegenerative dementias, mild cognitive impairment and cognitively normal controls. All participants underwent a comprehensive neurological and neuropsychological assessment, along with blood sampling and lumbar puncture for CSF AD biomarker analysis as part of their diagnostic evaluation.[101] Written consent was obtained from all participants for inclusion in the biomarker research program. Additional details about the SPIN cohort are available at https://santpaumemoryunit.com/our-research/spin-cohort.

A total of 20 CSF samples were included in the study, comprising samples from control individuals (n=10) and patients with AD dementia (n=10). All CSF samples were obtained via lumbar puncture under standardized conditions.[101]

1.2. CSF AD biomarker analysis

APOE genotype was determined by Sanger sequencing based on two single nucleotide polymorphisms: rs429358 and rs7412. Core AD biomarkers were analyzed in CSF, including markers of brain amyloidosis ($A\beta_{1-40}$, $A\beta_{1-42}$ and the $A\beta_{42}/A\beta_{40}$ ratio), tau pathology (p-Tau) and neurodegeneration (t-Tau). All biomarker measurements were performed using chemiluminescent immunoassay on the fully automated LUMIPULSE G600II platform (Fujirebio, Tokyo, Japan).

1.3. CSF lipid-related parameters measurement

Total CSF cholesterol and free cholesterol were measured by Amplex Red Cholesterol Assay Kit (Thermo Fisher Scientific). APOE, APOJ and APOA1 concentrations were measured by Human ELISA Kits (Thermo Fisher Scientific). PCSK9 concentrations were determined using the Quantikine® ELISA kit (R&D Systems, Minneapolis, USA). The kits were designed for plasma samples quantification; therefore, CSF samples dilutions were adapted to the cholesterol, APOs, or PCSK9 concentrations in the CSF.

2. Synthesis and characterization of rHDL nanoparticles

2.1. Synthesis of rHDL nanoparticles

The synthesis of rHDL nanoparticles containing APOE3 or APOE4 (rHDL-APOE3 and rHDL-APOE4) was performed using the sodium deoxycholate-dialysis method (**Figure 20**).[102] Briefly, the lipid mixture was prepared in chloroform using 1,2-dimyristoyl-sn-glycero-3-phosphocoline (DMPC, Merck) and free cholesterol (Merck) at a 9:1 molar ratio. For fluorescent labeling, Oregon Green™ 488 1,2-Dihexadecanoyl-sn-Glycero-3-Phosphoethanolamine (DHPE, Thermo Fisher Scientific) was added at a final concentration of 0.03 mmol/L. The organic solvent was evaporated under vacuum and nitrogen to form a dry lipid film, which was rehydrated in PBS containing 60 g/L sodium deoxycholate (Merck) and incubated at 37°C for 30 minutes to obtain clear mixed micelles.

Recombinant APOE3 or APOE4 (Thermo Fisher Scientific) was added to the micelles at a 59:7:1 molar ratio of DMPC:cholesterol:APOE. Afterward, the mixture underwent three temperature cycles between 4°C and 37°C to facilitate lipid-protein interactions. Sodium deoxycholate was then removed by extensive dialysis against 1000-fold volume excess of PBS at 4°C for 48 hours, using 3.5 kDa Slide-A-Lyzer™ G3 Dialysis Cassettes (Thermo Fisher Scientific) with two buffer changes. Finally, samples were centrifuged at 16,000 x *g* for 30 minutes at 4°C to remove unbound lipids.

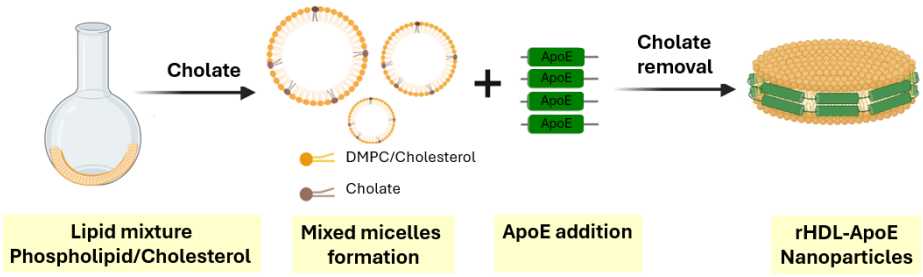

Figure 20. Schematic representation of the synthesis of rHDL-APOE nanoparticles. rHDL nanoparticles were generated using a cholate dialysis method. A lipid film composed of DMPC and cholesterol was first formed by solvent evaporation and then rehydrated in the presence of sodium cholate to form mixed micelles. Recombinant APOE3 or APOE4 was added to the micelles, and the mixture was subjected to three cycles of vortexing and temperature shifts to facilitate lipid-protein interaction. Final rHDL-APOE nanoparticles were obtained following cholate removal via extensive dialysis. Created with *Biorender.com*.

2.2. Characterization of rHDL-APOE3- and rHDL-APOE4

The composition of rHDL-APOE3 and rHDL-APOE4 nanoparticles, including unesterified cholesterol and APOE content, was determined using enzymatic and immunoturbidimetric assays, respectively, with commercial kits adapted for a COBAS 6000 autoanalyzer (Roche Diagnostics and Randox, Crumlin, UK). To assess protein profiles, rHDL-APOE nanoparticles, along with CSF, isolated HDL, and lipid-free APOA1, were separated by electrophoresis on a 4–15% Mini-PROTEAN® TGX™ Precast Protein Gel (Bio-Rad). Afterwards, proteins were fixed using 40% methanol (Merck) and 10% acetic acid (Merck) solution and stained with GelCode™ Blue Staining Reagent (Thermo Fisher Scientific). Images were captured using a ChemiDoc XRS Gel Documentation System (Bio-Rad) and Image Lab software (version 6.0.1, Bio-Rad).

Particle-size distributions were analyzed using dynamic light scattering with non-invasive backscatter detection (Malvern Zetasizer, Malvern Instruments, Malvern, United Kingdom). In addition, the morphology of rHDL-APOE3 and rHDL-

APOE4 nanoparticles was visualized by transmission electron microscopy with negative staining. Briefly, 8 µL aliquot of each sample was applied to glow-discharged carbon-coated 300 Mesh copper grids (Ted Pella Inc., Redding, CA) for 1 minute, followed by staining with 8 µL of 5% uranyl acetate (Merck) for 1 minute. Grids were examined using a JEM-1400 Transmission Electron Microscope (JEOL USA Inc., Peabody, MA).

3. Cell culture models, treatments and analysis

3.1. Cell culture models

A172 human glioblastoma cells (ATCC® CRL-1620™) were maintained in DMEM high glucose with L-glutamine and with sodium pyruvate supplemented with 10% FBS and 100 U/mL penicillin/streptomycin.

SH-SY5Y human neuroblastoma cells (ATCC® CRL-2266™) were maintained in DMEM high glucose with L-glutamine and Ham's Nutrient Mixture F12 with L-glutamine (Cytiva, Marlborough, MA) 1:1 v/v supplemented with 10% FBS (Pan Biotech) and 100 U/mL penicillin/streptomycin.

Cells were seeded and grown in 75 cm^2 cell culture flasks and incubated in a humidified incubator (5% CO_2, 37°C). The medium was renewed every 48 hours and cells were trypsinized once they reached confluence.

3.2. Cell treatments

Previous to any experiment, human neuroblastoma SH-SY5Y cells were differentiated into functional neurons by replacing maintenance medium with differentiation culture medium for 7 days and refreshment every 72h. Differentiation culture medium consisted of DMEM high glucose with L-glutamine and Ham's Nutrient Mixture F12 with L-glutamine 1:1 v/v supplemented with 1% FBS, 100 U/mL penicillin/streptomycin and 10 µM retinoic acid (RA, Merck).

3.3. qRT-PCR analysis

For qRT-PCR analyses, total cellular RNA was extracted, cDNA was synthesized and qRT-PCR was performed as described in **section 1.5, Work 2**. Specific Taqman probes for genes (Thermo Fisher Scientific) were *ABCA1* (Hs01059118_m1), *ABCG1* (Hs00245154_m1) and *GAPDH* (Hs02758991_g1), the latter used as internal control gene.

3.4. Confocal microscopy and flow cytometry

SH-SY5Y neurons were seeded in individual plates of 3.5 cm^2 at a cell density of 50,000 cells per well and differentiated as previously described. Subsequently, 1 mL of serum-free medium with or without synthetic rHDL-APOE3 or rHDL-APOE4 (5 µg/mL), was added to each plate and incubated for 4 hours to facilitate the internalization of synthetic rHDL-APOE nanoparticles. The cells were stained with a solution of 0.5 µL of Hoechst and 1 µL of CellMask™ (Thermo Fisher Scientific) diluted in 1 mL of PBS. Imaging of SH-SY5Y neurons was conducted using a Leica TCS SP5 X Tune confocal microscope (Leica Microsystems).

The uptake of synthetic rHDL-APOE3 and rHDP-APOE4 nanoparticles labeled with Oregon Green™ 488 DHPE fluorophore by SH-SY5Y cells was analyzed using flow cytometry. SH-SY5Y cells were seeded at a density of 200,000 cells per well in 12-well plates, and the differentiation protocol was performed. Upon reaching differentiation, the cells were incubated with or without synthetic rHDL-APOE3 or rHDL-APOE4 (5 µg/mL) in serum-free medium for 4 hours. After incubation, cells were washed with PBS, trypsinized for 5 minutes at 37ºC and resuspended in 100 µL of PBS. Flow cytometry analysis was performed as described in **section 1.4, Work 2**.

1. *In vitro* cholesterol transport studies

1.1. Astrocyte-derived cholesterol efflux assay

Astrocyte cholesterol efflux was assessed using a modified radiochemical method based on the previously described protocol (**section 3.1, Work 1**) and illustrated in **Figure 21**. A172 cells were seeded at a density of 5 x 10^5 cells per well in 24-well plates and cultured in complete medium. After 24 hours, cells were labeled with 0.5 µCi/well of [^{3}H]cholesterol for 48 hours. Subsequently, cells were equilibrated overnight in serum-free medium, either with or without 2 µM LXR agonist T0901317. The next day, cells were washed and incubated for 4 hours in serum-free medium containing cholesterol acceptors: CSF (30% v/v) or rHDL (5 µg of APOE/mL) was added to the cells. Radiolabeled cholesterol in the medium and cellular fractions was quantified by liquid scintillation counting, and the percentage of cholesterol efflux was calculated.

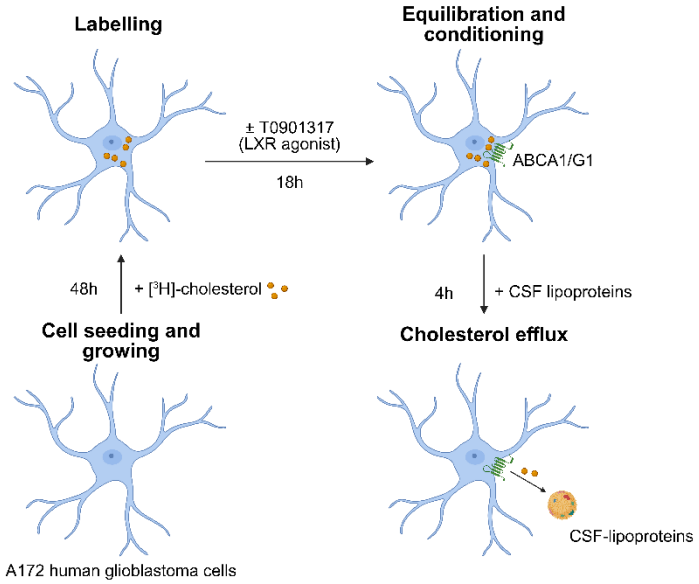

Figure 21. Astrocyte cholesterol efflux assay. A172 human glioblastoma cells were cultured for 24 hours, followed by a 48-hour incubation with radiolabeled cholesterol. Cells were then treated for 18 hours with or without the LXR agonist T0901317 to activate ABCA1/G1 pathways. Finally, serum-free medium containing CSF was added for 4 hours. Created with *Biorender.com*.

3.5. Neuronal-derived cholesterol uptake assay

Neuronal cholesterol uptake assay was optimized to quantify the internalization of cholesterol from CSF-lipoproteins by SH-SY5Y neurons (**Figure 22**). First, CSF samples or rHDL nanoparticles were radiolabeled by incubation with evaporated [^{3}H]cholesterol solution (0.1 µCi/µL and 0.2 µCi/µL, respectively) overnight at 37ºC. Successful incorporation into lipoproteins was confirmed by isolating CSF lipoproteins within the 1.063–1.210 g/mL density range using density gradient ultracentrifugation (see **Section 1.3, Work 1**).

SH-SY5Y cells were seeded at a density of 1 x 10^5 cells per well in 24-well plates. Twenty-four hours after reaching differentiation, cells were incubated with serum-free medium containing radiolabeled CSF (10% v/v) or rHDL (5 µg of APOE/mL). In selected experiments, Human Tau-441/2N4R Protein (ACROBiosystems, Bejing, China) or Aβ Protein Fragment 1-42 (Merck) was added to the medium at varying concentrations.

After 4 hours, the medium and cellular fractions were collected and processed as described in cholesterol efflux assay (**section 3.2, Work 1**). to quantify [^{3}H]cholesterol via liquid scintillation counting. Cholesterol uptake was expressed as the percentage of total radiolabeled cholesterol found in the cellular fraction:

$$\text{Cholesterol uptake (\%)} = \frac{[^3\text{H}]\text{cholesterol in the cells}}{\text{Total } [^3\text{H}]\text{cholesterol (medium + cells)}} x\ 100$$

Values were normalized to protein content, determined using the Pierce™ BCA Protein Assay Kit (Thermo Fisher Scientific).

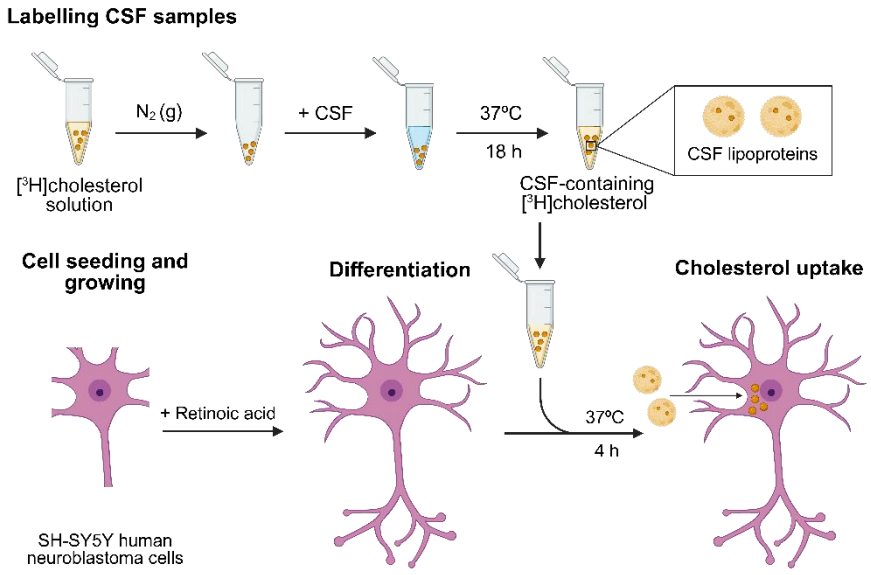

Figure 22. CSF HDL-like-mediated cholesterol uptake assay. Labelling of CSF lipoproteins was performed by evaporating [^{3}H]cholesterol solution and incubating it with CSF for 18 hours at 37ºC. SH-SY5Y human neuroblastoma cells were seeded and differentiated into neurons in a low-serum medium containing retinoic acid. Afterwards, the cells were incubated with medium containing the radiolabeled CSF for 4 hours to induce cholesterol uptake of [^{3}H]cholesterol into the neurons. Created with *Biorender.com*

4. Statistical methods

Continuous data are presented as the mean ± SD, while qualitative data are expressed as percentages and analyzed using Fisher's exact test. The Shapiro-Wilk normality test was performed to assess the Gaussian distribution.

The number of CSF samples per group was estimated using an α value of 0.05, a power of 80%, and an effect size of 1.28 in the cholesterol efflux and uptake assays. Unpaired t-test was used to compare statistical differences between AD and control groups. One-way ANOVA, followed by a post-test for linear trend, was used to evaluate relative cholesterol uptake in human neuroblastoma cells, mediated by control CSF HDL-like particles, in the absence or presence of t-Tau or Aβ1-42. Associations between variables were assessed using Pearson's correlation coefficient

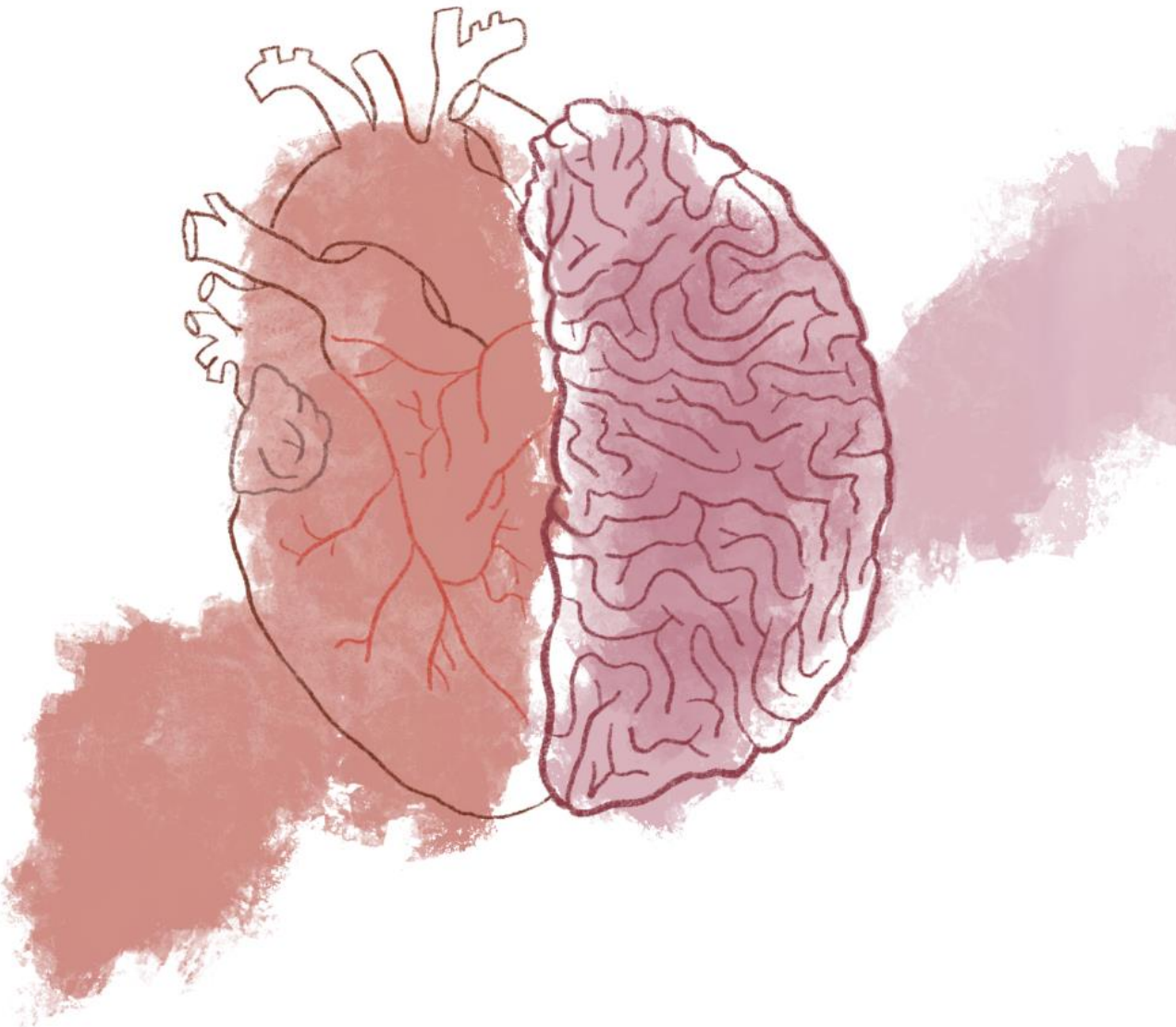

CHAPTER IV

RESULTS

1. RESULTS FROM WORK 1

The results presented in this section derive from our work published in *Publication 2* (see Annex).

1.1. LDL-cholesterol is efficiently reduced after evolocumab treatment in heterozygous FH patients

Plasma lipid parameters before and after evolocumab treatment are summarized in **Table 1**. As expected, treatment with this PCSK9 inhibitor significantly reduced LDL-cholesterol and APOB concentrations. In contrast, the levels of HDL-cholesterol and APOA1 remained unchanged following treatment.

Importantly, PCSK9 inhibition did not significantly affect the activity of major HDL-associated lipid transfer proteins and remodeling enzymes. Specifically, PLTP, CETP and LCAT activities remained stable post-treatment (**Table 1**).

Table 1. Plasma lipid parameters from FH patients treated with evolocumab.

	Evolocumab treatment (n=14)		
	Pre	**Post**	**P-value**
Total cholesterol (mmol/L)	5.51 ± 1.11	3.52 ± 1.21	< 0.001
LDL-cholesterol (mmol/L)	3.75 ± 1.00	1.75 ± 1.13	< 0.001
HDL-cholesterol (mmol/L)	1.21 ± 0.29	1.22 ± 0.29	0.53
APOA1 (g/L)	1.49 ± 0.28	1.57 ± 0.32	0.15
APOB100 (g/L)	1.19 ± 0.23	0.66 ± 0.27	< 0.001
Triglycerides (mmol/L)	1.18 ± 0.41	1.16 ± 0.54	0.86
PLTP activity (nmol/mL/h)	63.02 ± 24.69	61.83 ± 18.14	0.79
CETP activity (nmol/mL/h)	1.26 ± 0.67	1.18 ± 0.64	0.64
LCAT activity (ratio 390/470) [a]	0.68 ± 0.08	0.67 ± 0.06	0.52

Values are presented as mean ± SD. [a]The ratio between the 390 nm emission and 470 nm emission peak in the LCAT assay indicates the rate of substrate hydrolysis by LCAT.

1.2.PCSK9 inhibition alters the lipoprotein distribution of macrophage-derived cholesterol efflux in heterozygous FH

To assess whether PCSK9 inhibition affects the ability of plasma to promote cholesterol efflux, we first quantified total cholesterol efflux from macrophages to whole plasma from heterozygous FH patients before and after evolocumab treatment. As shown in **Figure 23A**, total cholesterol efflux remained unchanged following evolocumab treatment.

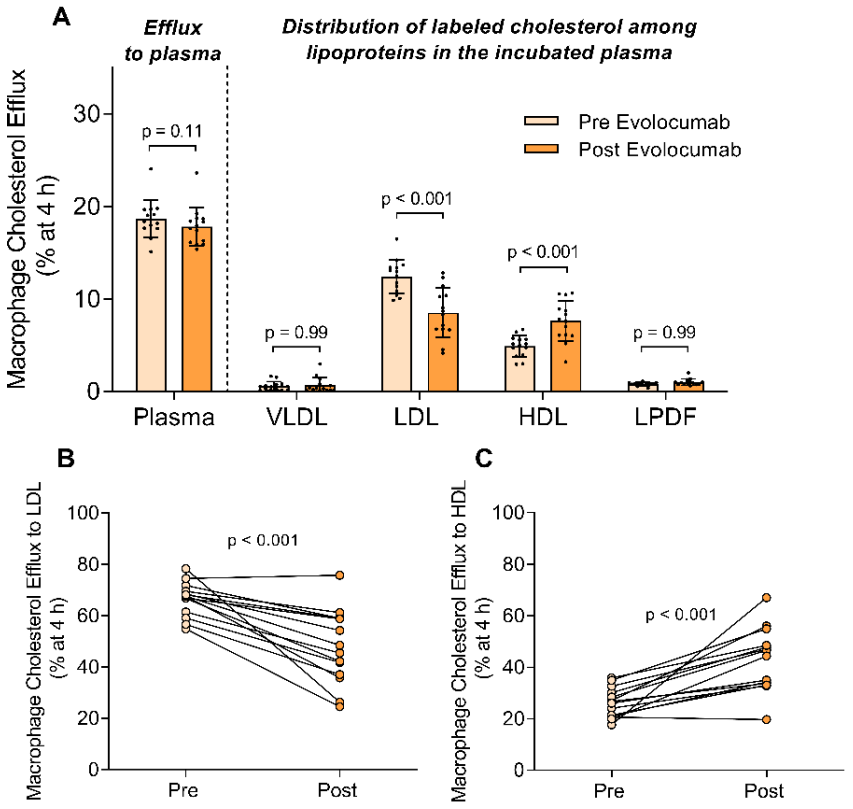

Figure 23. Anti-PCSK9 therapy alters the amount of macrophage-derived cholesterol in LDL and HDL *ex vivo*. (A) Macrophage cholesterol efflux to plasma samples collected from heterozygous FH subjects (n=14) before and after treatment with evolocumab. The distribution of radiolabeled cholesterol among lipoprotein fractions was analyzed after the efflux assay. Values are expressed as mean ± SD. **(B)** Matched-pair analysis of the percentage of total radiolabeled cholesterol in the LDL. **(C)** Matched-pair analysis of the percentage of total radiolabeled cholesterol in the HDL.

Given that plasma is a complex mixture of cholesterol acceptors, comprising both HDL and APOB-containing lipoproteins, and considering that LDL can act as a transient reservoir for macrophage-derived cholesterol,[99] we next examined the distribution of effluxed cholesterol across plasma lipoprotein fractions.

Evolocumab therapy led to a significant reduction in radiolabeled cholesterol associated with LDL particles, accompanied by a corresponding increase in the proportion of cholesterol associated with HDL particles (**Figures 23B and 23C**).

No significant changes were observed in the radioactivity associated with VLDL particles or the LPDF, both of which together accounted for less than 15% of total radiolabeled cholesterol (**Figure 10A**).

1.3.LDL competes with HDL for macrophage-derived cholesterol and promotes passive transfer from HDL

To further elucidate the mechanism by which PCSK9 inhibition alters the distribution of macrophage-derived cholesterol among lipoproteins, we assessed the competitive dynamics between LDL and HDL in cholesterol acceptance and transfer.

Radiolabeled macrophages were incubated with conditioned media containing either isolated HDL (**Figure 24A**) or whole plasma (**Figure 24B**), supplemented with different concentrations of isolated LDL obtained from normolipidemic plasmas, and the distribution of [^{3}H]cholesterol between the HDL and LDL fractions was quantified. As shown in **Figure 24A and 24B**, decreasing LDL protein levels resulted in a dose-dependent increase of macrophage-derived cholesterol in HDL particles. Notably, decreasing the LDL/HDL protein ratio (APOB/APOA1) from 15/25 to 5/25 significantly increased the percentage of radiolabel retained in HDL from 13.3% to 37.3% of total radiolabeled cholesterol, while reducing the proportion recovered in LDL (**Figure 24A**).

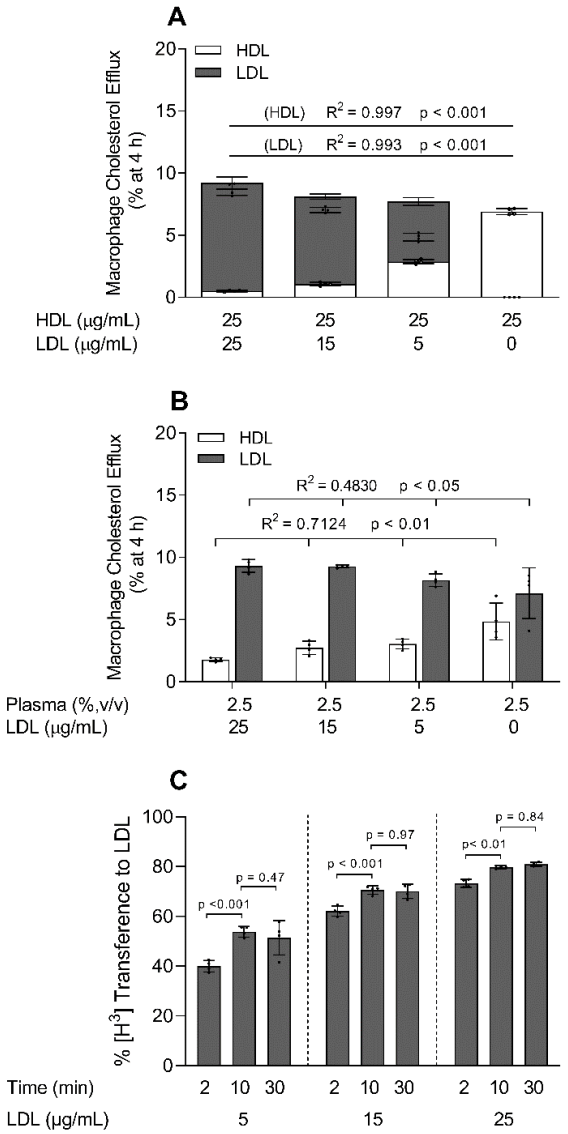

Figure 24. The capacity of HDL to serve as a macrophage cholesterol acceptor is enhanced by low levels of LDL *in vitro*. (A) Macrophage cholesterol efflux to HDL (25µg/mL APOA1) in the presence of LDL (up to 25µg/mL APOB). The distribution of radiolabeled cholesterol between HDL and LDL was assessed after APOB precipitation. **(B)** Macrophage cholesterol efflux to plasma (2.5% v/v) with or without LDL. Radiolabeled cholesterol distribution was analyzed after lipoprotein isolation by sequential ultracentrifugation. **(C)** Redistribution of radiolabeled cholesterol from HDL incubated with unlabeled LDL over 2, 10, and 30 minutes. The distribution of radiolabeled cholesterol was assessed after APOB precipitation. Values are presented as mean ± SD of four independent experiments per condition.

To determine whether LDL can passively acquire cholesterol from HDL in the absence of cells, we isolated [^{3}H]HDL from macrophage-conditioned media following the efflux period and incubated it with unlabeled LDL for up to 30 minutes (**Figure 24C**). Under these cell-free conditions, we observed a rapid and dose-dependent transfer of radiolabeled cholesterol from HDL to LDL, reaching a maximum plateau within 10 minutes.

1.4.PCSK9 inhibition recapitulates LDL-cholesterol-lowering effects in a transgenic mouse model of FH

To evaluate the *in vivo* relevance of PCSK9 inhibition on macrophage-specific RCT, a mouse model expressing human APOB100 under conditions of heterozygous LDL receptor deficiency (LDLR+/– hAPOB100) was used. Mice were fed a Western-type diet, and simultaneously injected either the PCSK9 monoclonal antibody PL-45134 (PCSK9-mAb1) or vehicle every 7 days for 4 weeks.

As shown in **Table 2**, vehicle-treated mice displayed elevated total cholesterol and LDL-cholesterol, consistent with a phenotype resembling FH. Treatment with PCSK9-mAb1 significantly reduced plasma LDL-cholesterol and APOB100 levels, while HDL-cholesterol levels and the activities of PLTP and LCAT remained unchanged. These lipid profile changes are in line with those observed in FH patients receiving evolocumab.

Table 2. Plasma and HDL parameters in heterozygous LDLR-deficient mice expressing hAPOB100 treated with the PCSK9-mAb1 or the vehicle solution.

	Vehicle (n=6)	PCSK9-mAb1 (n=6)	P-value
Body weight (g)	31.54 ± 4.35	27.23 ± 3.30	0.08
Food intake (g/day)	2.12 ± 0.60	2.00 ± 0.53	0.72
Total cholesterol (mmol/L)	14.38 ± 1.14	9.34 ± 1.12	< 0.001
LDL cholesterol (mmol/L)	9.77 ± 1.66	5.58 ± 0.66	< 0.001
HDL cholesterol (mmol/L)	4.36 ± 0.51	3.56 ± 0.74	0.05
Triglycerides (mmol/L)	2.81 ± 0.35	2.67 ± 0.77	0.71
APOB100 (g/L)	2.22 ± 0.31	1.46 ± 0.25	< 0.001
PLTP activity (nmol/mL/h)	141.06 ± 18.38	152.66 ± 24.86	0.38
LCAT activity (ratio 390/470) [a]	1.52 ± 0.57	2.02 ± 0.91	0.28

Values are presented as mean ± SD. [a]The ratio between the 390 nm emission and 470 nm emission peak in the LCAT assay indicates the rate of substrate hydrolysis by LCAT.

1.5.Macrophage-to-feces RCT is promoted by anti-PCSK9 treatment *in vivo*

To quantify macrophage-specific RCT rate, [^{3}H]cholesterol-labeled macrophages were intraperitoneally injected into treated mice, and [^{3}H]cholesterol recovery was measured in plasma, HDL, liver, and feces after 48 hours.

Plasma radioactivity levels were similar between groups (**Figure 25A**); however, PCSK9-mAb1 treatment significantly reduced the proportion of [^{3}H]cholesterol in LDL (**Figure 25A, inset**), while increasing its presence in the HDL fraction (**Figure 25A**). This redistribution is consistent with *ex vivo* findings in FH patients, where PCSK9 inhibition shifted the amount of radiolabeled cholesterol away from LDL and toward HDL particles.

Although hepatic [^{3}H]cholesterol levels were not affected by PCSK9-mAb1-treatment (**Figure 25B**), total recovery of [^{3}H]cholesterol in feces was significantly higher compared to controls (**Figure 25C**), indicating an overall enhancement of macrophage-to-feces RCT.

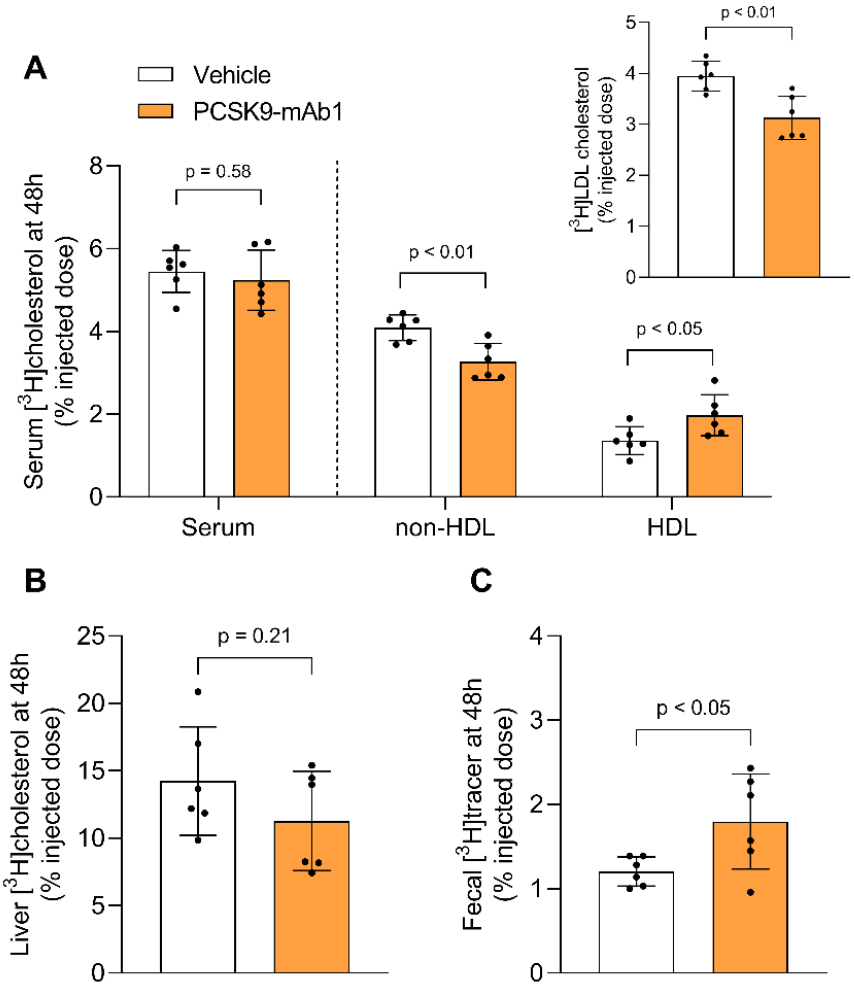

Figure 25. PCSK9 inhibition enhances macrophage-to-feces RCT in a mouse model of heterozygous FH. Eight-to-ten-week-old mice were treated with the PCSK9-mAb1 or the vehicle weekly and fed a Western-type diet for 4 weeks. RCT was assessed using radiolabeled cholesterol-loaded macrophages. **(A)** [^{3}H]cholesterol recovery in serum, HDL, and non-HDL fractions. Inset: [^{3}H]LDL cholesterol levels present in the non-HDL fraction. **(B)** [3H]cholesterol accumulation in the liver. **(C)** [^{3}H]cholesterol and [3H]bile acids recovered in feces over 48 hours. Values are expressed as the mean ± SD of 6 mice per group. Radioactivity is expressed as a percentage of the injected [^{3}H]tracer dose.

1.6.PCSK9 inhibition promotes LDL-derived cholesterol clearance in FH mice

To further elucidate the mechanism behind enhanced macrophage-specific RCT following PCSK9 inhibition, we performed kinetic studies using radiolabeled endogenous LDL and HDL in LDLR+/– hAPOB100 mice. Given the absence of CETP in mouse serum, this model allowed us to examine the direct effect of PCSK9 inhibition on lipoprotein [^{3}H]cholesterol clearance and its transfer to feces. Treated mice were intravenously injected with [^{3}H]cholesterol ester-labeled mouse LDL or HDL, and radiotracer clearance was monitored in the blood and feces over 48 hours.

In mice treated with PCSK9-mAb1, [^{3}H]LDL-cholesterol ester clearance from plasma was significantly accelerated compared to vehicle-treated controls (**Figure 26A**). This was accompanied by a reduction in hepatic [^{3}H]cholesterol levels (**Figure 26B**) and a notable increase in [^{3}H]cholesterol recovered in feces (**Figure 26C**), indicating enhanced excretion of LDL-derived cholesterol.

These changes were accompanied by a marked upregulation of hepatic LDLR expression, while the expression of the cholesterol transporters ABCG5 and ABCG8 remained unchanged (**Figure 26D**).

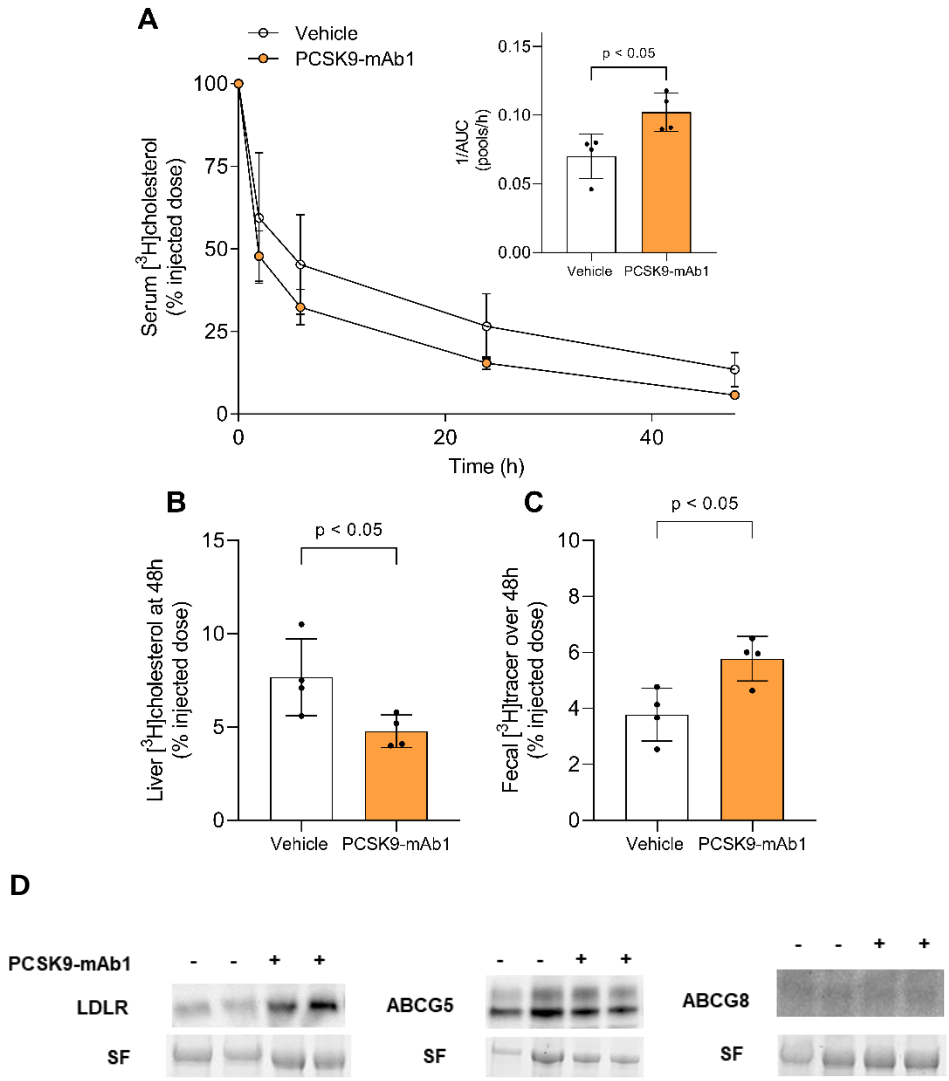

Figure 26. PCSK9 inhibition promotes the transfer of LDL-derived cholesterol esters to feces in a mouse model of heterozygous FH. Eight-to ten-week-old mice were treated weekly with either PCSK9-mAb1 or vehicle, and fed a Western-type diet for 4 weeks. LDL kinetic assays were performed using [^{3}H]cholesteryl oleate–labeled LDL (A) *In vivo* clearance of radiolabelled LDL. Inset: clearance rate expressed as the inverse of the area under the curve (AUC, pools/hour). (B) [^{3}H]cholesterol accumulation in the liver. (C) [^{3}H]cholesterol and [^{3}H]bile acids derived from LDL recovered in feces over 48 hours. Values are expressed as the mean ± SD of 4 mice per group. Radiotracer recovery is expressed as a percentage of the injected dose. (D) Protein was extracted from mice livers and western blot analysis of LDLR, ABCG5 and ABCG8, and the corresponding stain free (SF) images are shown.

In contrast to the LDL findings, [^{3}H]HDL-cholesterol ester clearance kinetics, as well as hepatic and fecal recovery of HDL-derived cholesterol, were not significantly altered by PCSK9-mAb1 treatment (**Figures 27A–C**).

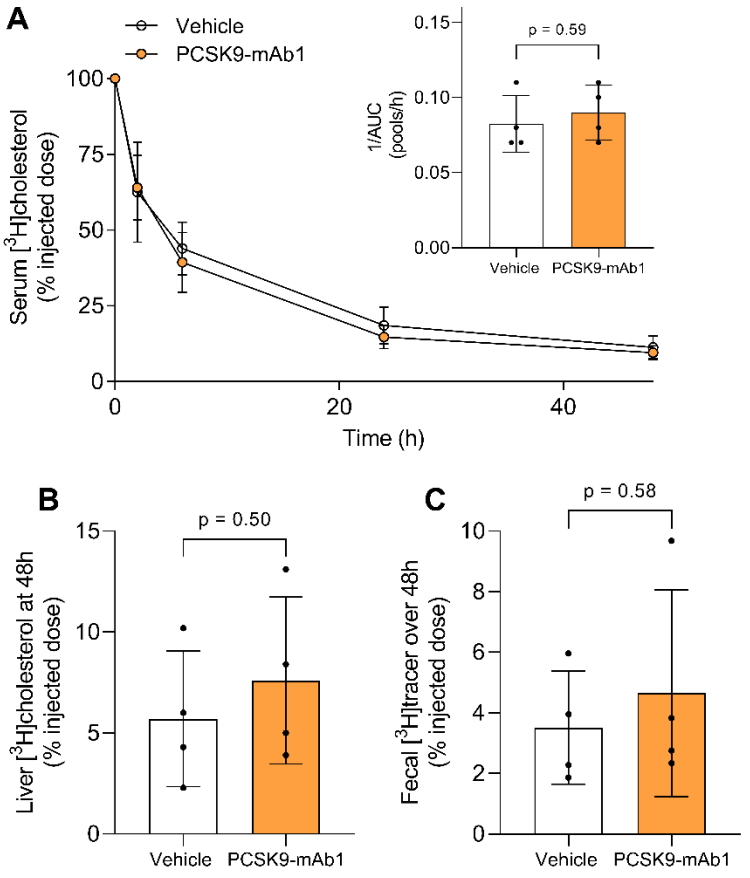

Figure 27. HDL-cholesterol ester transfer to feces is not altered by anti-PCSK9 treatment in a mouse model of FH. Eight-to ten-week-old mice were treated weekly with either PCSK9-mAb1 or vehicle, and fed a Western-type diet for 4 weeks. HDL kinetic assays were performed using [^{3}H]cholesteryl oleate–labeled HDL. **(A)** *In vivo* clearance of radiolabelled HDL. Inset: clearance rate expressed as the inverse of the area under the curve (AUC, pools/hour). **(B)** [^{3}H]cholesterol accumulation in the liver. **(C)** [^{3}H]cholesterol and [^{3}H]bile acids derived from HDL recovered in feces over 48 hours. Values are expressed as the mean ± SD of 4 mice per group. Radiotracer recovery is expressed as a percentage of the injected dose.

2. RESULTS FROM WORK 2

The results presented in this section derive from our work published in *Publication 3* (see Annex).

2.1.VSMCs exposed to MBD-cholesterol acquire foam cell features

To model foam cell formation in VSMCs, we treated immortalized mouse aortic VSMCs with MBD-cholesterol and evaluated hallmark characteristics of foam cell transition.

Following cholesterol loading, VSMCs exhibited a pronounced increase in neutral lipid accumulation, as evidenced by Oil Red O staining (**Figure 28A**). This phenotype was further supported by a significant increase in Bodipy-cholesterol incorporation from the media (**Figure 28B**), confirming enhanced uptake and intracellular retention of cholesterol.

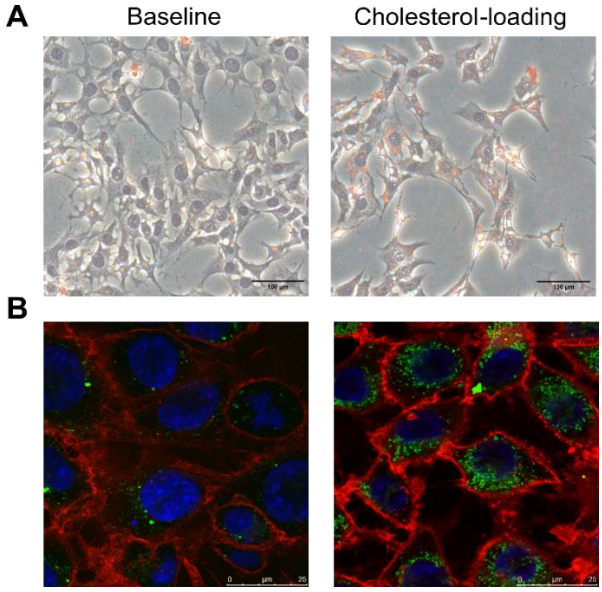

Figure 28. MBD-cholesterol loading increases neutral lipid accumulation in VSMCs. **(A)** Oil Red O staining of VSMCs under baseline conditions or following cholesterol loading with MBD-cholesterol. **(B)** Confocal imaging of VSMC incubated with Bodipy-cholesterol to VSMCs cultured under baseline or cholesterol loading conditions. Bodipy-cholesterol (green) indicates cholesterol localization, Hoechst (blue) stains nuclei, and CellMask (red) outlines the plasma membrane.

Consistently, total cellular cholesterol content was markedly elevated following MBD-cholesterol exposure (**Figure 29A**).

To determine whether cholesterol-loaded VSMCs undergo phenotypic changes associated with foam cell transition, we analyzed the expression of key molecular markers. MBD-cholesterol treatment significantly upregulated the mRNA expression of *Cd68*, a macrophage-associated marker, while concurrently diminishing the VSMC-specific canonical marker *Tagln* (**Figures 29B and 29C**).

Flow cytometry analysis further confirmed a significant increase in CD68 expression in MBD-cholesterol–treated VSMCs (**Figure 29D**), supporting the induction of macrophage-like features during foam cell transformation.

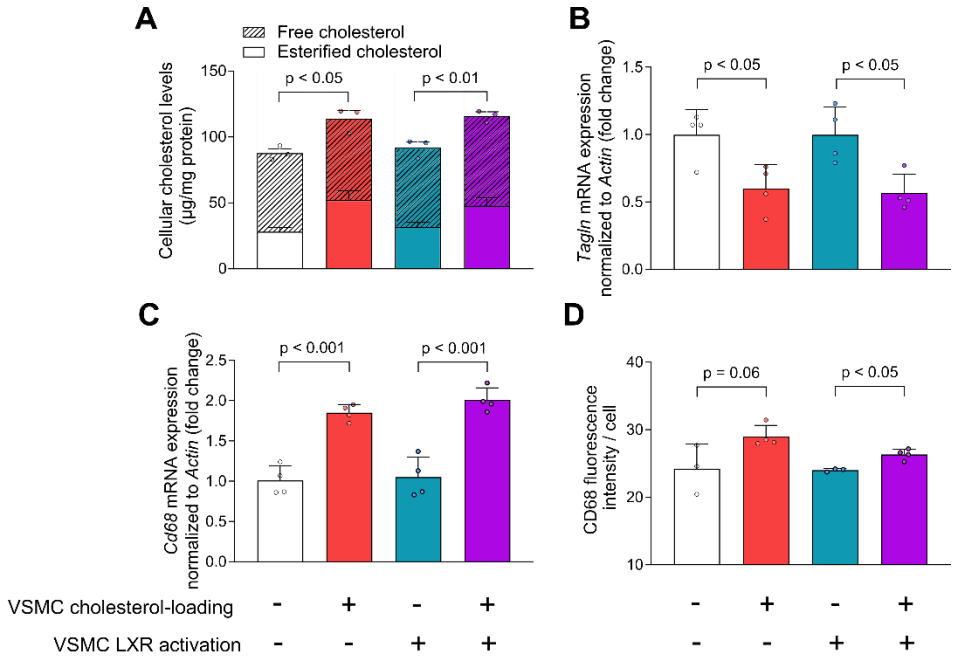

Figure 29. VSMCs exposed to MBD-cholesterol effectively mimic foam cell transformation characteristics. VSMCs were cultured under baseline or cholesterol-loading conditions, and treated with either vehicle or the LXR agonist T0901317. **(A)** Quantification of cellular esterified and unesterified cholesterol by thin-layer chromatography. **(B, C)** Relative mRNA expression of Tagln and Cd68, normalized to Actin; baseline expression was set to 1 arbitrary unit. **(D)** CD68-associated fluorescence intensity per cell measured by flow cytometry. Data are shown as mean ± SD from 3 or 4 independent experiments per group.

2.2.LXR agonist enhances cholesterol efflux in VSMCs *in vitro,* even after foam cell-induced reduction

We next assessed the cholesterol efflux capacity of VSMCs and VSMC-derived foam cells and how this process is modulated by LXR activation.

Cholesterol efflux assays using whole serum and APOB-depleted serum (enriched in HDL, preβ-HDL, albumin, and lipid transfer proteins) showed a robust efflux capacity in VSMCs under baseline conditions. However, exposure to MBD-cholesterol led to a marked reduction in cholesterol efflux to both acceptors, consistent with foam-like transformation (**Figures 30A and 30B**).
Importantly, treatment with the LXR agonist T0901317 significantly enhanced cholesterol efflux, not only in native VSMCs but also in cholesterol-loaded, foam-like VSMCs, although the effect was less prominent (**Figures 30A and 30B**).

To elucidate the mechanism underlying LXR-mediated efflux enhancement, we assessed *Abca1* expression. Cholesterol loading increased *Abca1* mRNA, and this was further upregulated by LXR agonist treatment (**Figure 30C**). In addition, the functional relevance of ABCA1 was confirmed using probucol, an ABCA1-specific inhibitor, which blunted LXR-stimulated cholesterol efflux to APOB-depleted serum under baseline and cholesterol-loading conditions (**Figure 30D**).

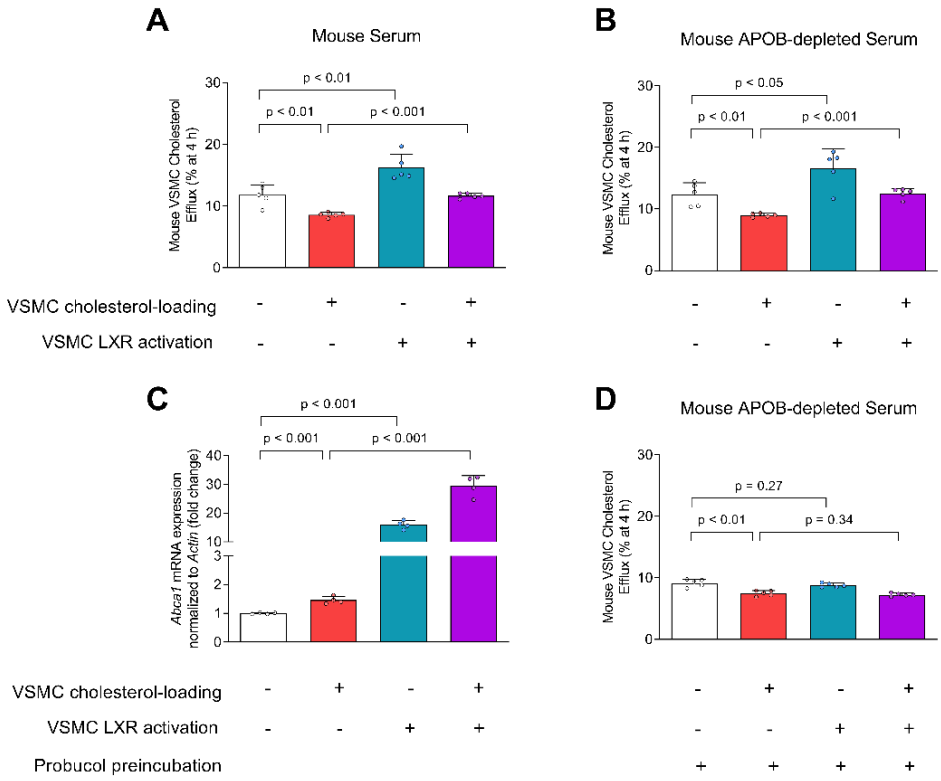

Figure 30. LXR agonist enhances cholesterol efflux in mouse VSMCs, including those exposed to MBD-cholesterol. VSMCs were cultured under baseline or cholesterol-loading conditions, and treated with either vehicle or the LXR agonist T0901317. **(A, B)** Cholesterol efflux to whole serum and APOB-depleted serum. **(C)** Relative mRNA expression of *Abca1*, normalized to *Actin*; baseline expression set to 1 arbitrary unit. (D) Cholesterol efflux to APOB-depleted serum following preincubation with probucol. Data are shown as mean ± SD from 5 independent experiments per group.

2.3.LXR agonist treatment in mouse VSMCs is sufficient to substantially promote RCT to feces *in vivo*

To determine whether activation of LXR influences VSMCs-to feces RCT *in vivo*, [^{3}H]cholesterol-labeled mouse VSMCs –either pre-loaded or not with MBD-cholesterol, and pretreated with either vehicle or an LXR agonist– were injected into wild-type mice maintained on a Western-type diet for 4 weeks. After 48 hours, the recovery of [^{3}H]cholesterol was measured in serum, HDL, liver, and feces.

MBD-cholesterol loading reduced the *in vivo* transfer of VSMC-derived cholesterol to serum and HDL, which was accompanied by decreased [^{3}H]cholesterol recovery in the liver and feces (**Figures 31A–D**). Notably, LXR agonist treatment of VSMCs prior to injection significantly increased [^{3}H]cholesterol levels across all compartments compared to vehicle-treated control cells (**Figures 31A–D**). In MBD-cholesterol-loaded VSMCs, LXR agonist treatment similarly enhanced RCT metrics, with increased [^{3}H]cholesterol detected in serum, HDL, and feces. However, [^{3}H]cholesterol accumulation in the liver showed only a modest, non-significant upward trend following LXR treatment (**Figures 31A–D**).

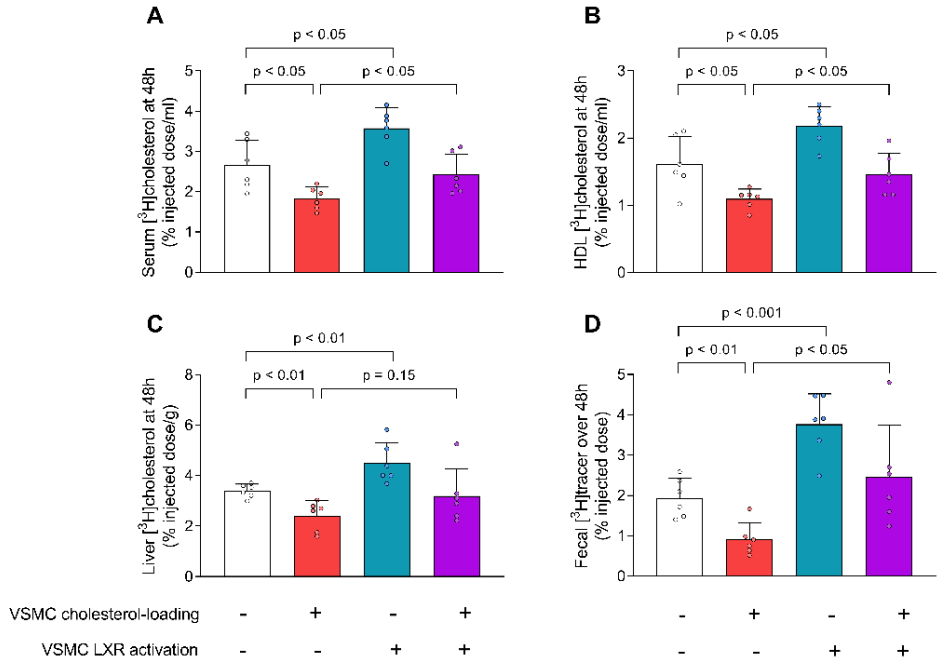

Figure 31. VSMC-to-feces RCT rate is promoted by cellular LXR agonist activation. Eight-to ten-week-old mice were fed a Western-type diet for 4 weeks. RCT was assessed using radiolabeled cholesterol-loaded VSMCs under baseline or cholesterol-loading conditions, treated with either vehicle or the LXR agonist T0901317. **(A, B)** [^{3}H]cholesterol recovery in serum and HDL fractions. **(C)** [^{3}H]cholesterol accumulation in the liver. **(D)** [^{3}H]cholesterol and [^{3}H]bile acids recovered in feces over 48 hours. Values are expressed as the mean ± SD of 6 mice per group. Radioactivity is expressed as a percentage of the injected [^{3}H]tracer dose.

2.4.ACAT inhibition normalizes the rate of RCT from VSMCs loaded with MBD-cholesterol to feces *in vivo*

To further investigate the mechanism by which MBD-cholesterol reduces the VSMC-to-feces RCT rate, we examined the bioavailability of radiolabeled unesterified cholesterol within VSMCs and assessed whether ACAT inhibition could restore cholesterol mobilization and transport.

Thin-layer chromatography analysis showed that over 94% of the radiolabeled cholesterol was found in its unesterified form in control VSMCs. In contrast, exposure to MBD-cholesterol led to a marked reduction in the proportion of radiolabeled unesterified cholesterol, lowering it to 75% (**Figure 32A**). Notably, treatment of MBD-cholesterol-loaded VSMCs with an ACAT inhibitor effectively reversed this effect, restoring radiolabeled unesterified cholesterol levels to those observed in control cells (**Figure 32A**). Functionally, ACAT inhibition fully normalized cholesterol efflux from MBD-cholesterol-loaded VSMCs to serum *in vitro*, and this effect was further enhanced by concomitant treatment with the LXR agonist (**Figure 32B**).

In vivo, when MBD-cholesterol-loaded VSMCs treated with the ACAT inhibitor were injected into wild-type mice, the levels of [^{3}H]cholesterol recovered in both serum and feces were similar to those observed following injection of unloaded, untreated VSMCs. Moreover, pretreatment with the LXR agonist further enhanced the overall transfer of [^{3}H]cholesterol from MBD-cholesterol-loaded, ACAT-inhibited VSMCs to serum and feces (**Figures 32C and 32D**).

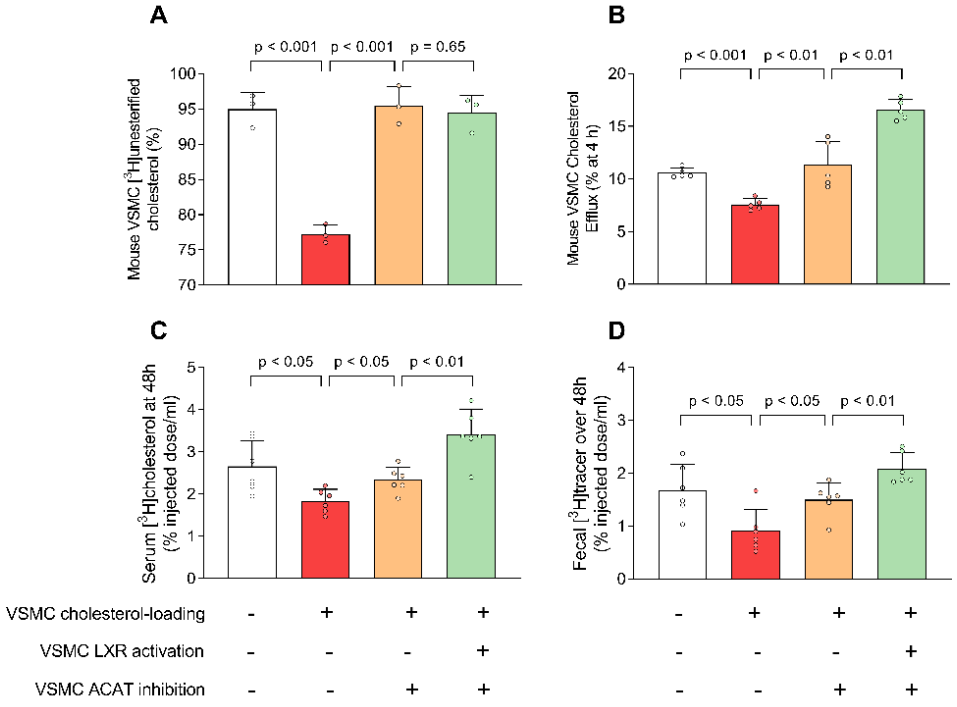

Figure 32. ACAT inhibition restores VSMC-derived cholesterol bioavailability and promotes cholesterol efflux and RCT rates. VSMCs were radiolabeled under baseline or cholesterol-loading conditions and treated with vehicle or the LXR agonist T0901317, with or without an ACAT inhibitor. **(A)** Thin-layer chromatography analysis of cellular [^{3}H]unesterified and esterified cholesterol. Three independent experiments per group are shown. **(B)** Cholesterol efflux from VSMCs to serum. Five independent experiments per group are shown. **(C, D)** RCT was assessed in eight-to ten-week-old mice fed a Western-type diet for 4 weeks using radiolabeled VSMCs. [^{3}H]cholesterol recovery in serum and feces. Six mice per group were used. Radioactivity is expressed as a percentage of the injected [^{3}H]tracer dose. Data are presented as mean ± SD.

3. RESULTS FROM WORK 3

The results presented in this section derive from our work published in *Publication 4* (see Annex).

3.1. CSF cholesterol and APO levels are similar in patients with AD and control individuals

CSF AD biomarkers and CSF cholesterol and APO levels are shown in **Table 3**.

Table 3. Population characteristics and CSF parameters in control subjects (n=10) and AD patients (n=10).

	Control (n=10)	AD (n=10)	p-value
Biological sex (Males/Females)	8/2	4/6	-
Age (years)	68.6 ± 3.1	72.3 ± 2.7	< 0.05
APOE-ε4 carriers	0/10	7/10	< 0.01
CSF parameters			
$A\beta_{1-42}$ (pg/mL)	1198.0 ± 330.2	479.1 ± 117.1	< 0.001
$A\beta_{1-40}$ (pg/mL)	11762.4 ± 2730.6	11041.3 ± 2615.8	0.55
$A\beta_{1-42}/A\beta_{1-40}$ ratio	0.10 ± 0.01	0.04 ± 0.01	< 0.001
t-Tau (pg/mL)	258.5 ± 52.3	763.4 ± 429.82	< 0.01
p-Tau (pg/mL)	36.3 ± 6.7	121.15 ± 62.8	< 0.001
Total cholesterol (µg/mL)	3.23 ± 0.71	3.21 ± 1.27	0.79
Free cholesterol (µg/mL)	1.63 ± 0.35	1.67 ± 0.83	0.91
APOA1 (µg/mL)	0.60 ± 1.01	0.34 ± 0.52	0.48
APOE (µg/mL)	17.3 ± 9.2	16.5 ± 7.2	0.83
APOJ (µg/mL)	10.1 ± 2.2	10.7 ± 4.0	0.67
PCSK9 (ng/mL)	3.23 ± 1.08	3.18 ± 1.56	0.94

Data are presented as the mean ± SD.

As expected, AD patients displayed significantly higher CSF concentrations of t-Tau and p-Tau, along with decreased levels of $A\beta_{1-42}$ and a lower $A\beta_{1-42}/A\beta_{1-40}$ ratio compared to control individuals (**Table 3**). Among AD patients, APOE-ε4 allele was more frequent, including individuals with APOE-ε4/ε3 (n = 6) and APOE-ε4/ε4 (n = 1) genotypes, whereas all control participants carried the APOE-ε3/ε3 genotype (**Table 3**).

CSF concentrations of total cholesterol, free cholesterol, APOA1, APOE, APOJ, and PCSK9 were similar between AD patients and cognitively healthy control individuals (**Table 3**). Importantly, APOE levels did not differ significantly between male and female AD patients (p=0.41).

3.2.Astrocyte cholesterol efflux to CSF is similar in patients with AD and control individuals

To determine the cholesterol efflux capacity of CSF from AD patients and control individuals, A172 human glioblastoma astrocytes were radiolabeled with [^{3}H]cholesterol and incubated with CSF samples. Under baseline conditions, astrocytes showed low cholesterol efflux, whereas treatment with the LXR agonist significantly increased cholesterol release to the media (**Figure 33A, left panel**). Consistent with this response, astrocytes exposed to the LXR agonist showed marked upregulation of ABCA1 and ABCG1 gene expression (**Figure 33B and 33C**).

When astrocytes were incubated with CSF from either control individuals or AD patients, cholesterol efflux was similar between groups under baseline conditions (**Figure 33A, left panel**). Furthermore, ABCA1/G1-dependent cholesterol efflux—calculated as the net increase in efflux after LXR agonist treatment—did not differ between CSF from AD and control individuals (**Figure 33A, right panel**).

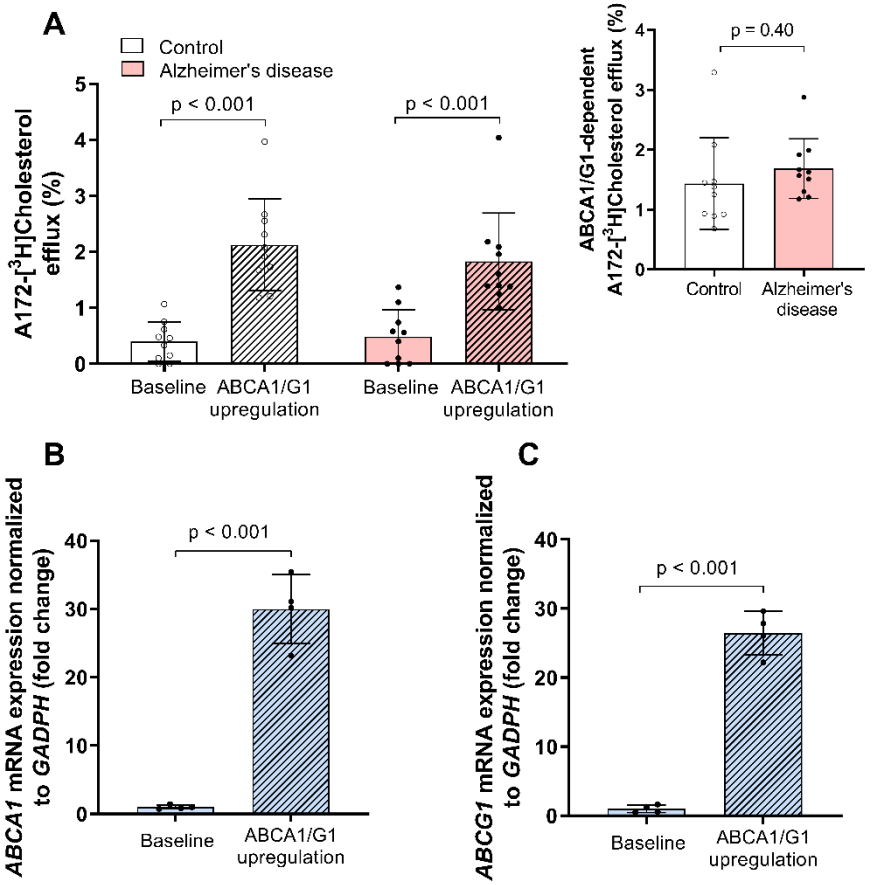

Figure 33. Astrocyte cholesterol efflux to CSF remains similar in AD and control groups. Human glioblastoma astrocytes were loaded with radiolabeled cholesterol and treated with vehicle or the LXR agonist T0901317. **(A)** Cholesterol efflux was assessed by incubating cells with serum-free medium containing CSF from control (n=10) or AD individuals (n=10) for 4 hours. Left panel: Cholesterol efflux under baseline and LXR-activated conditions. Right panel: ABCA1/G1-dependent efflux calculated by subtracting baseline values from LXR-induced responses. **(B, C)** Relative mRNA expression of ABCA1 and ABCG1, normalized to GAPDH. Baseline expression set to 1 arbitrary unit. Four independent experiments are shown. Data are expressed as the mean ± SD.

3.3. Cholesterol delivery to neurons is impaired in patients with AD

To evaluate the ability of CSF to mediate cholesterol delivery to neurons, [^{3}H]cholesterol was incorporated into HDL-like particles present in CSF samples, and its uptake was assessed in differentiated SH-SY5Y human neurons.

We compared HDL-like-mediated cholesterol uptake from CSF samples acquired from AD patients and control individuals. Within a 4-hour incubation period, neurons exposed to CSF from AD patients exhibited a significantly lower uptake of radiolabeled cholesterol compared to those incubated with CSF from control individuals (**Figure 34A**).

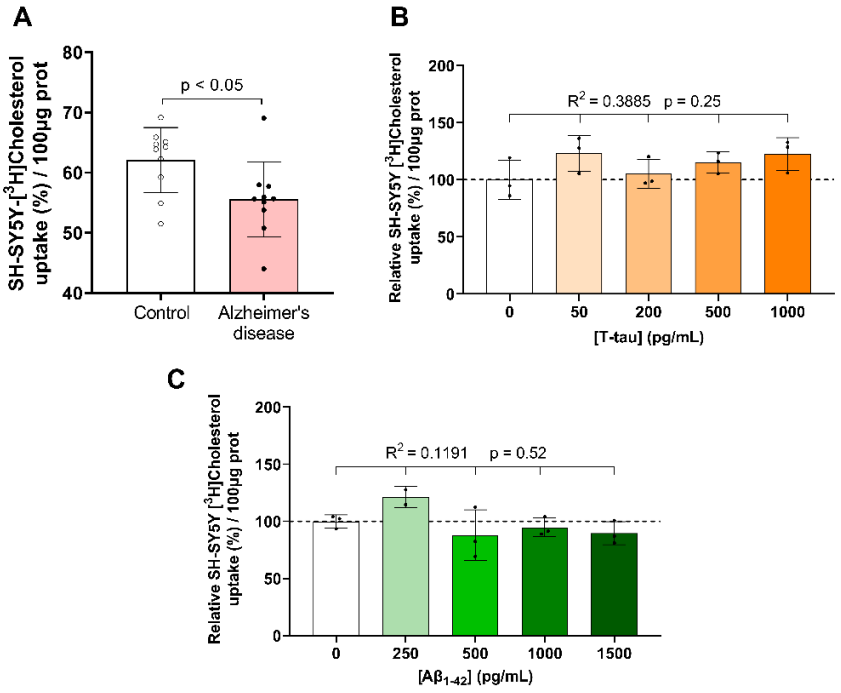

Figure 34. CSF HDL-like–mediated cholesterol delivery to neurons is impaired in AD. Differentiated human neuroblastoma cells were incubated with radiolabeled CSF HDL-like particles, with [^{3}H]cholesterol, for 4 hours. **(A)** Cholesterol uptake from radiolabeled CSF-derived HDL-like particles from control individuals (n=10) and patients with AD (n=10). **(B, C)** Cholesterol uptake from radiolabeled control CSF HDL-like particles in the presence of increasing concentrations of Tau (up to 1,000 pg/mL) or Aβ1-42 (up to 1,500 pg/mL) added to the culture medium. Three independent experiments per condition are shown. Data are presented as mean ± SD.

We then investigated whether Tau protein or Aβ peptide could directly impact cholesterol uptake from CSF in neurons. To test this, increasing concentrations of purified t-Tau protein or $A\beta_{1-42}$were added to the conditioned media during the cholesterol uptake assay. Under these conditions, neither t-Tau or $A\beta_{1-42}$ significantly affected the percentage of radiolabeled cholesterol uptake by neurons (**Figure 34B and 34C**). Consistent with these findings, correlation analyses revealed no significant associations between impaired neuronal cholesterol uptake and CSF levels of AD biomarkers or cholesterol-related parameters (**Table 4**).

Table 4. Association of cholesterol uptake with CSF biochemical parameters.

	Pearson r	p-value
$A\beta_{1-42}$ (pg/mL)	0.4081	0.07
$A\beta_{1-40}$ (pg/mL)	0.2206	0.35
$A\beta_{1-42}/A\beta_{1-40}$ ratio	0.4359	0.05
t-Tau (pg/mL)	- 0.0145	0.95
p-Tau (pg/mL)	- 0.0960	0.68
Total cholesterol (µg/mL)	- 0.1300	0.59
Free cholesterol (µg/mL)	0.2029	0.39
APOA-I (µg/mL)	0.0601	0.80
APOE (µg/mL)	- 0.1484	0.53
APOJ (µg/mL)	0.1086	0.65
PCSK9 (ng/mL)	- 0.1105	0.64

Furthermore, cholesterol uptake was not associated with age in either control subjects (Pearson r = 0.37, p = 0.29) or AD patients (Pearson r = –0.10, p = 0.66). Additionally, within the AD group, where sex distribution was balanced, no significant differences in cholesterol uptake were observed between males and females (p = 0.70).

3.4.APOE4-containing HDL displays reduced efficiency in delivering cholesterol to neurons

To explore the impact of APOE isoforms on cholesterol transport, synthetic rHDL nanoparticles were assembled using recombinant human APOE3 or APOE4, phospholipids, and cholesterol. Both rHDL-APOE3 and rHDL-APOE4 nanoparticles exhibited similar electrophoretic migration patterns (Figure 35A). Dynamic light scattering confirmed that particle sizes were similar between the two nanoparticle types (Figure 35B and 35C). Additionally, the cholesterol-to-APOE ratios were nearly identical (0.278 for rHDL-APOE3 and 0.287 for rHDL-APOE4).

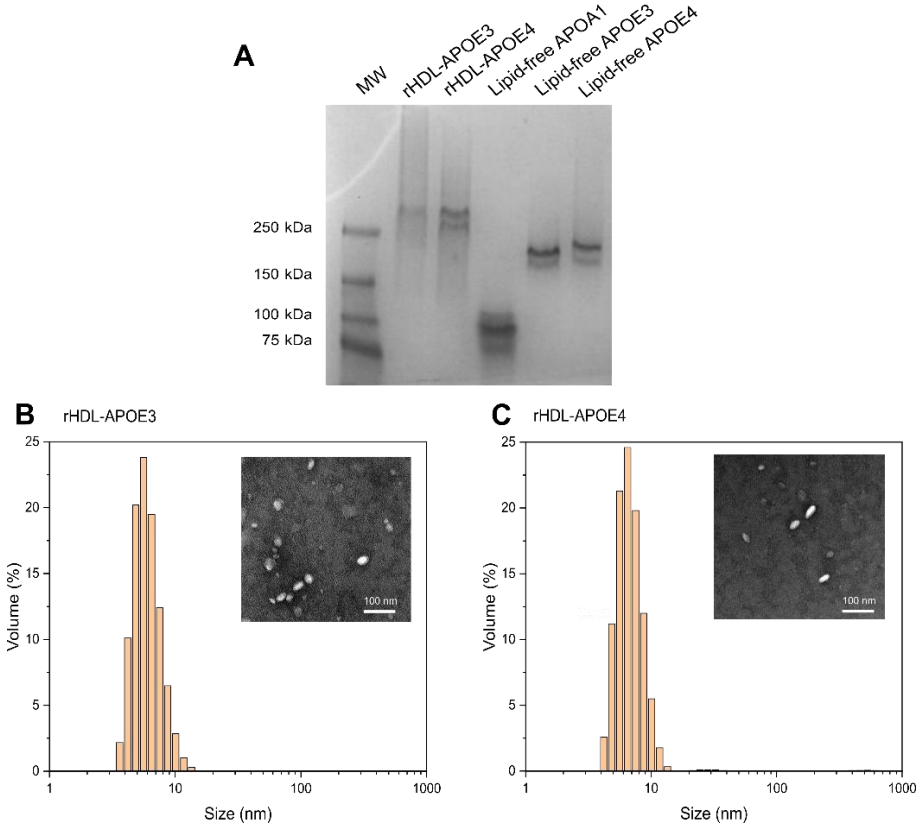

Figure 35. rHDL-APOE nanoparticles exhibit similar electrophoretic mobility and size distribution. (A) Native gel electrophoresis visualized by Coomassie Blue staining. **(B, C)** Particle size distributions of rHDL-APOE3 and rHDL-APOE4 nanoparticles analyzed by dynamic light scattering. Representative intensity-based size profiles are shown, with corresponding images of nanoparticles displayed as insets.

We next examined whether these rHDL nanoparticles could mediate cholesterol efflux. Both rHDL-APOE3 and rHDL-APOE4 nanoparticles induced similar levels of cholesterol efflux from astrocytes (**Figure 36A**).

To evaluate neuronal interaction with rHDL nanoparticles, Oregon Green–labeled phospholipid was incorporated in their core and incubated with SH-SY5Y neurons for 4 hours. No fluorescence was detected in control cells, whereas both rHDL-APOE3 and rHDL-APOE4 delivered fluorescent phospholipids to neurons, as visualized by confocal microscopy (**Figures 36B**). Flow cytometry analysis revealed a trend toward reduced internalization of rHDL-APOE4–associated phospholipids compared to rHDL-APOE3 (**Figure 36C**). Furthermore, when assessing cholesterol uptake by SH-SY5Y neurons, rHDL-APOE4 particles promoted significantly lower uptake of radiolabeled cholesterol than rHDL-APOE3 (**Figure 36D**).

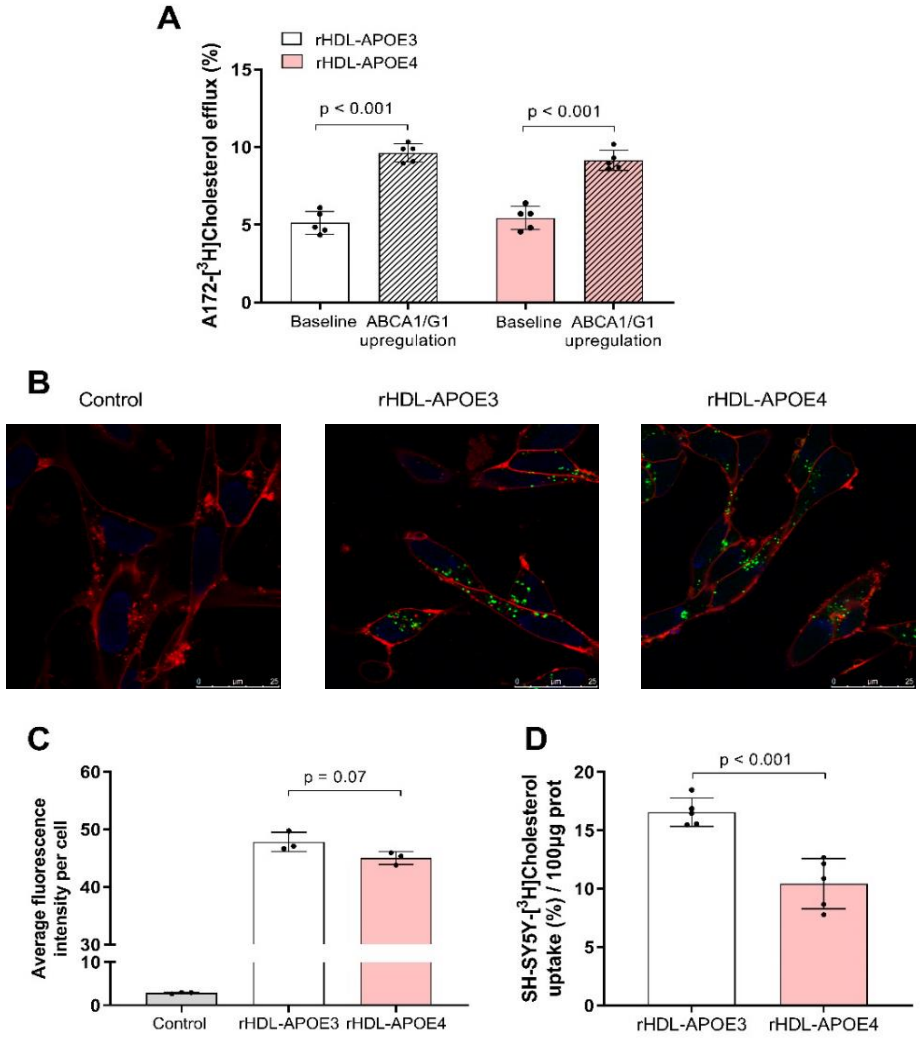

Figure 36. APOE4-containing rHDL has a lower ability to deliver cholesterol to neurons. **(A)** Cholesterol efflux from human astrocytes to rHDL-APOE3 or rHDL-APOE4 under baseline conditions and following LXR agonist T0901317 treatment. Five independent experiments are shown. **(B)** Confocal microscopy images of human neurons under three conditions: untreated (control), incubated with rHDL-APOE3, and incubated with rHDL-APOE4. Oregon Green–labeled phospholipids were used to assess nanoparticle uptake. **(C)** Quantification of phospholipid internalization in neurons by flow cytometry under the same conditions. Three independent experiments are shown. **(D)** Neuronal cholesterol uptake mediated by rHDL-APOE3 and rHDL-APOE4 nanoparticles. Five independent experiments are shown. Data are presented as the mean ± SD.

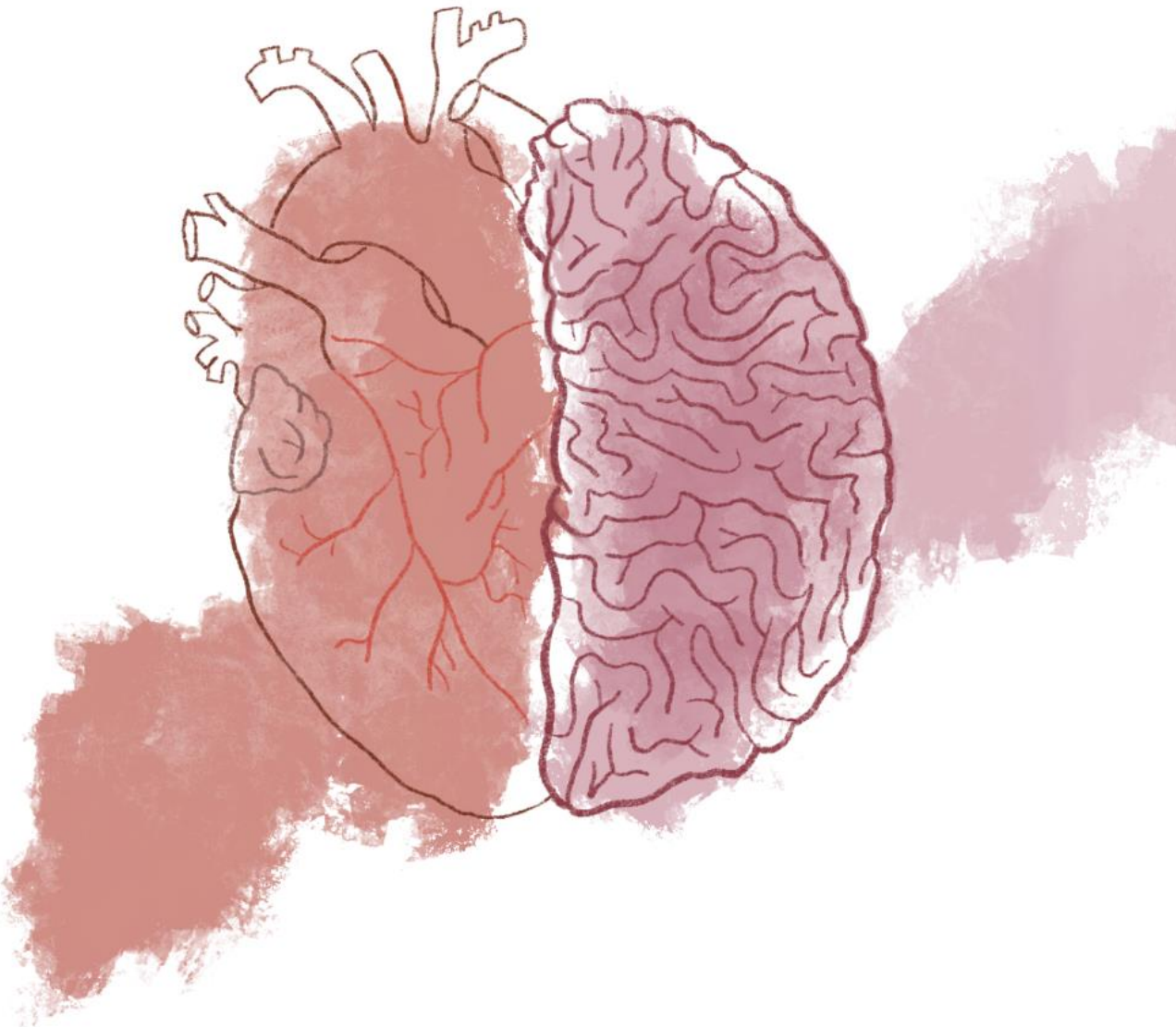

CHAPTER V

DISCUSSION

DISCUSSION OF RESULTS FROM WORK 1

The identification of PCSK9 as a therapeutic target marked a turning point in cholesterol-lowering strategies, offering a promising option for patients with FH or those unresponsive to conventional lipid-lowering treatments. PCSK9-neutralizing antibodies, such as evolocumab and alirocumab, have since emerged as effective tools in clinical practice, helping to achieve LDL-cholesterol goals in high-risk individuals.[64,65] In the present study, we evaluated 14 heterozygous FH patients before and after treatment with evolocumab. As expected, the therapy significantly reduced circulating LDL-cholesterol and APOB levels, confirming its efficacy in this cohort.

Evolocumab treatment modulates the lipoprotein distribution of macrophage-derived cholesterol efflux towards the HDL fraction

Previous studies have shown that plasma or HDL derived from untreated heterozygous FH patients exhibits a reduced capacity to promote cholesterol efflux from macrophages compared to normolipidemic controls.[103] Intriguingly, while HDL functions as the primary cholesterol efflux acceptor, LDL has been identified as the major intermediate reservoir for unesterified cholesterol effluxed from macrophages,[99,103] indicating a more relevant role of this lipoprotein in the overall RCT pathway. PCSK9 inhibitors have been reported to cause modest alterations in HDL particle number and size; however, findings across studies have been inconsistent,[104,105] and these changes do not appear to significantly impact the overall cholesterol efflux capacity mediated by HDL.[106–108] However, the potential influence of PCSK9 inhibitors on the role of LDL as a macrophage-derived cholesterol reservoir has remained unexplored.

Our data show that evolocumab therapy did not significantly alter the total cholesterol efflux capacity of plasma from FH patients assessed *ex vivo*. However, when analyzing the plasma lipoprotein fractions post-efflux, a redistribution of radiolabeled macrophage-derived cholesterol was observed. Specifically, HDL-

associated radiolabeled cholesterol was increased, while radiolabeled cholesterol associated with LDL was significantly reduced in post-treatment samples. These findings suggest that, although total efflux remained unchanged, evolocumab was able to modulate the trafficking of macrophage-derived cholesterol between lipoproteins, favoring its association with HDL over LDL.

Importantly, PCSK9 inhibition treatment did not affect the activities of CETP, PLTP, or LCAT, which are key lipoprotein remodeling enzymes. These findings indicate that the observed lipoprotein shifts occurred independently of major lipid transfer or esterification processes. They also reveal that PCSK9 inhibition could not restore the enzymatic activity alterations reported in FH patients.[103]

In our experiments investigating the competitive dynamics between LDL and HDL in cholesterol acceptance and trafficking, we observed that at high LDL concentrations, this lipoprotein efficiently acquired macrophage-derived radiolabeled cholesterol, acting as a transient reservoir. Conversely, as LDL concentrations decreased, radiolabeled cholesterol was predominantly recovered in the HDL fraction, indicating a shift in reservoir preference. Importantly, in plasma from anti-PCSK9-treated FH patients, the transfer of cholesterol from macrophages to LDL was markedly reduced, with unesterified cholesterol instead accumulating within HDL particles. This redistribution suggests a PCSK9 inhibitor–induced shift in lipoprotein-mediated cholesterol trafficking of macrophages, potentially influencing the efficiency of RCT. However, whether this altered redistribution among lipoproteins translates into enhanced cholesterol elimination *in vivo* required further investigation.

PCSK9 inhibition mimics lipoprotein redistribution of macrophage-derived cholesterol and enhances macrophage-to-feces RCT *in vivo*

To address this point, we established a murine model of FH by crossbreeding LDLR-deficient mice with human APOB100 transgenic mice, generating heterozygous LDLR-deficient mice expressing human APOB100, which

recapitulates key aspects of human FH pathology. In this model, treatment with the PCSK9-mAb1 significantly reduced plasma APOB100 and LDL-cholesterol levels induced by Western-type diet feeding.

When assessing the macrophage-specific RCT pathway *in vivo*, we found that PCSK9 inhibition led to a reduced retention of macrophage-derived cholesterol in the LDL fraction, accompanied by a corresponding increase in radioactivity within the HDL fraction. This lipoprotein redistribution closely mirrored the pattern observed in FH patient plasma following PCSK9 inhibitor therapy. Consistently, PCSK9-mAb1 therapy did not alter the PLTP and LCAT activities in FH mice, supporting that lipoprotein redistribution occurred independently of the main lipoprotein remodeling factors also in mice.

Notably, mice treated with PCSK9-mAb1 exhibited increased recovery of radiolabeled cholesterol in feces, indicating enhanced cholesterol elimination. These findings suggest that by preventing the sequestration of macrophage-derived cholesterol in LDL, PCSK9 inhibitors may also facilitate its transfer to HDL, thereby promoting the overall efficiency of the RCT pathway.

It is important to emphasize that cholesterol efflux from macrophages is a key protective mechanism against atherosclerosis.[109] While the peritoneal cavity does not fully replicate the arterial intima, where LDL particles are predominantly retained within the extracellular matrix via proteoglycan binding and subsequently modified and taken up by macrophages,[110] it does share relevant physiological features. Specifically, HDL particles exit both environments through the lymphatic circulation, which constitutes a central route in the RCT pathway.[111] Therefore, the observed increase in radiolabeled HDL-cholesterol derived from macrophages, including in FH subjects, likely reflects enhanced mobilization and clearance of macrophage-derived cholesterol from the body.

LDL-cholesterol clearance is potentiated by PCSK9 antibody treatment

We next aimed to determine whether the enhanced RCT observed in LDLR+/-hAPOB100 mice following PCSK9 inhibition was attributable to increased clearance of LDL- or HDL-associated cholesterol. Previous studies have demonstrated that functional LDLR is essential for sustaining CETP-independent RCT *in vivo* by mediating the hepatic uptake and subsequent fecal excretion of macrophage-derived cholesterol transported in LDL particles.[99] In contrast, HDL-cholesterol is primarily taken up by the liver via SR-BI and to a lesser extent through ABCA1-mediated pathways.[21,23]

Following the injection of [^{3}H]LDL-cholesterol ester, mice treated with PCSK9-mAb1 exhibited a more rapid clearance of [^{3}H]cholesterol from plasma, accompanied by a reduced hepatic accumulation and increased fecal excretion. These findings indicate that PCSK9 inhibition enhances the removal of LDL-associated cholesterol in LDLR+/- hAPOB100 mice. In contrast, PCSK9-mAb1 treatment had no effect on the clearance of [^{3}H]HDL-cholesterol ester, suggesting that the treatment mainly enhances the catabolism of LDL-derived cholesterol.

Notably, hepatic cholesterol is ultimately secreted into bile and the intestinal lumen as unesterified cholesterol via the ABCG5 and ABCG8 transporters.[112] Although the expression of these transporters was not directly modulated by anti-PCSK9 treatment, their levels are known to be upregulated by dietary cholesterol such as that provided by a Western-type diet.[113] Therefore, the marked upregulation of functional LDLR in PCSK9 antibody-treated LDLR+/-hAPOB100 mice, in conjunction with the sustained high expression of ABCG5 and ABCG8, supports the hypothesis that the hepatobiliary route of LDL-cholesterol elimination plays a central role in mediating the enhanced fecal cholesterol excretion observed in this model. Taken together, our data indicate that PCSK9 inhibition promotes an efficient pathway for LDL-derived cholesterol clearance, thereby contributing to improved RCT.

Altogether, our work demonstrates that treatment with evolocumab in FH patients, and with a PCSK9 monoclonal antibody in a humanized FH mouse model, promotes a redistribution of macrophage-derived cholesterol from LDL to HDL, without altering total efflux capacity or the activity of key remodeling enzymes. This shift was accompanied by increased fecal cholesterol excretion in heterozygous LDLR-deficient mice expressing human APOB100, driven specifically by enhanced clearance of LDL-associated cholesterol via upregulated LDLR (**Figure 37**). These findings highlight a mechanistic pathway through which PCSK9 inhibitors increase RCT, contributing to atheroprotection beyond their LDL-lowering effects alone.

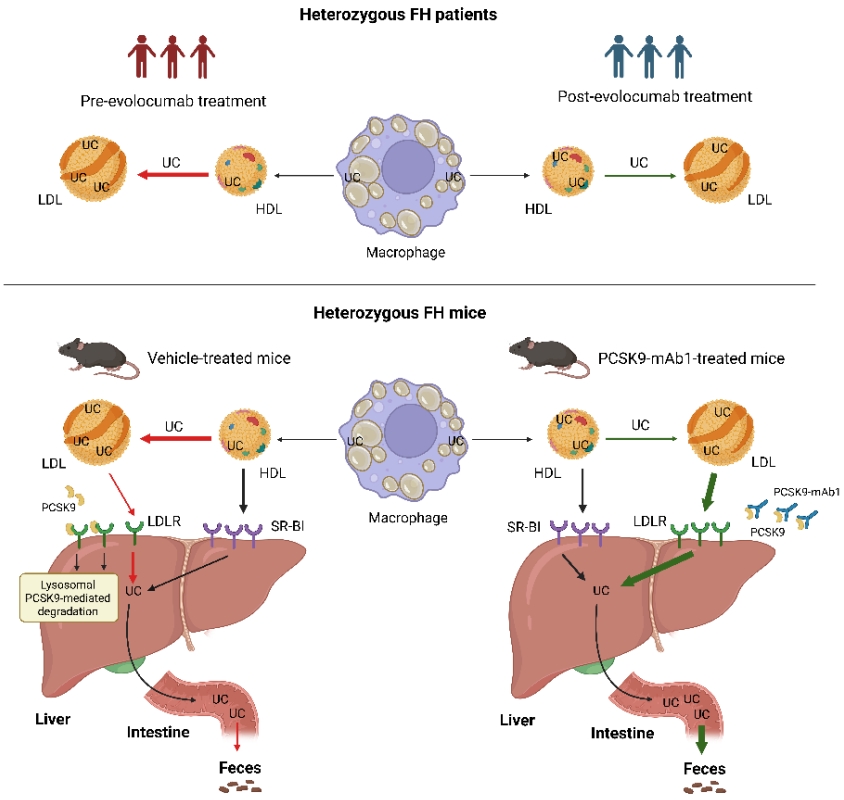

Figure 37. Proposed model for work 1. PCSK9 inhibition promotes the redistribution of macrophage-derived cholesterol from LDL to HDL and enhances macrophages-to-feces RCT pathway by accelerating hepatic clearance of LDL particles. UC: unesterified cholesterol. Created with *Biorender.com*

DISCUSSION OF RESULTS FROM WORK 2

The present work builds on the increasing recognition of VSMCs as a substantial source of foam cells within atherosclerotic plaques. While foam cells were traditionally considered to originate predominantly from macrophages, recent studies have demonstrated that VSMC may account for 30–70% of foam cell population in human atherosclerotic lesions.[50,114–118] This paradigm shift has changed our understanding of plaque development and progression, emphasizing the phenotypic plasticity of VSMCs and their active involvement in lipid accumulation. Despite these insights, the molecular and cellular mechanisms governing cholesterol handling in lipid-loaded VSMCs remain poorly understood. In particular, the capacity of VSMC-derived foam cells to participate in RCT, and whether this process can be modulated by LXR activation has yet to be assessed.

Cholesterol loading drives phenotypic switching and dysfunctional cholesterol efflux in VSMCs

To begin addressing this, we first evaluated whether immortalized mouse aortic VSMCs are capable of undergoing a foam cell-like transformation characterized by intracellular lipid accumulation and phenotypic plasticity. The cholesterol-loading model using MBD-cholesterol effectively induced lipid accumulation in VSMCs, demonstrating their ability to uptake and store cholesterol. In parallel, the observed changes in gene expression, including increased CD68 and decreased TAGLN, further corroborate a phenotypic switch toward a macrophage-like state, as previously reported.[48] These findings reinforce the evolving understanding that VSMCs actively contribute to foam cell populations within atherosclerotic plaques, in addition to their traditional structural role.

Initially, we confirmed that both whole serum and APOB-depleted serum, rich in HDL and lipid transfer proteins, effectively promoted cholesterol efflux from immortalized mouse aortic VSMCs. In contrast, cholesterol efflux capacity was significantly impaired following MBD-cholesterol loading, reflecting features

commonly associated with macrophage-derived foam cells. This dysfunction underscores a substantial disruption in cholesterol handling in foam-like VSMCs, further supporting their active role in plaque lipid accumulation.

Interestingly, we observed that ABCA1 expression was upregulated in VSMCs exposed to MBD-cholesterol. This finding contrasts with reports showing reduced ABCA1 expression in human intimal and rat intimal-like VSMCs.[50,119] However, it aligns with other studies demonstrating increased expression in cholesterol-loaded mouse VSMCs.[48,114,115] Although we did not evaluate ABCA1 protein expression in our work, discrepancies in mRNA *Abca1* expression suggest that ABCA1 regulation in VSMCs may differ depending on the context, and may be influenced by species or the nature of cholesterol loading. The observed ABCA1 upregulation may represent a compensatory response aimed at limiting intracellular lipid accumulation. Nevertheless, this response is not sufficient to prevent foam cell transformation under hypercholesterolemic conditions, featuring a functional disconnect between ABCA1 expression and effective cholesterol efflux in VSMCs.

LXR activation enhances cholesterol efflux in VSMCs, but foam cell transformation limits its efficacy

The activation of LXRs has been well established as a potent enhancer of macrophage-specific cholesterol efflux and RCT *in vivo*,[120–122] and thus represents a promising strategy for attenuating atherosclerosis. In this context, elucidating the role of LXR signaling in regulating the entire VSMC-specific RCT pathway, under both baseline conditions and following foam-cell like transformation, is of particular interest.

Consistent with its known effects in macrophages, treatment with the LXR agonist T0901317 significantly enhanced cholesterol efflux from VSMCs. This supports the concept that LXR-mediated upregulation of ABCA1 is an effective mechanism to facilitate lipid removal from VSMCs.

Differently, the cholesterol efflux response to LXR activation was markedly attenuated in MBD-cholesterol–loaded VSMCs. While LXR stimulation still promoted efflux in these lipid-laden cells, the extent of this response was substantially reduced compared to non-lipid-laden VSMCs, even though ABCA1 expression was more strongly induced. This reveals intrinsic limitations in the ability of foam cells to mobilize intracellular cholesterol effectively, likely due to altered cellular architecture, impaired transporter trafficking, or reduced interaction with cholesterol acceptors following phenotypic transformation.

The critical role of ABCA1 in mediating this process was further confirmed by the complete abrogation of LXR-stimulated cholesterol efflux in the presence of probucol, an ABCA1 specific inhibitor that specifically blocks APOA1 binding without affecting passive lipid exchange mechanisms.

In contrast to our findings, previous studies have reported a complete failure of LXR-mediated cholesterol efflux in intimal-like VSMCs derived from Wistar-Kyoto rat arteries, possibly as a result of the absence of key membrane or cytoskeletal component required for APOA1 interaction.[119] Together, these findings manifest species-specific differences in cholesterol efflux regulation in VSMCs and emphasize the need for further investigation into the molecular mechanisms and structural factors that modulate this pathway across different experimental models.

Targeted LXR activation restores *in vivo* RCT from cholesterol-loaded VSMCs

In line with our *in vitro* findings, the *in vivo* RCT assay revealed a markedly impaired cholesterol clearance from MBD-cholesterol-loaded VSMCs. Radiolabeled cholesterol recovery in serum, HDL, liver, and feces was significantly reduced compared to non-lipid-laden VSMCs, reflecting the physiological limitations of cholesterol mobilization from foam cell–like VSMCs.

This impairment underscores the pathological relevance of VSMC-derived foam cells as inefficient contributors to RCT in the atherosclerotic context.

Importantly, pre-treatment of both native and lipid-loaded VSMCs with the LXR agonist T0901317 significantly enhanced RCT efficiency. Increased radiolabeled cholesterol levels were detected in serum, HDL fraction, and feces, demonstrating that LXR activation boosts the mobilization and excretion of cholesterol from VSMCs *in vivo*, even under foam cell–like conditions. These results confirm that pharmacological activation of LXR restores, at least partially, the efflux and transport defects inherent to cholesterol-laden VSMCs.

Crucially, these findings support cell-specific activation of LXR in VSMCs as a more desirable therapeutic strategy over systemic activation. While systemic LXR stimulation is effective in promoting RCT,[122] it has also been reported to induce lipogenesis and hepatic lipid accumulation, raising concerns over potential adverse effects such as hepatic steatosis.[123] By contrast, targeted modulation of LXR activity within the vascular wall, particularly in VSMCs, could facilitate cholesterol removal from plaques while minimizing hepatic side effects, offering a safer and more focused approach to atherosclerosis treatment.

ACAT inhibition and LXR activation synergistically enhance cholesterol mobilization from VSMC-derived foam cells

Given that ACAT is the key enzyme catalyzing the esterification of free cholesterol into cholesteryl esters for storage within lipid droplets, we sought to determine whether its inhibition could enhance cholesterol mobilization in foam cell–like VSMCs. Selective pharmacological inhibition of ACAT restored the pool of bioavailable, unesterified radiolabeled cholesterol in cholesterol-loaded VSMCs. This increase in free cholesterol coincided with a significant recovery of cholesterol efflux and RCT rates, reaching levels similar to those observed in non-lipid-laden control cells. These findings support the notion that blocking

cholesterol esterification facilitates the redistribution of intracellular cholesterol toward transport pathways rather than storage compartments.

Notably, ACAT inhibition has previously been shown to reduce cholesterol accumulation and promote cholesterol efflux in human macrophages,[124–126] highlighting its role as a modulator of intracellular cholesterol homeostasis. Nonetheless, the therapeutic potential of ACAT inhibitors has been questioned due to cytotoxic effects observed in foam cells derived from mouse macrophages, where pharmacological inactivation of ACAT led to cholesterol-induced cell toxicity and death.[127,128] In contrast, both human and rat aortic VSMCs appear to be more resilient to cholesterol accumulation and ACAT inhibition. These cells demonstrate an ability to reduce foam cell formation in response to ACAT inhibition without triggering cytotoxic responses.[129] These results emphasize the sensitivity of different cell types and species to cholesterol ester accumulation and mobilization, and reinforce the selective inhibition of ACAT in VSMCs as a feasible targeted therapeutic strategy.

Building on this, our experiments demonstrated that the combined application of an LXR agonist and an ACAT inhibitor synergistically enhanced cholesterol efflux and markedly promoted *in vivo* RCT from VSMC-derived foam cells. This combinatorial approach appeared to overcome the intrinsic limitations of cholesterol mobilization in heavily lipid-laden VSMCs, where either treatment alone achieved only partial restoration. By simultaneously increasing the bioavailability of unesterified cholesterol (via ACAT inhibition) and upregulating efflux transporters (via LXR activation), this strategy effectively reestablished cholesterol trafficking.

Overall, our study highlights the active and pathological role of VSMC-derived foam cells in atherosclerosis. Cholesterol loading induced a phenotypic switching and functional dysfunction in VSMCs, resulting in defective cholesterol efflux. While LXR activation enhanced cholesterol efflux in baseline conditions, its

efficacy was diminished in lipid-loaded cells, revealing intrinsic limitations in cholesterol mobilization. Importantly, the combination of LXR activation and ACAT inhibition synergistically restored cholesterol efflux and significantly improved *in vivo* RCT (**Figure 38**). These findings underscore the therapeutic potential of targeting VSMC-specific mechanisms to mobilize cholesterol and reduce plaque lipid burden, offering a novel and more precise approach to atherosclerosis treatment beyond macrophage-centered strategies.

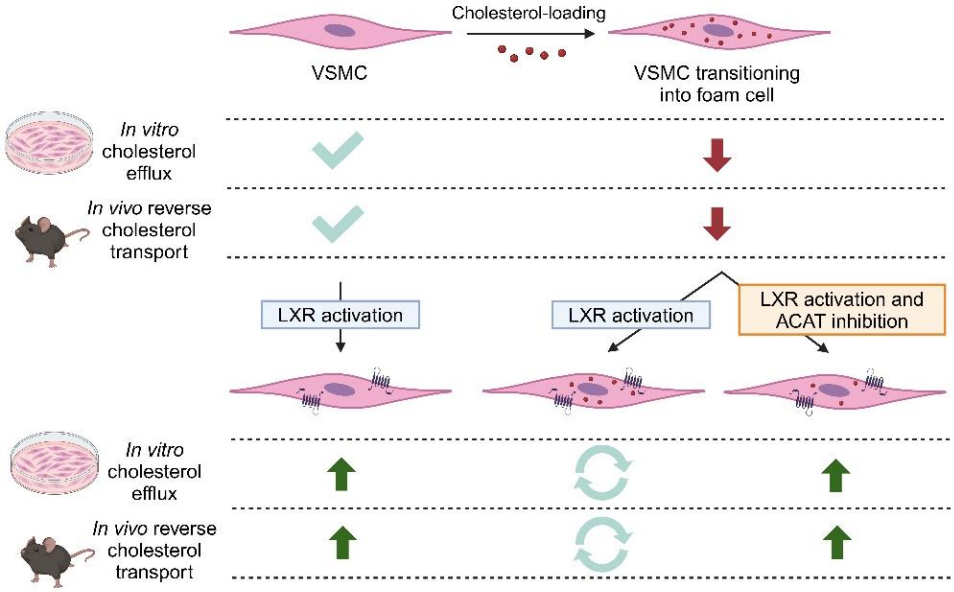

Figure 38. Proposed model for work 2. Cholesterol loading of VSMCs impairs cholesterol efflux and RCT. These defects are restored by LXR activation or ACAT inhibition, with a synergistic enhancement observed when both strategies are combined. Created with *Biorender.com*

DISCUSSION OF RESULTS FROM WORK 3

Growing evidence has increasingly highlighted the role of lipid dysregulation in AD pathogenesis. It is noteworthy that APOE-ε4 is the most well-established genetic risk factor for the disease.[85] However, the specific impact of this isoform on brain cholesterol transport is not yet fully understood. Given the essential role of cholesterol in maintaining neuronal membrane integrity and supporting synaptic function, we aimed to investigate how AD and APOE isoform status influence cholesterol transport mediated by CSF HDL-like particles.

Increased APOE-ε4 prevalence in AD patients does not alter CSF HDL-like lipid composition

The individuals included in this study were selected from the well-characterized SPIN cohort. As expected, biochemical analysis of CSF confirmed hallmark alterations associated with AD, including elevated levels of t-Tau and p-Tau, along with decreased concentrations of Aβ1-42 peptide and a reduced Aβ1-42/Aβ1-40 ratio. These findings are consistent with the established biomarker profile of AD.[130] Moreover, a higher prevalence of the APOE-ε4 allele was observed among AD patients, further supporting its strong genetic association with the disease.

Significant differences in sex distribution and age were also noted between the groups, with the AD cohort comprising a higher proportion of female patients and older individuals. These observation align with epidemiological data and meta-analyses that identify advanced age as the strongest risk factor for AD[131,132] and report a higher prevalence of the disease among women.[133]

Regarding lipid-related CSF components, our analysis revealed no significant differences in APOE concentrations between AD and control groups, which were unaffected by sex distribution. Previous studies reported conflicting results on APOE levels in AD patients,[33,134–140] and suggested that its associated risk may be

more tightly linked to APOE isoform function than to overall protein abundance. Similarly, levels of other key constituents of CSF HDL-like particles, including APOA1, APOJ, and total cholesterol, were similar between groups. Notably, although PCSK9 has been implicated in AD pathophysiology,[141] with several reports reporting elevated plasma and CSF levels in AD patients,[142–144] our data did not show significant differences in CSF PCSK9 concentrations between the two groups.

Taken together, our results indicate that despite the higher presence of the APOE-ε4 genotype in the AD group, the main lipid and protein components of CSF HDL-like particles remain unaltered.

Astrocyte cholesterol efflux to CSF HDL-like particles is similar between AD patients and control subjects

Astrocyte-mediated cholesterol efflux to CSF HDL-like lipoproteins, which mainly contain APOE, occurs via both passive diffusion and active pathways facilitated by the transporters ABCA1 and ABCG1.[145,146] We evaluated the ability of human A172 glioblastoma astrocytes to mediate cholesterol efflux to CSF under basal conditions and following activation of the ABCA1- and ABCG1-dependent pathways.

In line with findings from rat astrocyte models,[33] we observed no significant difference in cholesterol efflux to CSF between AD and control groups, regardless of transporter pathway activation. However, this results contrast with a previous report using human U373-MG astrocytoma cells, where CSF from AD patients exhibited a reduced capacity to promote cholesterol efflux following ABCA1/ABCG1 stimulation.[147] Notably, that study reported elevated CSF APOE levels in AD, which may have contributed to the impaired efflux, an effect similarly described in macrophages.[148]

CSF HDL-like-mediated cholesterol delivery to neurons is impaired in AD patients

To investigate cholesterol delivery to neurons, we developed a sensitive isotopic uptake assay that involved the incorporation of radiolabeled unesterified cholesterol into the CSF HDL-like particles. This approach allowed us to evaluate the ability of differentiated SH-SY5Y human neurons to acquire cholesterol directly from the radiolabeled CSF HDL-like particles.

Our findings revealed a significant reduction in cholesterol uptake by neurons when exposed to CSF from AD patients compared to control CSF. This suggests a compromised efficiency of cholesterol delivery to neurons in the context of AD, potentially contributing to impaired neuronal membrane synthesis, synaptic function, and overall neurodegeneration.

To determine whether hallmark pathological proteins of AD might influence this transport deficit, we next examined the effect of Aβ and tau on cholesterol uptake. The addition of these proteins to the assay system did not alter neuronal cholesterol acquisition from CSF, indicating that their presence alone does not account for the observed impairment in cholesterol delivery. This implies that the reduced uptake is likely driven by intrinsic changes in the lipid or protein composition of HDL-like particles in AD CSF, rather than by direct interference from Aβ or tau.

These results highlight a previously underexplored aspect of lipid dysregulation in AD and suggest that altered cholesterol transport dynamics—particularly reduced delivery to neurons—may be an early and contributing factor in disease progression.

APOE4 in rHDL-like particles impairs cholesterol delivery to neurons

To explore whether the cholesterol transport alterations observed in AD could stem from functional differences among APOE isoforms, we directly compared the effects of rHDL nanoparticles containing either APOE3 or APOE4 on cholesterol efflux and uptake.

Our results showed that cholesterol efflux from human A172 glioblastoma astrocytes did not differ between rHDL-APOE3 and rHDL-APOE4, indicating similar capacity to accept cholesterol from these cells. Previous studies have reported conflicting results regarding the lipidation and cholesterol-handling capacity of different APOE isoforms in astrocytes. Some findings suggest that ABCA1-mediated cholesterol and phosphatidylcholine efflux to lipid-free APOE does not significantly differ between isoforms,[149] while others demonstrate that APOE3 more efficiently facilitates cholesterol efflux than APOE4.[150] This difference aligns with findings showing that ABCA1 membrane trafficking is impaired in the presence of APOE4, ultimately leading to reduced cholesterol efflux from astrocytes.[151] In line with this, transcriptomic and functional analyses of human iPSC-derived astrocytes have shown that APOE4 alters cholesterol and extracellular matrix pathway regulation[30] and diminishes neurotrophic support, including impaired cholesterol transport capacity.[152]

In cholesterol uptake assays using differentiated SH-SY5Y neurons, radiolabeled cholesterol delivered by rHDL-APOE4 was internalized significantly less efficiently than that delivered by rHDL-APOE3, demonstrating a compromised capacity of APOE4-containing rHDL particles to deliver cholesterol to neurons. In this context, prior studies using rat hippocampal neurons also showed APOE isoform-dependent differences in cholesterol uptake, with APOE4 displaying an impaired lipid delivery.[153] This reduced uptake may result from lower binding affinity for neuronal APOE receptors or impaired receptor-mediated

internalization and trafficking, such as LRP1 which has been shown to be critical for lipid metabolism homeostasis in neurons.[154]

Collectively, our data show that despite the increased prevalence of APOE-ε4 and the presence of hallmark AD biomarkers, the overall composition of CSF HDL-like particles and their capacity to accept cholesterol from astrocytes remain unchanged. Nevertheless, a significant impairment in neuronal cholesterol uptake from AD CSF was observed, implicating a functional deficiency in cholesterol delivery. This defect was recapitulated using reconstituted HDL particles, where APOE4-containing particles exhibited reduced neuronal uptake compared to APOE3 (**Figure 39**). These findings support a critical APOE isoform–dependent mechanism by which cholesterol trafficking to neurons is compromised in AD, potentially contributing to synaptic dysfunction and neurodegeneration. Targeting APOE4-mediated cholesterol transport deficits may offer a novel therapeutic approach to restoring neuronal lipid homeostasis in AD.

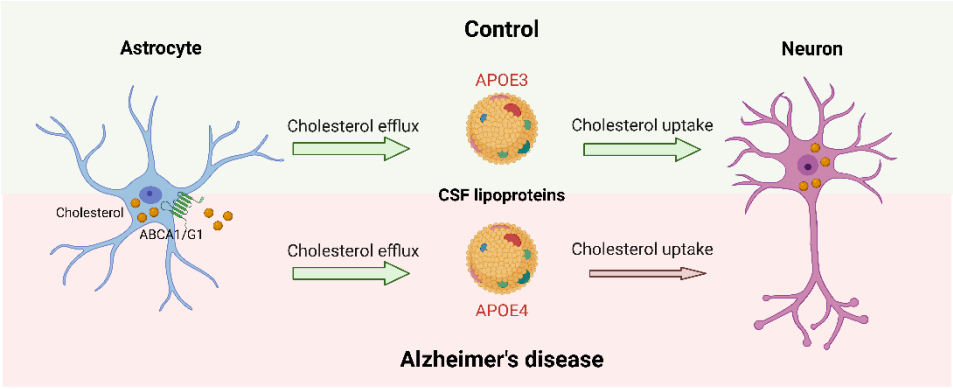

Figure 39. Proposed model for work 3. While cholesterol efflux from astrocytes is similar between control and AD patients, cholesterol uptake by neurons is significantly reduced when mediated by CSF HDL-like particles from AD patients. This impairment is primarily attributed to the presence of APOE4 isoform. Created with *Biorender.com*

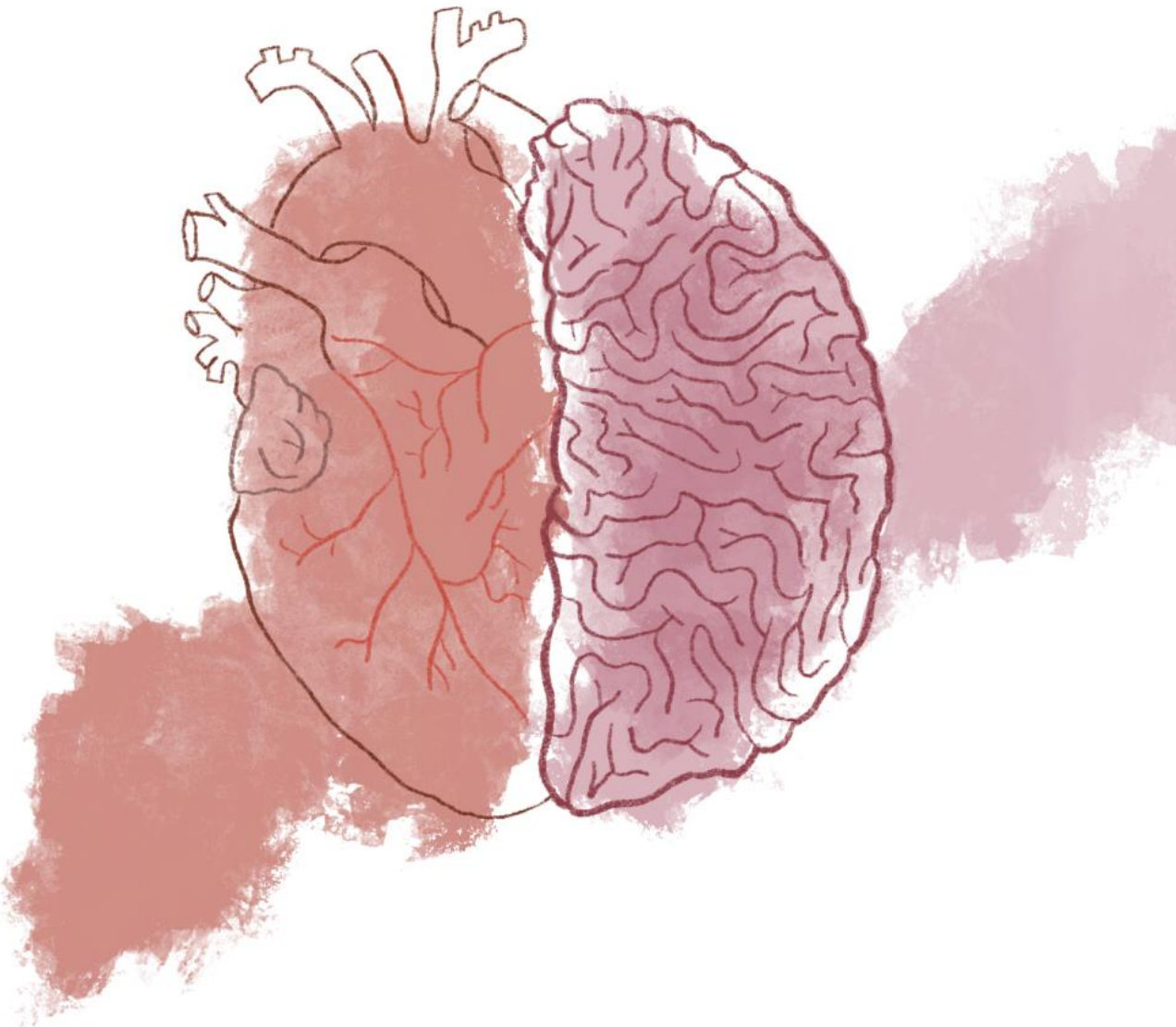

CHAPTER VI

CONCLUSIONS

Work 1: PCSK9 Inhibition and Cholesterol Efflux in FH

- Macrophage cholesterol efflux capacity remains unchanged following PCSK9 inhibitor treatment in FH patients.
- PCSK9 inhibitor therapy induces a shift in the distribution of macrophage-derived cholesterol to lipoproteins in FH plasma during the cholesterol efflux process; this results in a reduction of LDL's capacity to act as a macrophage-derived cholesterol reservoir and an increase in the acceptor function of HDL.
- In a humanized FH mouse model, PCSK9 antibody treatment significantly enhances the overall macrophage-to-feces RCT pathway, mainly via accelerated hepatic clearance of LDL particles.

Work 2: Cholesterol Efflux from VSMCs in Atherogenesis

- Cholesterol loading induces a phenotypic switch in VSMCs, accompanied by a marked impairment in cholesterol efflux to HDL.
- LXR activation enhances cholesterol efflux and promotes the VSMC-to-feces RCT pathway *in vivo*, even after foam-cell like transformation.
- ACAT inhibition restores the cholesterol efflux capacity in lipid-laden VSMCs by increasing the bioavailability of unesterified cholesterol for transport.
- The combination of LXR activation and ACAT inhibition synergistically enhances cholesterol efflux from VSMC-derived foam cells, effectively overcoming the limitations of each treatment alone.

Work 3: CSF-Mediated Cholesterol Transport in AD

- Cholesterol efflux from astrocytes is similar between AD patients and control individuals, both under baseline conditions and following ABCA1/ABCG1 transporter upregulation.
- CSF HDL-like particles from AD patients exhibit defective cholesterol delivery to neurons, resulting in reduced neuronal cholesterol uptake that is not influenced by Aβ peptide or tau protein.
- rHDL particles containing APOE4 show similar cholesterol efflux from astrocytes and lower cholesterol delivery to neurons compared to rHDL-APOE3, emphasizing the role of APOE4 in compromising neuronal cholesterol homeostasis.

-

REFERENCES

1. Sonal Sekhar, M., Marupuru, S., Reddy, B. S., Kurian, S. J. & Rao, M. Chapter 21 - Physiological role of cholesterol in human body. in *Dietary Sugar, Salt and Fat in Human Health* (eds. Preuss, H. G. & Bagchi, D.) 453–481 (Academic Press, 2020).
2. Zhang, J. & Liu, Q. Cholesterol metabolism and homeostasis in the brain. *Protein Cell* **6**, 254–264 (2015).
3. Luo, J., Yang, H. & Song, B.-L. Mechanisms and regulation of cholesterol homeostasis. *Nat. Rev. Mol. Cell Biol.* **21**, 225–245 (2020).
4. Vitali, C., Wellington, C. L. & Calabresi, L. HDL and cholesterol handling in the brain. *Cardiovasc. Res.* **103**, 405–413 (2014).
5. Dominiczak, M. H. & Caslake, M. J. Apolipoproteins: metabolic role and clinical biochemistry applications. *Ann. Clin. Biochem.* **48**, 498–515 (2011).
6. Balazs, Z. *et al.* Uptake and transport of high-density lipoprotein (HDL) and HDL-associated alpha-tocopherol by an in vitro blood-brain barrier model. *J. Neurochem.* **89**, 939–950 (2004).
7. Hinsdale, M. E., Sullivan, P. M., Mezdour, H. & Maeda, N. ApoB-48 and apoB-100 differentially influence the expression of type-III hyperlipoproteinemia in APOE*2 mice. *J. Lipid Res.* **43**, 1520–1528 (2002).
8. Picard, C. *et al.* Apolipoprotein B is a novel marker for early tau pathology in Alzheimer's disease. *Alzheimers Dement.* **18**, 875–887 (2022).
9. Lanfranco, M. F., Ng, C. A. & Rebeck, G. W. ApoE Lipidation as a Therapeutic Target in Alzheimer's Disease. *Int. J. Mol. Sci.* **21**, 6336 (2020).
10. Liu, C.-C., Kanekiyo, T. & Bu, G. Apolipoprotein E and Alzheimer disease: risk, mechanisms and therapy. *Nat. Rev. Neurol.* **9**, 106–118 (2013).

11. Feingold, K. R. Introduction to Lipids and Lipoproteins. in *Endotext [Internet]* (MDText.com, Inc., 2024).

12. Qiao, Y.-N., Zou, Y.-L. & Guo, S.-D. Low-density lipoprotein particles in atherosclerosis. *Front. Physiol.* **13**, (2022).

13. Thomas, S. R., Zhang, Y. & Rye, K.-A. The pleiotropic effects of high-density lipoproteins and apolipoprotein A-I. *Best Pract. Res. Clin. Endocrinol. Metab.* **37**, 101689 (2023).

14. Thakkar, H., Vincent, V., Sen, A., Singh, A. & Roy, A. Changing Perspectives on HDL: From Simple Quantity Measurements to Functional Quality Assessment. *J. Lipids* **2021**, 5585521 (2021).

15. Wasan, K. M., Brocks, D. R., Lee, S. D., Sachs-Barrable, K. & Thornton, S. J. Impact of lipoproteins on the biological activity and disposition of hydrophobic drugs: implications for drug discovery. *Nat. Rev. Drug Discov.* **7**, 84–99 (2008).

16. Sirinian, M. I. *et al.* Adaptor protein ARH is recruited to the plasma membrane by low density lipoprotein (LDL) binding and modulates endocytosis of the LDL/LDL receptor complex in hepatocytes. *J. Biol. Chem.* **280**, 38416–38423 (2005).

17. Yang, H. *et al.* Cholesterol in LDL receptor recycling and degradation. *Clin. Chim. Acta* **500**, 81–86 (2020).

18. Go, G. & Mani, A. Low-Density Lipoprotein Receptor (LDLR) Family Orchestrates Cholesterol Homeostasis. *Yale J. Biol. Med.* **85**, 19–28 (2012).

19. Goldstein, J. L., DeBose-Boyd, R. A. & Brown, M. S. Protein Sensors for Membrane Sterols. *Cell* **124**, 35–46 (2006).

20. Horton, J. D., Cohen, J. C. & Hobbs, H. H. Molecular biology of PCSK9: its role in LDL metabolism. *Trends Biochem. Sci.* **32**, 71–77 (2007).

21. Shen, W.-J., Azhar, S. & Kraemer, F. B. SR-B1: A Unique Multifunctional Receptor for Cholesterol Influx and Efflux. *Annu. Rev. Physiol.* **80**, 95–116 (2018).

22. Rees, D. C., Johnson, E. & Lewinson, O. ABC transporters: the power to change. *Nat. Rev. Mol. Cell Biol.* **10**, 218–227 (2009).

23. Matsuo, M. ABCA1 and ABCG1 as potential therapeutic targets for the prevention of atherosclerosis. *J. Pharmacol. Sci.* **148**, 197–203 (2022).

24. Patel, S. B., Graf, G. A. & Temel, R. E. Thematic Review Series: Lipid Transfer Proteins ABCG5 and ABCG8: more than a defense against xenosterols. *J. Lipid Res.* **59**, 1103–1113 (2018).

25. Fessler, M. B. The challenges and promise of targeting the Liver X Receptors for treatment of inflammatory disease. *Pharmacol. Ther.* **181**, 1–12 (2018).

26. Davis, H. R. & Altmann, S. W. Niemann-Pick C1 Like 1 (NPC1L1) an intestinal sterol transporter. *Biochim. Biophys. Acta* **1791**, 679–683 (2009).

27. Afonso, M. S. *et al.* Molecular Pathways Underlying Cholesterol Homeostasis. *Nutrients* **10**, 760 (2018).

28. Duan, Y. *et al.* Regulation of cholesterol homeostasis in health and diseases: from mechanisms to targeted therapeutics. *Signal Transduct. Target. Ther.* **7**, 1–29 (2022).

29. Pownall, H. J., Rosales, C., Gillard, B. K. & Gotto, A. M. High-density lipoproteins, reverse cholesterol transport and atherogenesis. *Nat. Rev. Cardiol.* **18**, 712–723 (2021).

30. Tcw, J. *et al.* Cholesterol and matrisome pathways dysregulated in astrocytes and microglia. *Cell* **185**, 2213-2233.e25 (2022).

31. Vance, J. E. & Hayashi, H. Formation and function of apolipoprotein E-containing lipoproteins in the nervous system. *Biochim. Biophys. Acta BBA - Mol. Cell Biol. Lipids* **1801**, 806–818 (2010).

32. Koch, S. *et al.* Characterization of four lipoprotein classes in human cerebrospinal fluid. *J. Lipid Res.* **42**, 1143–1151 (2001).

33. Demeester, N. *et al.* Characterization and functional studies of lipoproteins, lipid transfer proteins, and lecithin:cholesterol acyltransferase in

CSF of normal individuals and patients with Alzheimer's disease. *J. Lipid Res.* **41**, 963–974 (2000).

34. Hirsch-Reinshagen, V. *et al.* Deficiency of ABCA1 impairs apolipoprotein E metabolism in brain. *J. Biol. Chem.* **279**, 41197–41207 (2004).

35. DeMattos, R. B. *et al.* Purification and characterization of astrocyte-secreted apolipoprotein E and J-containing lipoproteins from wild-type and human apoE transgenic mice. *Neurochem. Int.* **39**, 415–425 (2001).

36. Mahley, R. W. Central Nervous System Lipoproteins. *Arterioscler. Thromb. Vasc. Biol.* **36**, 1305–1315 (2016).

37. Li, X. *et al.* Astrocytic ApoE reprograms neuronal cholesterol metabolism and histone-acetylation-mediated memory. *Neuron.* **109**, 957-970.e8 (2021).

38. Borràs, C. *et al.* HDL-like-Mediated Cell Cholesterol Trafficking in the Central Nervous System and Alzheimer's Disease Pathogenesis. *Int. J. Mol. Sci.* **23**, 9356 (2022).

39. Cardiovascular diseases. https://www.who.int/health-topics/cardiovascular-diseases.

40. Netala, V. R., Teertam, S. K., Li, H. & Zhang, Z. A Comprehensive Review of Cardiovascular Disease Management: Cardiac Biomarkers, Imaging Modalities, Pharmacotherapy, Surgical Interventions, and Herbal Remedies. *Cells* **13**, 1471 (2024).

41. Vaduganathan, M., Mensah, G. A., Turco, J. V., Fuster, V. & Roth, G. A. The Global Burden of Cardiovascular Diseases and Risk. *J. Am. Coll. Cardiol.* **80**, 2361–2371 (2022).

42. Adhikary, D., Barman, S., Ranjan, R. & Stone, H. A Systematic Review of Major Cardiovascular Risk Factors: A Growing Global Health Concern. *Cureus* **14**, e30119.

43. Hajar, R. Genetics in Cardiovascular Disease. *Heart Views Off. J. Gulf Heart Assoc.* **21**, 55–56 (2020).

44. Björkegren, J. L. M. & Lusis, A. J. Atherosclerosis: Recent developments. *Cell* **185**, 1630–1645 (2022).

45. Jebari-Benslaiman, S. *et al.* Pathophysiology of Atherosclerosis. *Int. J. Mol. Sci.* **23**, 3346 (2022).

46. Bax, M. *et al.* Arterial dissections: Common features and new perspectives. *Front. Cardiovasc. Med.* **9**, (2022).

47. Rosenfeld, M. E. Converting smooth muscle cells to macrophage-like cells with KLF4 in atherosclerotic plaques. *Nat. Med.* **21**, 549–551 (2015).

48. Rong, J. X., Shapiro, M., Trogan, E. & Fisher, E. A. Transdifferentiation of mouse aortic smooth muscle cells to a macrophage-like state after cholesterol loading. *Proc. Natl. Acad. Sci.* **100**, 13531–13536 (2003).

49. Francis, G. A. The Greatly Under-Represented Role of Smooth Muscle Cells in Atherosclerosis. *Curr. Atheroscler. Rep.* **25**, 741–749 (2023).

50. Allahverdian, S., Chehroudi, A. C., McManus, B. M., Abraham, T. & Francis, G. A. Contribution of intimal smooth muscle cells to cholesterol accumulation and macrophage-like cells in human atherosclerosis. *Circulation* **129**, 1551–1559 (2014).

51. Libby, P., Ridker, P. M. & Hansson, G. K. Progress and challenges in translating the biology of atherosclerosis. *Nature* **473**, 317–325 (2011).

52. Libby, P. *et al.* Atherosclerosis. *Nat. Rev. Dis. Primer* **5**, 56 (2019).

53. Hu, P. *et al.* Prevalence of Familial Hypercholesterolemia Among the General Population and Patients With Atherosclerotic Cardiovascular Disease: A Systematic Review and Meta-Analysis. *Circulation* **141**, 1742–1759 (2020).

54. Nordestgaard, B. G. *et al.* Familial hypercholesterolaemia is underdiagnosed and undertreated in the general population: guidance for clinicians to prevent coronary heart disease: consensus statement of the European Atherosclerosis Society. *Eur. Heart J.* **34**, 3478–3490a (2013).

55. Vaezi, Z. & Amini, A. Familial Hypercholesterolemia. in *StatPearls* (StatPearls Publishing, Treasure Island (FL), 2025).

56. Nikasa, P. *et al.* A case of autosomal recessive hypercholesterolemia with a novel mutation in the LDLRAP1 gene. *Clin. Pediatr. Endocrinol.* **30**, 201–204 (2021).

57. Mach, F. *et al.* 2019 ESC/EAS Guidelines for the management of dyslipidaemias: lipid modification to reduce cardiovascular risk: The Task Force for the management of dyslipidaemias of the European Society of Cardiology (ESC) and European Atherosclerosis Society (EAS). *Eur. Heart J.* **41**, 111–188 (2020).

58. Catapano, A. L. *et al.* 2016 ESC/EAS Guidelines for the Management of Dyslipidaemias. *Eur. Heart J.* **37**, 2999–3058 (2016).

59. Cuchel, M. *et al.* Homozygous familial hypercholesterolaemia: new insights and guidance for clinicians to improve detection and clinical management. A position paper from the Consensus Panel on Familial Hypercholesterolaemia of the European Atherosclerosis Society. *Eur. Heart J.* **35**, 2146–2157 (2014).

60. Hindi, N. N., Alenbawi, J. & Nemer, G. Pharmacogenomics Variability of Lipid-Lowering Therapies in Familial Hypercholesterolemia. *J. Pers. Med.* **11**, 877 (2021).

61. Sultan, S. *et al.* Chapter 6 - Statins: Rationale, Mode of Action, and Side Effects. in *The Impact of Nutrition and Statins on Cardiovascular Diseases* (eds. Zabetakis, I., Lordan, R. & Tsoupras, A.) 171–200 (Academic Press, 2019).

62. Chen, R., Lin, S. & Chen, X. The promising novel therapies for familial hypercholesterolemia. *J. Clin. Lab. Anal.* **36**, e24552 (2022).

63. Alradwan, I. *et al.* Emerging Trends and Innovations in the Treatment and Diagnosis of Atherosclerosis and Cardiovascular Disease: A Comprehensive Review towards Healthier Aging. *Pharmaceutics* **16**, 1037 (2024).

64. Sabatine, M. S. *et al.* Evolocumab and Clinical Outcomes in Patients with Cardiovascular Disease. *N. Engl. J. Med.* **376**, 1713–1722 (2017).

65. Robinson, J. G. *et al.* Efficacy and Safety of Alirocumab in Reducing Lipids and Cardiovascular Events. *N. Engl. J. Med.* **372**, 1489–1499 (2015).

66. Masana Marín, L. & Plana Gil, N. Bempedoic acid. Mechanism of action and pharmacokinetic and pharmacodynamic properties. *Clin. E Investig. En Arterioscler. Publicacion Of. Soc. Espanola Arterioscler.* **33 Suppl 1**, 53–57 (2021).

67. Lee, Y. T. *et al.* Mouse models of atherosclerosis: a historical perspective and recent advances. *Lipids Health Dis.* **16**, 12 (2017).

68. Ramírez, C. *et al.* ApoB100/LDLR-/- Hypercholesterolaemic Mice as a Model for Mild Cognitive Impairment and Neuronal Damage. *PLOS ONE* **6**, e22712 (2011).

69. Benitez-Amaro, A. *et al.* Targeting LDL aggregation decreases atherosclerotic lipid burden in a humanized mouse model of familial hypercholesterolemia: Crucial role of ApoB100 conformational stabilization. *Atherosclerosis* 118630 (2024).

70. Dementia. https://www.who.int/news-room/fact-sheets/detail/dementia.

71. Blennow, K., Leon, M. J. de & Zetterberg, H. Alzheimer's disease. *The Lancet* **368**, 387–403 (2006).

72. Association, A. 2019 Alzheimer's disease facts and figures. *Alzheimers Dement.* **15**, 321–387 (2019).

73. Scheltens, P. *et al.* Alzheimer's disease. *The Lancet* **397**, 1577–1590 (2021).

74. Hampel, H. *et al.* The Amyloid-β Pathway in Alzheimer's Disease. *Mol. Psychiatry* **26**, 5481–5503 (2021).

75. Bachurin, S. O., Bovina, E. V. & Ustyugov, A. A. Drugs in Clinical Trials for Alzheimer's Disease: The Major Trends. *Med. Res. Rev.* **37**, 1186–1225 (2017).

76. Sadigh-Eteghad, S. *et al.* Amyloid-Beta: A Crucial Factor in Alzheimer's Disease. *Med. Princ. Pract.* **24**, 1–10 (2014).

77. Goate, A. *et al.* Segregation of a missense mutation in the amyloid precursor protein gene with familial Alzheimer's disease. *Nature* **349**, 704–706 (1991).

78. Sherrington, R. *et al.* Cloning of a gene bearing missense mutations in early-onset familial Alzheimer's disease. *Nature* **375**, 754–760 (1995).

79. Abyadeh, M. *et al.* Amyloid-beta and tau protein beyond Alzheimer's disease. *Neural Regen. Res.* **19**, 1262 (2024).

80. Holtzman, D. M. *et al.* Tau: From research to clinical development. *Alzheimers Dement.* **12**, 1033–1039 (2016).

81. Lambert, J.-C. *et al.* Genome-wide association study identifies variants at CLU and CR1 associated with Alzheimer's disease. *Nat. Genet.* **41**, 1094–1099 (2009).

82. Kunkle, B. W. *et al.* Genetic meta-analysis of diagnosed Alzheimer's disease identifies new risk loci and implicates Aβ, tau, immunity and lipid processing. *Nat. Genet.* **51**, 414–430 (2019).

83. Lambert, J.-C. *et al.* Meta-analysis of 74,046 individuals identifies 11 new susceptibility loci for Alzheimer's disease. *Nat. Genet.* **45**, 1452–1458 (2013).

84. Farfel, J. M., Yu, L., De Jager, P. L., Schneider, J. A. & Bennett, D. A. Association of *APOE* with tau-tangle pathology with and without β-amyloid. *Neurobiol. Aging* **37**, 19–25 (2016).

85. Corder, E. H. *et al.* Gene dose of apolipoprotein E type 4 allele and the risk of Alzheimer's disease in late onset families. *Science* **261**, 921–923 (1993).

86. Poirier, J. *et al.* Apolipoprotein E polymorphism and Alzheimer's disease. *The Lancet* **342**, 697–699 (1993).

87. Fortea, J. *et al.* APOE4 homozygosity represents a distinct genetic form of Alzheimer's disease. *Nat. Med.* **30**, 1284–1291 (2024).

88. Jack, C. R. *et al.* Revised criteria for diagnosis and staging of Alzheimer's disease: Alzheimer's Association Workgroup. *Alzheimers Dement. J. Alzheimers Assoc.* **20**, 5143–5169 (2024).

89. Porsteinsson, A. P., Isaacson, R. S., Knox, S., Sabbagh, M. N. & Rubino, I. Diagnosis of Early Alzheimer's Disease: Clinical Practice in 2021. *J. Prev. Alzheimers Dis.* **8**, 371–386 (2021).

90. Masters, C. L. *et al.* Alzheimer's disease. *Nat. Rev. Dis. Primer* **1**, 1–18 (2015).

91. Anitha K *et al.* Recent Insights into the Neurobiology of Alzheimer's Disease and Advanced Treatment Strategies. *Mol. Neurobiol.* **62**, 2314–2332 (2025).

92. Vaz, M. & Silvestre, S. Alzheimer's disease: Recent treatment strategies. *Eur. J. Pharmacol.* **887**, 173554 (2020).

93. Friedewald, W. T., Levy, R. I. & Fredrickson, D. S. Estimation of the concentration of low-density lipoprotein cholesterol in plasma, without use of the preparative ultracentrifuge. *Clin. Chem.* **18**, 499–502 (1972).

94. Radding, C. M. & Steinberg, D. Studies on the synthesis and secretion of serum lipoproteins by rat liver slices. *J. Clin. Invest.* **39**, 1560–1569 (1960).

95. Escolà-Gil, J. C. *et al.* Quantification of In Vitro Macrophage Cholesterol Efflux and In Vivo Macrophage-Specific Reverse Cholesterol Transport. *Methods Mol. Biol.* **1339**, 211–233 (2015).

96. Chan, J. C. Y. *et al.* A proprotein convertase subtilisin/kexin type 9 neutralizing antibody reduces serum cholesterol in mice and nonhuman primates. *Proc. Natl. Acad. Sci. U. S. A.* **106**, 9820–9825 (2009).

97. Neris, R. L. S., Dobles, A. M. C. & Gomes, A. V. Western Blotting Using In-Gel Protein Labeling as a Normalization Control: Advantages of Stain-Free Technology. *Methods Mol. Biol. Clifton NJ* **2261**, 443–456 (2021).

98. Taylor, S. C. & Posch, A. The design of a quantitative western blot experiment. *BioMed Res. Int.* **2014**, 361590 (2014).

99. Cedó, L. *et al.* LDL Receptor Regulates the Reverse Transport of Macrophage-Derived Unesterified Cholesterol via Concerted Action of the HDL-LDL Axis. *Circ. Res.* **127**, 778–792 (2020).

100. Livak, K. J. & Schmittgen, T. D. Analysis of relative gene expression data using real-time quantitative PCR and the 2(-Delta Delta C(T)) Method. *Methods San Diego Calif* **25**, 402–408 (2001).

101. Alcolea, D. *et al.* The Sant Pau Initiative on Neurodegeneration (SPIN) cohort: A data set for biomarker discovery and validation in neurodegenerative disorders. *Alzheimers Dement. N. Y. N* **5**, 597–609 (2019).

102. Fernández-de-Retana, S. *et al.* Characterization of ApoJ-reconstituted high-density lipoprotein (rHDL) nanodisc for the potential treatment of cerebral β-amyloidosis. *Sci. Rep.* **7**, 14637 (2017).

103. Cedó, L. *et al.* Altered HDL Remodeling and Functionality in Familial Hypercholesterolemia. *J. Am. Coll. Cardiol.* **71**, 466–468 (2018).

104. Rehues, P. *et al.* PCSK9 Inhibitors Have Apolipoprotein C-III-Related Anti-Inflammatory Activity, Assessed by 1H-NMR Glycoprotein Profile in Subjects at High or very High Cardiovascular Risk. *Int. J. Mol. Sci.* **24**, 2319 (2023).

105. Koren, M. J. *et al.* Effect of PCSK9 Inhibition by Alirocumab on Lipoprotein Particle Concentrations Determined by Nuclear Magnetic Resonance Spectroscopy. *J. Am. Heart Assoc.* **4**, e002224 (2015).

106. Lappegård, K. T. *et al.* Lipoprotein apheresis affects lipoprotein particle subclasses more efficiently compared to the PCSK9 inhibitor evolocumab, a pilot study. *Transfus. Apher. Sci.* **57**, 91–96 (2018).

107. Ying, Q. *et al.* Effect of a PCSK9 inhibitor and a statin on cholesterol efflux capacity: A limitation of current cholesterol-lowering treatments? *Eur. J. Clin. Invest.* **52**, e13766 (2022).

108. Palumbo, M. *et al.* Effects of PCSK9 inhibitors on HDL cholesterol efflux and serum cholesterol loading capacity in familial hypercholesterolemia subjects: a multi-lipid-center real-world evaluation. *Front. Mol. Biosci.* **9**, 925587 (2022).

109. Lee-Rueckert, M., Escola-Gil, J. C. & Kovanen, P. T. HDL functionality in reverse cholesterol transport--Challenges in translating data emerging from

mouse models to human disease. *Biochim. Biophys. Acta* **1861**, 566–583 (2016).

110. Borén, J. *et al.* Low-density lipoproteins cause atherosclerotic cardiovascular disease: pathophysiological, genetic, and therapeutic insights: a consensus statement from the European Atherosclerosis Society Consensus Panel. *Eur. Heart J.* **41**, 2313–2330 (2020).

111. Martel, C. *et al.* Lymphatic vasculature mediates macrophage reverse cholesterol transport in mice. *J. Clin. Invest.* **123**, 1571–1579 (2013).

112. Graf, G. A. *et al.* ABCG5 and ABCG8 are obligate heterodimers for protein trafficking and biliary cholesterol excretion. *J. Biol. Chem.* **278**, 48275–48282 (2003).

113. Escolà-Gil, J. C. *et al.* The cholesterol content of Western diets plays a major role in the paradoxical increase in high-density lipoprotein cholesterol and upregulates the macrophage reverse cholesterol transport pathway. *Arterioscler. Thromb. Vasc. Biol.* **31**, 2493–2499 (2011).

114. Shankman, L. S. *et al.* KLF4-dependent phenotypic modulation of smooth muscle cells has a key role in atherosclerotic plaque pathogenesis. *Nat. Med.* **21**, 628–637 (2015).

115. Vengrenyuk, Y. *et al.* Cholesterol loading reprograms the microRNA-143/145-myocardin axis to convert aortic smooth muscle cells to a dysfunctional macrophage-like phenotype. *Arterioscler. Thromb. Vasc. Biol.* **35**, 535–546 (2015).

116. Feil, S. *et al.* Transdifferentiation of vascular smooth muscle cells to macrophage-like cells during atherogenesis. *Circ. Res.* **115**, 662–667 (2014).

117. Chappell, J. *et al.* Extensive Proliferation of a Subset of Differentiated, yet Plastic, Medial Vascular Smooth Muscle Cells Contributes to Neointimal Formation in Mouse Injury and Atherosclerosis Models. *Circ. Res.* **119**, 1313–1323 (2016).

118. Misra, A. *et al.* Integrin beta3 regulates clonality and fate of smooth muscle-derived atherosclerotic plaque cells. *Nat. Commun.* **9**, 2073 (2018).

119. Choi, H. Y. *et al.* ATP-binding cassette transporter A1 expression and apolipoprotein A-I binding are impaired in intima-type arterial smooth muscle cells. *Circulation* **119**, 3223–3231 (2009).

120. Zanotti, I. *et al.* The LXR agonist T0901317 promotes the reverse cholesterol transport from macrophages by increasing plasma efflux potential. *J. Lipid Res.* **49**, 954–960 (2008).

121. Yasuda, T. *et al.* Tissue-Specific Liver X Receptor Activation Promotes Macrophage Reverse Cholesterol Transport In Vivo. *Arterioscler. Thromb. Vasc. Biol.* **30**, 781–786 (2010).

122. Naik, S. U. *et al.* Pharmacological activation of liver X receptors promotes reverse cholesterol transport in vivo. *Circulation* **113**, 90–97 (2006).

123. Lee, S. D. & Tontonoz, P. Liver X receptors at the intersection of lipid metabolism and atherogenesis. *Atherosclerosis* **242**, 29–36 (2015).

124. Rodriguez, A., Bachorik, P. S. & Wee, S. B. Novel effects of the acyl-coenzyme A:Cholesterol acyltransferase inhibitor 58-035 on foam cell development in primary human monocyte-derived macrophages. *Arterioscler. Thromb. Vasc. Biol.* **19**, 2199–2206 (1999).

125. Rodriguez, A. & Usher, D. C. Anti-atherogenic effects of the acyl-CoA:cholesterol acyltransferase inhibitor, avasimibe (CI-1011), in cultured primary human macrophages. *Atherosclerosis* **161**, 45–54 (2002).

126. Cignarella, A. *et al.* Pharmacological regulation of cholesterol efflux in human monocyte-derived macrophages in the absence of exogenous cholesterol acceptors. *Atherosclerosis* **179**, 229–236 (2005).

127. Warner, G. J., Stoudt, G., Bamberger, M., Johnson, W. J. & Rothblat, G. H. Cell toxicity induced by inhibition of acyl coenzyme A:cholesterol acyltransferase and accumulation of unesterified cholesterol. *J. Biol. Chem.* **270**, 5772–5778 (1995).

128. Feng, B. & Tabas, I. ABCA1-mediated cholesterol efflux is defective in free cholesterol-loaded macrophages. Mechanism involves enhanced ABCA1

degradation in a process requiring full NPC1 activity. *J. Biol. Chem.* **277**, 43271–43280 (2002).

129. Rong, J. X., Kusunoki, J., Oelkers, P., Sturley, S. L. & Fisher, E. A. Acyl-coenzymeA (CoA):cholesterol acyltransferase inhibition in rat and human aortic smooth muscle cells is nontoxic and retards foam cell formation. *Arterioscler. Thromb. Vasc. Biol.* **25**, 122–127 (2005).

130. Olsson, B. *et al.* CSF and blood biomarkers for the diagnosis of Alzheimer's disease: a systematic review and meta-analysis. *Lancet Neurol.* **15**, 673–684 (2016).

131. Evans, S. *et al.* Alzheimer's disease progression and risk factors: A standardized comparison between six large data sets. *Alzheimers Dement. Transl. Res. Clin. Interv.* **5**, 515–523 (2019).

132. Qiu, C., Kivipelto ,Miia & and von Strauss, E. Epidemiology of Alzheimer's disease: occurrence, determinants, and strategies toward intervention. *Dialogues Clin. Neurosci.* **11**, 111–128 (2009).

133. Niu, H., Álvarez-Álvarez, I., Guillén-Grima, F. & Aguinaga-Ontoso, I. Prevalence and incidence of Alzheimer's disease in Europe: A meta-analysis. *Neurol. Barc. Spain* **32**, 523–532 (2017).

134. Marchi, C. *et al.* ABCA1- and ABCG1-mediated cholesterol efflux capacity of cerebrospinal fluid is impaired in Alzheimer's disease. *J. Lipid Res.* **60**, 1449–1456 (2019).

135. Yassine, H. N. *et al.* ABCA1-Mediated Cholesterol Efflux Capacity to Cerebrospinal Fluid Is Reduced in Patients With Mild Cognitive Impairment and Alzheimer's Disease. *J. Am. Heart Assoc.* **5**, e002886 (2016).

136. Fukuyama, R. *et al.* Age-dependent decline in the apolipoprotein E level in cerebrospinal fluid from control subjects and its increase in cerebrospinal fluid from patients with Alzheimer's disease. *Eur. Neurol.* **43**, 161–169 (2000).

137. Hesse, C. *et al.* Measurement of apolipoprotein E (apoE) in cerebrospinal fluid. *Neurochem. Res.* **25**, 511–517 (2000).

138. Kandimalla, R. J. L. *et al.* Apolipoprotein E levels in the cerebrospinal fluid of north Indian patients with Alzheimer's disease. *Am. J. Alzheimers Dis. Other Demen.* **28**, 258–262 (2013).

139. Merched, A. *et al.* Cerebrospinal fluid apolipoprotein E level is increased in late-onset Alzheimer's disease. *J. Neurol. Sci.* **145**, 33–39 (1997).

140. Talwar, P. *et al.* Meta-analysis of apolipoprotein E levels in the cerebrospinal fluid of patients with Alzheimer's disease. *J. Neurol. Sci.* **360**, 179–187 (2016).

141. Testa, G. *et al.* The Emerging Role of PCSK9 in the Pathogenesis of Alzheimer's Disease: A Possible Target for the Disease Treatment. *Int. J. Mol. Sci.* **25**, 13637 (2024).

142. Kang, S. *et al.* PiB-PET Imaging-Based Serum Proteome Profiles Predict Mild Cognitive Impairment and Alzheimer's Disease. *J. Alzheimer's Dis.* **53**, 1563–1576 (2016).

143. Zimetti, F. *et al.* Increased PCSK9 Cerebrospinal Fluid Concentrations in Alzheimer's Disease. *J. Alzheimers Dis. JAD* **55**, 315–320 (2017).

144. O'Connell, E. M. & Lohoff, F. W. Proprotein Convertase Subtilisin/Kexin Type 9 (PCSK9) in the Brain and Relevance for Neuropsychiatric Disorders. *Front. Neurosci.* **14**, (2020).

145. Chen, J., Zhang, X., Kusumo, H., Costa, L. G. & Guizzetti, M. Cholesterol efflux is differentially regulated in neurons and astrocytes: implications for brain cholesterol homeostasis. *Biochim. Biophys. Acta* **1831**, 263–275 (2013).

146. Cipollari, E. *et al.* Correlates and Predictors of Cerebrospinal Fluid Cholesterol Efflux Capacity from Neural Cells, a Family of Biomarkers for Cholesterol Epidemiology in Alzheimer's Disease. *J. Alzheimers Dis. JAD* **74**, 563–578 (2020).

147. Turri, M. *et al.* Plasma and cerebrospinal fluid cholesterol esterification is hampered in Alzheimer's disease. *Alzheimers Res. Ther.* **15**, 95 (2023).

148. Pamir, N. *et al.* Proteomic analysis of HDL from inbred mouse strains implicates APOE associated with HDL in reduced cholesterol efflux capacity via the ABCA1 pathway[S]. *J. Lipid Res.* **57**, 246–257 (2016).

149. Lindner, K. *et al.* Isoform- and cell-state-specific lipidation of ApoE in astrocytes. *Cell Rep.* **38**, 110435 (2022).

150. Minagawa, H. *et al.* Mechanism underlying apolipoprotein E (ApoE) isoform-dependent lipid efflux from neural cells in culture. *J. Neurosci. Res.* **87**, 2498–2508 (2009).

151. Rawat, V. *et al.* ApoE4 Alters ABCA1 Membrane Trafficking in Astrocytes. *J. Neurosci. Off. J. Soc. Neurosci.* **39**, 9611–9622 (2019).

152. Zhao, J. *et al.* APOE ε4/ε4 diminishes neurotrophic function of human iPSC-derived astrocytes. *Hum. Mol. Genet.* **26**, 2690–2700 (2017).

153. Rapp, A., Gmeiner, B. & Hüttinger, M. Implication of apoE isoforms in cholesterol metabolism by primary rat hippocampal neurons and astrocytes. *Biochimie* **88**, 473–483 (2006).

154. Liu, Q. *et al.* Neuronal LRP1 knockout in adult mice leads to impaired brain lipid metabolism and progressive, age-dependent synapse loss and neurodegeneration. *J. Neurosci. Off. J. Soc. Neurosci.* **30**, 17068–17078 (2010).

ANNEX

Related publications

Publication 1:

Borràs, C., A. Mercer, S. Sirisi, D. Alcolea, J. C. Escolà-Gil, F. Blanco-Vaca, and M. Tondo. 2022. HDL-like-Mediated Cell Cholesterol Trafficking in the Central Nervous System and Alzheimer's Disease Pathogenesis. *Int J Mol Sci*. **23**: 9356. https://doi.org/10.3390/ijms23169356

Publication 2:

Borràs, C., M. Canyelles, J. Girona, D. Ibarretxe, D. Santos, G. Revilla, V. Llorente-Cortes, N. Rotllan, P. T. Kovanen, M. Jauhiainen, M. Lee-Rueckert, L. Masana, F. Arrieta, J. Martínez-Botas, D. Gómez-Coronado, J. Ribalta, M. Tondo, F. Blanco-Vaca, and J. C. Escolà-Gil. 2024. PCSK9 Antibodies Treatment Specifically Enhances the Macrophage-specific Reverse Cholesterol Transport Pathway in Heterozygous Familial Hypercholesterolemia. *JACC Basic Transl Sci*. **9**: 1195–1210. https://doi.org/10.1016/j.jacbts.2024.06.008

Publication 3:

Borràs, C., N. Rotllan, R. Griñán, D. Santos, A. Solé, C. Dong, Q. Zhao, V. Llorente-Cortes, M. Mourín, B. Soto, M. Camacho, M. Tondo, M. Canyelles, F. Blanco-Vaca, and J. C. Escolà-Gil. 2025. Restoring cholesterol efflux in vascular smooth muscle cells transitioning into foam cells through Liver X receptor activation. *Biomed Pharmacother*. **188**: 118178. https://doi.org/10.1016/j.biopha.2025.118178

Publication 4:

Borràs, C., M. Canyelles, D. Santos, N. Rotllan, E. Núñez, J. Vázquez, D. Maspoch, M. Cano-Sarabia, M. Carmona-Iragui, S. Sirisi, A. Lleó, J. Fortea, D. Alcolea, F. Blanco-Vaca, J. C. Escolà-Gil, and M. Tondo. 2024. Impaired Cerebrospinal Fluid Lipoprotein-Mediated Cholesterol Delivery to Neurons in Alzheimer's Disease. *Res Sq*. rs.3.rs-5682870. https://doi.org/10.21203/rs.3.rs-5682870/v1

ACKNOWLEDGEMENTS

I aquest últim apartat voldria dedicar-lo a tots aquells que heu format part d'aquesta aventura i que heu estat imprescindibles perquè pogués completar-la.

En primer lloc, voldria donar les gràcies als meus directors, ja que sense ells aquesta tesi no hagués estat possible. Gràcies Joan Carles per tots els consells, per les teves gesticulacions del més entenedores i per sempre tenir un Seguim! després de cada assoliment. Gràcies Mireia per les teves bones paraules i la teva admiració per la recerca bàsica, per la perseverança i el positivisme a cada pas en aquest projecte que no ha estat fàcil, però si molt gratificant. I gràcies Xisco per guiar-me, per confiar en mi i obrir-me les portes d'aquest grup i de la ciència.

Marina, has sigut la meva referent des de que vaig arribar. Tu et vas alegrar per la meva beca com si fos teva, i això només va ser el principi d'aquesta gran amistat. Gràcies per tot el que m'has ensenyat, pels esmorzars (o berenars) plens de cotis, per totes les reunions amb esquemes al despatx del JC, i pels congressos amb mil anècdotes (el lago i el petit gran secret de Lyon) que m'encantaria repetir.

Núria i Raquel, el meu equip Western Blot, aquelles companyes que tothom desitjaria tenir. Heu estat un pilar durant aquest camí, gràcies per tots els experiments en equip, pels congressos juntes, per organitzar berenars, activitats, regals i el que calgui. Quina visita més guai vaig tenir a Alemanya i quin festival de fi de tesi més èpic, us estimo molt!!

David, si la sala del ICCC tuviera oídos ya sabría todos los que preferirías embarazosos que me has hecho responder. Gracias por tus historias y tus bromas que, aunque a veces me quejo un poco, me encanta que me chinches por ser "la jefa" y compartir contigo el título de guarros de bioquímica.

Arnau, gràcies per ser el meu no ex tòxic i mai dir que no a una broma, la teva calma (encara que no la d'enviar albarans) sempre és la millor companyia. Jose, gràcies per ampliar el meu vocabulari, la veritat és que per ser una mica anodino no fas gens malament de profe de pool, però millor de compi de running. Lorena, sempre és un plaer unir forces contra el David, no deixis mai de portar-li la contraria. Gio, per mi ets una més del grup, gràcies pels teus ànims i consells. Aya, moltes gràcies per aquesta portada tan bonica, pels teus dibuixos i la teva paciència infinita. Qi, Chen and Kemin, your help over the past year has been invaluable.

Noe, Sònia i Jose Luís, gràcies per acollir-me al laboratori, per la vostra ajuda plena d'experiència i proximitat, pels congressos compartits i per deixar-vos enredar en les nostres bromes i activitats, sou uns jefes molt enrotllats.

A tots els estudiants que heu passat pel grup, gràcies per la vostra dedicació i esforç, l'aprenentatge ha sigut mutu.

Gràcies als que heu fet que Barcelona hagi sigut casa durant aquests cinc anys..

Xavier i Irene, amb vosaltres va començar aquesta experiència, el piset de Via Augusta va ser molt top, canviant fluorescents o fent receptes a hores intempestives com a ritme de vida. Cristina, gràcies per tots els viatges de tren juntes, per ser la cosineta gran exemplar i per l'energia positiva que desprens.

Marta, mi galleguiña favorita, todo empezó en el máster compartiendo los primeros pasos (y cagadas) en el laboratorio, me siento muy afortunada de poder compartir los días buenos y los no tan buenos a tu lado, gracias por estar aquí. Esther, que poc sabies com em vas salvar quan et vaig conèixer, la vida al teu costat és mil cops millor, gràcies per fer la rutina tan fàcil i els purés de carabassa (o carabassó) tan bons. Alba, m'encantaria tornar a les nits de This is Us i Los Bridgerton, que el que ha unit George no ho separi ningú.

Sergio, Mariona i Irene, els meus sapròfits de confiança, escolliria mil vegades més la uni amb vosaltres, gràcies per tots aquests anys celebrant alegries i posant

humor a les penes, viure més a prop aquí que a Tarragona és un privilegi. Carla, gràcies per les converses inacabables, que van des dels problemes diaris a rememorar anècdotes de les nostres nits d'estiu a Tivissa.

I per últim, voldria agrair també a tots els que m'heu recolzat des de la distància, i que heu fet que els dies junts fossin un al·licient més per seguir endavant.

A les yermanis i els nens del barri, sempre preparats per una bona calçotada, una festa d'aniversari o qualsevol pla improvisat, però sobretot per honrar les festes majors com els que més. Quina sort tenir-vos a la meva vida des de ben petits.

Anna, Oriol, Marta i Marc, quin gran descobriment, gràcies pels ànims, i per deixar-me formar part d'aquesta família tan bonica que ja creix amb l'arribada de la nostra estimada Anni.

Abril, tu sempre deies que una amistat de 7 anys ja és per tota la vida, i que feliç soc de tenir-te des de fa més de 12 anys ja sigui fent jazz, vòlei o running, però sempre descobrint algun nou hobby. Anna, quina connexió tan especial, gràcies pel teu suport incondicional i per acollir-me sempre com una sarralenca més.

Júlia, amb tu sobren les paraules, quina ironia quan els nostres àudios són eterns i les nostres trucades no acaben mai. Tot i estar lluny, sento que et tinc ben a prop. Tant de bo tothom tingués la sort de sentir-se tan estimada i recolzada com jo, gràcies per ser la meva persona, aquesta tesi també porta el teu nom.

Padrí, gràcies pels teus missatges cada setmana i per les nostres abraçades. Gràcies a tu, a Carles, a l'Arnau i la Eli per animar-me des de la distància.

Marta, Pep i Júlia, gràcies per fer-me sentir una més de casa vostra, per deixar-me formar part de les vostres bromes i cuidar-me tant.

Naima i Najla, gràcies per valorar-me i estimar-me amb tanta tendresa, pel vostre suport i per estar sempre a punt per una nova aventura juntes.

Diuen que la família no es tria, però jo us tornaria a triar cada vegada. Papa, gràcies per confiar en mi, per l'orgull que irradies quan parles de mi, i per donar-me tomates de l'hort encara que no vingui gaire. Mama, gràcies per fer-me sentir tan especial i per la teva intensitat que et fa ser la millor mare del món, una trucada amb tu m'arregla el dia. I gràcies també per portar el Bram a les nostres vides. Paula, tu estimes sense fi, sé que ho donaries tot per mi. Com a germana gran, m'has ensenyat que a la vida no tot és fàcil, però val moltíssim la pena lluitar pel que vols. Judit, gràcies per la teva senzillesa, tu saps molt bé el que vol dir la paraula esforç, em fa molt feliç que també formis part d'aquesta experiència.

Albert, gràcies per ensenyar-me la vida al teu costat, i per fer-ho tot tan fàcil. Gràcies per recolzar-me incondicionalment, i no sempre dir-me el que vull sentir sinó el que necessito. Has sigut imprescindible en aquest projecte. Que feliç de que aquest amor sigui recíproc i exponencial (milions de trilions).

Moltíssimes gràcies a tots per aportar el vostre granet de sorra en aquesta tesi.

I no voldria acabar aquests agraïments sense parlar d'aquelles persones que ja no hi són però que sempre portaré a dins. En especial, les que em van veure embarcar-me en aquesta aventura, però no han pogut veure'm acabar-la. Iaia, tio i Teresina, sé que estaríeu molt orgullosos de mi, aquesta tesi també és gràcies a vosaltres.

UAB
Universitat Autònoma
de Barcelona